MODELING BIOSORPTION OF CADMIUM, ZINC AND LEAD ONTO NATIVE AND IMMOBILIZED CITRUS PEELS IN BATCH AND FIXED BED REACTORS

A

Thesis

Presented to the Faculty

of the University of Alaska Fairbanks

in Partial Fulfillment of the Requirements

for the Degree of

DOCTOR OF PHILOSOPHY

By

Abhijit Chatterjee

Fairbanks, Alaska

December 2012

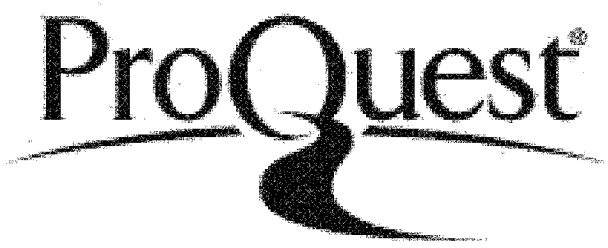

ProQuest LLC
789 East Eisenhower Parkway
P.O. Box 1346
Ann Arbor, MI 48106-1346

MODELING BIOSORPTION OF CADMIUM, ZINC AND LEAD

ONTO NATIVE AND IMMOBILIZED CITRUS PEELS

IN BATCH AND FIXED BED REACTORS

By

Abhijit Chatterjee

RECOMMENDED:

Advisory Committee Chair

Chair, Department of Civil and Environmental Engineering

APPROVED:

Dean, College of Engineering and Mines

Dean of the Graduate School

12/17/12

Date

The thesis is dedicated to
my late father Ajit Kumar Chatterjee and
my mother Banirupa Chatterjee
who sacrificed their comfort for my education

विद्या ददाति विनयं विनयाद्याति पात्रताम् ।
पात्रत्वाद्धनमाप्नोति धनाद्धर्मं ततः सुखम् ॥

"Education gives humility, humility gives character, from character one gets wealth, from wealth one gets righteousness, in righteousness there is joy"

Table of Contents

Page

Signature page i

Title page ii

Abstract iii

Dedication Page iv

Table of Contents v

List of Figures xiii

List of Tables xvi

Acknowledgements xviii

1 Biosorption- a literature review 1

1.1 What is biosorption? 1

1.2 Heavy metal contamination 1

1.3 Comparison with conventional methods 2

1.3.1 Chemical precipitation 2

1.3.2 Membrane filtration 2

1.3.3 Ion exchange 3

1.3.4 Comparison of conventional techniques and biosorption 3

1.4 Citrus peels as biosorbent 5

1.5 Hypotheses and objectives 6

1.6 Modeling biosorption equilibrium 11

1.6.1 Introduction 11

1.6.2 Batch equilibrium data 12

1.6.3 Equilibrium isotherm 13

1.6.4 Simple isotherm models 13

1.7 Fixed bed fundamentals 16

1.7.1 Basic terminology 16

1.7.2 Ideal situation: Equilibrium non-dispersive model 21

1.7.3 Causes and effect of non-ideality 22

1.7.4 Simplest non-ideal system: Equilibrium dispersive model 24

1.8 Rate equations 25

1.8.1 Anatomy of the biosorption process 25

1.8.2 Batch vs. Fixed-Bed 27

1.8.3 Rate equations for Mass Transfer Models (MTM) 27

1.8.3.1 Rate equations for film diffusion 28

1.8.3.2 Rate equations for intra-particle diffusion 28

a) Linear Driving Force (LDF) 28

b) Homogeneous Solid Diffusion Model (HSDM) 29

c) Pore diffusion 29

d) Pore diffusion with surface diffusion 29

e) Shrinking core model 29

1.8.3.3 Rate equations for Surface Reaction Models (SRM) 30

1.9 Kinetic modeling of biosorption in a batch reactor 32

1.9.1 Surface Reaction Models (SRM) 32

1.9.2 Mass Transfer Models (MTM) 33

1.9.2.1 Crank model for intraparticle diffusion with linear isotherm in infinite bath 33

1.9.2.2 Crank model for intraparticle diffusion with linear isotherm and mass balance 37

1.9.3 Applications of SRM and MTM for biosorption batch kinetics 38

1.10 Kinetic modeling of biosorption in a fixed bed reactor 44

1.10.1 Bohart Adams and Thomas Models 44

1.10.2 Bed Depth Service Time Model 45

1.10.3 Mass Transfer Models 48

1.11 Overview of thesis 57

1.12 References 65

2 Biosorption of cadmium (II) ions by citrus peels in a packed bed column: effect of process parameters and comparison of different breakthrough curve models 72

2.1 Abstract 72

2.2 Introduction 73

2.3 Materials and methods 74

2.3.1 Protonation of citrus peels 74

2.3.2 Column characteristics 75

2.3.3 Continuous flow column system 75

2.4 Theory 76

2.4.1 Analysis of breakthrough curve 76

2.4.2 Mathematical modeling of breakthrough curve 77

2.4.2.1 Thomas Model 78

2.4.2.2 Bohart-Adams Model 78

2.4.2.3 Yoon-Nelson Model 79

2.4.2.4 Dose-Response Model 79

2.5 Results and discussion 80

2.5.1 Effect of flow rate 80

2.5.2 Effect of inlet concentration 80

2.5.2.1 Effect of bed height 81

2.5.2.2 Application of models 82

2.6 Conclusions 85

2.7 Acknowledgments 86

2.8 References 97

3 Multi-resistance kinetic models for biosorption of Cd by raw and immobilized citrus peels in batch and packed bed columns 102

3.1 Abstract 102

3.2 Introduction 107

3.3 Materials and methods 108

3.3.1 Pretreatment of citrus peels 108

3.3.2 Scanning Electron Microscopy (SEM) 109

3.3.3 Immobilization 109

3.3.3.1 Immobilization using Ca-alginate gel 109

3.3.3.2 Immobilization within agar matrix 110

3.3.4 Batch experiment 110

3.3.5 Column characteristics 110

3.3.6 Fixed bed kinetic experiment 111

3.4 Theory: Mathematical modeling 111
3.4.1 Mass balance equation: 112
3.4.2 Rate equation for batch/fixed bed: 113
3.4.2.1 Mass Transfer Modeling (MTM) 113
3.4.2.2 Surface Reaction Modeling (SRM) 114
3.4.3 Isotherm equation 115
3.5 Results and discussion 116
3.5.1 Batch equilibrium 116
3.5.2 Batch kinetics: SRM 117
3.5.3 Fixed bed kinetics: SRM 118
3.5.4 Batch kinetics: MTM 119
3.5.4.1 Single resistance –intra-particle diffusion models 119
3.5.4.2 Single resistance –film diffusion models 123
3.5.4.3 Dual resistance model (intra-particle and film diffusion) 124
3.5.5 Fixed bed kinetics: MTM 126
3.5.6 Effect of operating variables and immobilization 130
3.6 Conclusions 131
3.7 Acknowledgements 132
3.8 References 145
4 Modeling competitive biosorption of cadmium(II) and zinc(II) ions by protonated citrus peels in batch systems 150
4.1 Abstract 150

4.2 Introduction 150
4.3 Modeling equations 152
4.3.1 Single metal isotherms 152
4.3.2 Binary metal isotherms 154
4.3.2.1 Langmuir Predictive Model (LPM) 154
4.3.2.2 Semi predictive models 155
4.3.2.3 Modified Langmuir type models 155
4.3.2.3.1 Competitive Langmuir Model (CLM) 155
4.3.2.3.2 Uncompetitive Langmuir Model (ULM) 156
4.3.2.3.3 Partially Competitive Langmuir Model (PCM) 156
4.3.2.3.4 Langmuir-Freundlich Competitive Model (LFCM) 157
4.4 Materials and methods 157
4.4.1 Protonation of citrus peels 157
4.4.2 Batch experiment 157
4.5 Results and discussion 158
4.5.1 Single metal biosorption 158
4.5.1.1 Comparison of models 158
4.5.1.2 Comparison of metals 159
4.5.2 Binary metal biosorption 160
4.5.2.1 Model fitting 160
4.5.2.2 3D Biosorption surface 162
4.5.2.3 Influence of co-cation on biosorption of primary metal 163

4.6 Conclusions 165

4.7 References 177

5 Effect of competing cations (Pb, Cd, Zn and Ca) in fixed bed column biosorption and desorption from citrus peels 180

5.1 Abstract 180

5.2 Introduction 180

5.3 Materials and methods 182

5.3.1 "Protonation" of citrus peels 182

5.3.2 Column characteristics 182

5.3.3 Continuous flow column system 183

5.4 Analysis of breakthrough and desorption curve 183

5.5 Results and discussion 186

5.5.1 Single metal biosorption 186

5.5.2 Binary metal biosorption 188

5.5.2.1 Effect on individual uptake 188

5.5.2.1.1 Effect of presence of other metals (Pb, Zn) on Cd biosorption 188

5.5.2.1.2 Effect of presence of other metals (Cd, Pb) on Zn biosorption 189

5.5.2.1.3 Effect of presence of other metals (Cd, Zn) on Pb biosorption 190

5.5.2.2 Comparison of the binary system with its mono-component counterparts 190

5.5.2.2.1 Comparison with respect to individual uptake 190

5.5.2.2.2 Comparison with respect to total uptake 191

5.5.2.3 Effect of calcium ions 191

5.5.2.4 Desorption 193

5.5.2.5 Treatment of mining wastewater 194

5.6 Conclusions 195

5.7 Acknowledgement 196

5.8 References 210

6 Overall conclusions and recommendations 213

6.1 Conclusions 213

6.2 Recommendations for future research 215

List of Figures

Page

Figure 1.1 Illustration of (a) metabolism-independent and (b) metabolism-dependent metal uptake in suspension of different biomass types. The figure was modified from [63]. 58
Figure 1.2 Biosorption articles published per year according to ISI web of knowledge.. 59
Figure 1.3 Overview of different approaches and mechanisms considered in fixed bed kinetic modeling 60
Figure 2.1 Schematic diagram of experimental set-up for packed bed column study 87
Figure 2.2 Breakthrough curves for biosorption of cadmium onto protonated citrus peels at different flow rates (bed height = 24 cm, inlet cadmium concentration = 10 mg/L, pH 5.5). 88
Figure 2.3 Breakthrough curves for biosorption of cadmium onto protonated citrus peels at different inlet cadmium concentrations (flow rate = 9 ml/min, bed height = 24 cm, pH 5.5). 89
Figure 2.4 Breakthrough curves for biosorption of cadmium onto protonated citrus peels at different bed heights (flow rate = 15.5 ml/min, inlet cadmium concentration = 10 mg/L, pH 5.5) 90
Figure 2.5 Breakthrough curves for biosorption of cadmium onto protonated citrus peels at different bed heights plotted in terms of number of bed volumes treated (flow rate = 15.5 ml/min, inlet cadmium concentration = 10 mg/L, pH 5.5). 91
Figure 2.6 Effect of EBCT on SUR at inlet cadmium concentration = 10 mg/L.. 92
Figure 3.1 Isotherm of Cd (II) biosorption by PRP, PALP and ALP in a batch reactor at pH 5.5 133
Figure 3.2 Isotherm of Cd (II) biosorption by PRP, PALP and AGP in a batch reactor at pH 5.5 134
Figure 3.3 Kinetics of Cd (II) biosorption by PRP and PALP in a batch reactor and predictions of different surface reaction models 135

Page

Figure 3.4 Breakthrough curves of Cd (II) biosorption by PRP or PALP in a fixed bed reactor under different conditions as detailed in Table 3.3. 136
Figure 3.5 Kinetics of Cd (II) biosorption by PRP and PALP in a batch reactor and predictions of different mass transfer models. 137
Figure 3.6 Weber-Morris plot for Cd (II) biosorption by PALP. 138
Figure 3.7 Breakthrough curve of Cd (II) biosorption by PALP at different bed heights plotted in terms of bed volumes treated (C_0 = 10 mg/L, Q = 2 ml/min) 139
Figure 3.8 SEM pictures of a) raw peels batch 1; b) raw peels batch 2, c) Ca-alginate beads with entrapped peels low magnification, d) Cross-section of Ca-alginate beads at higher magnification. 140
Figure 4.1 Single metal isotherms for Zn and Cd using citrus peels 170
Figure 4.2 3D biosorption surface (interpolated) for Zn in binary system 171
Figure 4.3 Uptake of Zn in bimetal system 172
Figure 4.4 Uptake of Cd in bimetal system 173
Figure 4.5 Total uptake (Cd and Zn) in bimetal system 174
Figure 4.6 Cd and Zn isotherm at 0.2 and 2 mmol/L co-cation concentration 175
Figure 4.7 Reduction of Cd and Zn uptake with increasing co-cation concentration 175
Figure 4.8 Scatter plots of 4 Langmuir type competitive models using F_{rel} 176
Figure 5.1 Schematic diagram of experimental set-up for packed bed column study. 202
Figure 5.2 Breakthrough curves for single metal biosorption of Cd, Zn and Pb onto protonated citrus peels. (inlet concentration 0.1meq/L, bed height 24 cm, flow rate 9 ml/min and pH 5.0) 203
Figure 5.3 Comparison of single and binary metal breakthrough curves to account for the influence of co-ions. (inlet concentration of each ion 0.1meq/L, bed height 24 cm, flow rate 9 ml/min and pH 5.0) a) Cd in presence of Pb and Zn, b) Zn in presence of Pb and Cd, c) Pb in presence of Cd and Zn. 204

Page

Figure 5.4 Experimental breakthrough curves for binary biosorption onto protonated citrus peels in presence of co-ions. (inlet concentration of each ion 0.1meq/L, bed height 24 cm, flow rate 9 ml/min and pH 5.0) a) Pb-Cd, b) Pb-Zn, c) Zn-Cd..... 205
Figure 5.5 Breakthrough curves for heavy metal biosorption onto protonated citrus peels in presence of different inlet concentrations of Ca (mg/L). (bed height 24 cm, flow rate 9 ml/min and pH 5.0) a) Pb inlet concentration of 20 mg/L, b) Cd inlet concentration 5 mg/L..... 206
Figure 5.6 Desorption curve for Cd, Zn and Pb using 0.1(N) nitric acid after mono-metal sorption. 207
Figure 5.7 Desorption curve for binary systems using 0.1 N nitric acid. a) Pb-Cd, b) Pb-Zn, c) Zn-Cd..... 208
Figure 5.8 Treatment of mining effluent (bed height 24 cm, flow rate 9 ml/min) 209

List of Tables

Page

Table 1.1 Fixed bed mass transfer models 61

Table 1.2 Biosorption capacity of Cd, Zn and Pb by different plant-based residues 63

Table 1.3 Comparison of Langmuir isotherm parameters obtained from batch versus column experiments. 64

Table 2.1 Influence of experimental conditions on biosorption of protonated citrus peels for removal of cadmium in a packed bed column 93

Table 2.2 Parameters 'a' and 'b' of general model Eq. (2.14) expressed in terms of parameters of different models 94

Table 2.3. Parameters of generalized model and DR Model and deviation from experimental data 95

Table 2.4 Comparison of equilibrium uptake capacities and Thomas rate constants for removal of Cd by different biosorbents and for removal of other metals by pectin-based biosorbents in packed bed column 96

Table 3.1 Batch Equilibrium: Comparison of isotherm models 141

Table 3.2 Batch Kinetics: Comparison of model parameters (MTM and SRM) 142

Table 3.3 Influence of experimental conditions on biosorption of cadmium by PRP and PALP in a fixed-bed column 143

Table 3.4 Fixed bed kinetics: Comparison of model parameters (MTM and SRM) 144

Table 4.1 Single metal isotherm 166

Table 4.2 Comparison of 2 parameter models with LF model 167

Table 4.3 Physicochemical properties of Cd and Zn [18] 167

Table 4.4 Modeling parameters for binary metal sorption (i = 1 for Zn, 2 for Cd) 168

Table 4.5 Goodness of fit analysis for binary metal sorption models 169

Table 4.6 Comparison of LM and CLM parameters with related studies 169

Table 5.1 Breakthrough curve parameters for removal of Pb, Zn and Cd from single and binary systems using protonated citrus peels. 197

Page

Table 5.2 Comparison of mono-component saturation uptake for Pb, Cd and Zn biosorption in fixed bed columns 198
Table 5.3 Physicochemical properties characterizing the binding strength of metals [29] 199
Table 5.4 Comparison of removal of Pb, Zn and Cd from single and binary metal mixtures using protonated citrus peels 199
Table 5.5 Biosorption performance of protonated citrus peels for removal of Pb or Cd in presence of variable amount of Ca 200
Table 5.6 Desorption curve parameters for breakthrough curves 1- 6 201

Acknowledgements

A mere thank you note would not be enough to acknowledge my mother's sacrifice and courage to let me leave the home just after she lost her husband. I am sincerely grateful for my mother and brother's efforts to manage the home and support me during this period of time.

I am thankful to the United States Department of Agriculture (USDA) for major funding of this research. I also acknowledge additional support from the United States Geological Survey (USGS). Thanks to the University of Alaska Fairbanks for supporting me with a thesis completion fellowship award. I also thank Alarma Corporation for providing the citrus peels.

I would like to express my gratitude to my major adviser, Dr Silke Schiewer, for giving me the opportunity to work on this project, giving me the liberty to investigate whatever I felt exciting and providing me suggestions whenever I stumbled.

I would like to thank my committee members, Dr Ron Johnson, Dr David L. Barnes and Dr Thomas P. Trainor for their time to evaluate my work. Special thanks to Eric Johanson and Ken Irving for helping me to assemble the packed-bed column system, Pete Condon for collecting mining wastewater and Shane Billings for his help with analytical equipment.

Finally, I would like to thank my colleagues in office and laboratory, faculty and staff of the Water and Environmental Research Center (WERC) and the Civil and Environmental Engineering Department (CEE) and other friends in town who kept me warm and cozy at -40° C/F.

1 Biosorption- a literature review

1.1 What is biosorption?

Biosorption, in a broad sense, may be defined as the uptake of pollutants from the aqueous phase by different biomass types. Recalcitrant contaminants such as heavy metals and dyes are the primary target pollutants for this process. Metals cannot be degraded, but can be "removed" from a solution by sequestration to a suitable adsorbing agent. Some pollutants can be accumulated by both living and dead biomass through different mechanisms. The term biosorption, in a stricter sense, denotes the metabolism-independent passive process and is differentiated from a related term bioaccumulation which refers to the metabolically regulated active uptake of elements. The difference between two is illustrated in Figure 1.1.

1.2 Heavy metal contamination

Since the classification of metals into 'heavy' and 'light' is not defined by any authoritative body (such as IUPAC), the term is often used inconsistently in biosorption literature due to variable definitions based on density, group, atomic mass, or atomic number. A rough generalization may be to include all metals of the periodic table except Groups I and II, with particular focus on those metals which are recognized as toxic pollutants by EPA or equivalent national organizations. This includes Cd, Pb, Zn, Cr, Cu, Hg, Ni and the metalloid As. Heavy metals may enter the human body directly (use of contaminated water for drinking, cooking and irrigation) or indirectly (bio-magnification through the food chain) and are eventually accumulated in human tissues. Cadmium was reported to have a half life of 6 to 38 years in the human body according to the Agency for Toxic Substances & Disease Registry (ATSDR) [1]. Metals cannot be 'degraded' biochemically and are therefore harmful for human health if consumed more than required (for trace elements) or permissible, which is usually in the order of ppm or ppb. Sources of heavy metals in the environment can be both natural (in rocks and soils) or of anthropogenic origin. The main anthropogenic sources are industrial activities such as

mining, coal combustion and waste disposal. The waste rock in mining is usually disposed in mine tailings or rock spoils. The typical acidity of mine tailings leachate mobilizes heavy metals from the waste rocks. Notable heavy metals in coal residues are As, Cd, Mo, Se and Zn. Coal combustion is used to generate electric power in coal burning power plants. A study [2] conducted by American Coal Ash Association (ACAA) in 2008 showed that approximately 72 million tons of fly ash was generated as a result of coal combustion.

1.3 Comparison with conventional methods

Conventional methods for removal of heavy metals from aquatic solution include chemical precipitation, membrane filtration and ion-exchange.

1.3.1 Chemical precipitation

The pH of the solution is adjusted to 8-10 by adding alkali, so that metals are converted to their insoluble hydroxide form and subsequently precipitated. Usually lime or caustic soda is used for the purpose. The process is not selective, and different metals will be precipitated at different pH, for example, Fe (III) will be precipitated at lower pH followed by Cd, Zn or Pb. A large amount of toxic sludge is generated from the process; an effluent containing 100 mg/L of Cd (II) will produce 900 mg/L of sludge [3] and metals cannot be economically recovered from the process. The final effluent may not meet the regulatory criteria.

1.3.2 Membrane filtration

This is a separation technique based on size exclusion or permeability based on ionic nature. Depending on the membrane pore size and the chemical nature of the membrane material, a membrane is selectively permeable to substances present in a water sample ranging from suspended particles visible to the naked eye (10^7Å) to dissolved salts (1Å). Flow of feed solution may be perpendicular to (dead end filtration) or parallel with (cross flow filtration) the membrane. The process requires a driving force for the transfer of solute from the bulk phase through the membrane. For the purpose of metal removal,

reverse osmosis (RO) and electro dialysis (ED) are used. In RO, a pressure gradient is generated by maintaining a pressure at the solution side of the membrane greater than the osmotic pressure caused by the dissolved metal ions. Due to this pressure gradient, pure water is able to pass through the membrane retaining the metal ions on the solution side of the membrane. On the other hand, ED requires lower pressure than RO, but it applies an electric current. Similar to the electrolysis process, an electric field is generated by passing an electric current through the reactor which is separated into smaller chambers by cation and anion permeable membranes. Accordingly, when feed solution flows through the reactor, cations and anions of the water sample remain in the respective chambers whereas purified water is obtained at the outlet. Unlike RO, the energy expense is proportional to the concentration of ions in the solution. The membrane filtration process produces high quality effluent, but is expensive.

1.3.3 Ion exchange

This unit operation is similar to biosorption from the point of view of mechanism and contacting methods and hence the primary competitor to biosorption. A cation exchange resin is a synthetic polymer having an ionizable functional group such as carboxylic, phenolic or sulphonic group where the cation (H^+ or Na^+) is replaced by the target metal cation(s) in water during the adsorption stage of the sorption-regeneration cycle. A saturated exchanger is then regenerated by using an acid (source of H^+) or brine (source of Na^+). Most of these resins are very costly and not selective towards target metals and become ineffective in the presence of large amounts of competing mono and divalent cations such as Na^+ or Ca^{++}. Presence of small amounts of cationic surface active agents may inhibit the normal function of a resin [4] and it may be permanently poisoned by irreversible deposition of non-target metals.

1.3.4 Comparison of conventional techniques and biosorption

Conventional techniques work best for low to moderate volumes of effluent having high to moderate concentrations of metals. These processes become ineffective for the

treatment of high volumes of dilute stream as the cost becomes too high. Biosorption, on the other hand is a 'cost effective' process [5]. A large number of biomass types may have the potential to adsorb a target pollutant. To ensure cheap and abundant availability of raw material, only those biomass types which occur naturally (such as seaweed) or as an industrial waste product (such as citrus peels, fermentation waste), are preferred. Metals can be recovered by eluting the spent biomass with a suitable desorbing agent, similarly as commonly done for synthetic ion exchange resins. The three main mechanisms of metal removal by biosorption are adsorption, ion-exchange and micro-precipitation. The driving force for both adsorption and ion-exchange is the affinity of metals for binding sites in the biomass, while micro-precipitation occurs due to the limited solubility of the metal ion in the aqueous phase without any metal-biomass interaction. Adsorption (equation (1.1)) refers to the attachment of ions onto the binding site by Van der Waals type interaction, covalent bonds or complex formation. The equilibrium constant of the reaction is symbolized as b which is the ratio of forward (k_{ad}) and backward rate (k_{de}) constant. Ion-exchange (equation (1.2)) involves electrostatic interaction where binding of an ion is always accompanied by the release of the equivalent amount of ions from the binding site. The affinity of the metal for the biomass depends on the physicochemical factors such as size of the metal ion, electronegativity, hydration enthalpy etc., which in turn control the strength of the bond between metal and biomass. The efficiency of a biosorption process depends on factors such as pH, temperature, ionic strength and presence of co-ions. There are other factors which are related to the type of reactor used.

Adsorption: $M + S \leftrightarrow M\text{-}S$ (1.1)

Ion exchange: $M^{2+} + S\text{-}H \leftrightarrow M\text{-}S^{+} + H^{+}$ (1.2)

Here S denotes the biosorbent binding site and M denotes the metal ion as the sorbate species.

1.4 Citrus peels as biosorbent

A large number of research articles are available describing the biosorption of different regulated metals by different biomass types. There are some review articles summarizing the results of these studies. In general, fewer articles focused on agricultural residues compared to microbial biomass. Even fewer of them studied citrus biosorbents. Citrus peels contain pectin which is a polymer of galacturonic acid. Past research proved that alginate plays the instrumental role in algal biosorbents. Due to the structural similarity between galacturonic acid and alginic acid, it was hypothesized that pectin rich materials may behave similarly which was tested in Patil's study [5]. A number of pectin rich biosorbent materials were examined and it was found that grape skins had the highest Cd binding capacity followed by orange peels, apple core and lemon peels. The orange peels, however, were found to be more stable than grape skins and apple residue at pH 5.0. A potentiometric study confirmed the presence of four acidic sites with pK_a values of 3.8, 6.4, 8.4 and 10.7, and a total site quantity of 1.14 meq/g in the citrus peels. The uptake capacity was found to increase with increasing pH in the acidic range, which is typical for other biosorption studies too. A pH sensitive isotherm was constructed to include the effect of pH. A preliminary study indicated that biosorption kinetics was limited by mass transfer but that was not backed up by any model. Later Balaria [6] studied the Pb-citrus peels interaction mechanism and found similar FTIR spectra for both citrus peels and citrus pectin, proving the role of pectin in citrus biosorbents. Carboxylic acid groups were identified to be the main binding site for Pb. Potentiometric titration at pH 5.0 and a background electrolyte concentration of 0.01 M $NaNO_3$ showed that the total surface charge of native peels was -0.014 meq/g which was increased to -0.23 meq/g after protonation. Within the experimental range, the maximum uptake by Pb was 0.97 meq/g. Throughout this thesis, the term 'citrus peels' indicated the waste peels obtained from the fruit processing industries after extracting the juice from fruits using a proprietary method.

1.5 Hypotheses and objectives

- In order to use an adsorbent in a packed bed column, it needs to be mechanically rigid and stable enough. Unlike most microbial biomass types, agricultural residues better satisfy these criteria.

  Hypothesis 1: Citrus peels, without any further processing, are suitable for use in a packed bed column.

  Objective 1: To test this hypothesis, a packed bed column was assembled and used with raw citrus peels.

- For successful fixed bed operation, adsorption needs to be completed within the residence time of the solution within the column, which depends on the flow rate and bed height of the column. Equilibrium is established at the influent metal concentration.

  Hypothesis 2: A breakthrough curve for biosorption of metals onto citrus peels depends on influent concentration, flow rate and bed height.

  Objective 2: To test this hypothesis, a number of fixed bed experiments were conducted under varying influent concentrations, flow rates and bed heights.

  Hypothesis 3: A mathematical model, similar to those used in other biosorption studies, can explain the influence of above mentioned operating variables.

  Objective 3: To test this hypothesis a number of different models were applied to the batch and fixed bed experimental data.

- Microbial biomass types are often immobilized within a suitable polymeric matrix to improve stability and lower hydraulic resistance.

  Hypothesis 4: Immobilization using commonly used polymeric materials can be customized to immobilize citrus peels such that they can be successfully applied in a column.

  Objective 4: To test hypothesis 4, citrus peels were immobilized using commonly available polymeric materials and fixed bed experiments were conducted using both native and immobilized citrus biosorbent.

- A real effluent may contain more than one regulated metal and other light metals which affect the biosorption of target metal.

  Hypothesis 5: The competitive influence of co-ions on target metal biosorption by citrus peels can be described by models similar to those in other biosorption studies.

  Objective 5: To test this hypothesis, both batch and fixed bed experiments were conducted with one or more combinations of the priority pollutants Cd, Pb and Zn as well as the most commonly occurring divalent light metal, Ca.

Notation

A	cm^2	Area of cross-section of fixed bed column
b	L/mg	Equilibrium constant for Langmuir surface reaction (equation 1.1) (= k_{ad}/k_{de})
C	mg/L	Concentration of adsorbate in aqueous phase at time t
C′	mg/L	Reference value of C to define X, typically maximum C value in an isotherm or over the course of an experiment (C_0 or C_∞)
C^*	mg/L	Equilibrium adsorbate concentration corresponding to q
C_0	mg/L	Initial or influent concentration of adsorbate in the batch or fixed bed reactor
C_∞	mg/L	C at t_∞ for batch experiment
C_i	mg/L	Aqueous concentration of adsorbate at the adsorbate-adsorbent interface
DoSU	%	Degree of sorbent used
D_L	cm^2/min	Axial dispersion coefficient
D_s	cm^2/min	Diffusion coefficient of adsorbate within the adsorbent
F	-	Fractional Approach to Equilibrium (FATE) (= q/q_∞)
h	cm	Bed height
K	L/g	Equilibrium constant for linear isotherm
k_1	1/min	PFO Rate constant
k_2	$\frac{g}{mg.min}$	PSO Rate constant
k_{ad}	$\frac{L}{mg.min}$	Mixed second order forward rate constant for Langmuir surface reaction (equation 1.1)
k_{BA}	$\frac{ml}{mg.min}$	Rate constant for Bohart-Adams model
k_{de}	1/min	First order reverse rate constant for Langmuir surface reaction (equation 1.1)

k_f	cm/min	External or film mass transfer coefficient
K_f	cm/min	Overall fluid phase mass transfer coefficient
K_F	$L^{1/\mu}/(g\ mmol^{1/\mu-1})$	Freundlich isotherm parameter
k_s	cm/min	Intra-particle mass transfer coefficient
K_s	cm/min	Overall solid phase mass transfer coefficient
M	g	Mass of adsorbent in the reactor (batch/fixed bed)
MTZ	cm	Mass Transfer Zone
N_0	mg/ml	Bohart-Adams sorption capacity
P_e	-	Peclet number (= u L/D_L), a measure of the relative importance of advection to diffusion
Q	ml/min	Flow rate
q	mg/g	Uptake i.e., average concentration of adsorbate within the adsorbent at time t
q′	mg/g	Reference value of q to define Y. Equilibrium uptake corresponding to C′
q*	mg/g	Equilibrium uptake corresponding to C
q_∞	mg/g	Uptake at t_∞
q_b	mg/g	Uptake at breakthrough time
q_i	mg/g	Uptake at the adsorbate-adsorbent interface
q_m	mg/g	Maximum uptake capacity according to Langmuir isotherm
q_r	mg/g	Uptake at a radius r from adsorbent center
q_s	mg/g	Uptake at t_s
R	cm	Radius of adsorbent particle
S′	cm^{-1}	Adsorbent particle surface area per solution volume (= $S_0M/(V_s \rho)$)
S_0	cm^{-1}	Adsorbent particle surface area per unit particle volume (= 3/R)
Sc	-	Schmidt number (= v/D)
SUR	g/L	Sorbent usage rate

t_∞	h	Duration of batch experiment or saturation time in fixed bed experiment
t_s	min	Saturation time in fixed bed experiment
u	cm/min	Superficial velocity within column
V	ml	Volume of reactor (batch or fixed bed)
v	cm/h	Interstitial velocity within column
V_s	ml	Volume of aqueous phase (= V ε)
X	-	Dimensionless concentration (= C/C'), $0 \leq X \leq 1$ (sorbent is initially free of sorbate)
Y_s	%	Removal at saturation
Y	-	Dimensionless equilibrium uptake corresponding to X, (= q^*/q'), $0 \leq Y \leq 1$ (sorbent is initially free of sorbate)
Z	cm	Axial distance coordinate, positive in the flow direction
β	-	Separation factor in equation (1.5)
β_L	-	Separation factor for Langmuir isotherm
ε	-	Void fraction in column
ε_p	-	Sorbent internal porosity
μ	-	Freundlich isotherm exponent
ρ	g/mL	Density of adsorbent particle (= M/(V(1-ε))

1.6 Modeling biosorption equilibrium

1.6.1 Introduction

Modeling biosorption processes is an important part of biosorption studies as it serves the following purposes:

1. A predictive model is commercially valuable as it can predict the biosorption performance in a given situation, requiring fewer actual experiments to be performed.

2. Regardless of its empirical or mechanistic nature, model parameters provide a tool to compare the performance of different biosorbents used for different target metals under different experimental conditions.

3. A mechanistic model can anchor the experimental data to a theoretical background and helps to explain observations.

On January 11, 2012, a search in ISI Web of Knowledge with the keyword "biosorption" and selecting time span as "all years" revealed a total of 7680 published journal articles, 127 of which were review articles. Refining the search with keyword "dye" and "metals" showed 817 and 5265 articles respectively. The top five countries contributing to this research include India (907), China (801), Turkey (616), USA (340), and Canada (228). There was a rapid increase in biosorption based research in the last 20 years, which is reflected in the dramatic increase in the number of published articles and citations within the last 20 years as shown in Figure 1.2. This trend confirms the need, efficacy and relevance of biosorption research in the contemporary world. At the same time, it is often criticized [7] that even this amount of research was not able to develop this promising alternative of the waste treatment into a commercially successful process. Since there is a large pool of biomass types and a similarly large pool of contaminants that could potentially be removed by these biosorbents, biosorption research often follows a

common template only with a different combination of sorbate and sorbent. It may be important to mention that a keyword as simple as 'modeling' may reduce the total number of published articles from 7680 to 3641. Pagnanelli [8] found that even though there is a huge increase in the number of publications per year, only half of all biosorption articles published during 1995-2009 include a model. A further analysis showed that most of these models are empirical ones to describe equilibrium and kinetic data in batch reactors whereas very few models consider modeling breakthrough curves in packed bed columns. To contribute towards an eventual commercialization of biosorption, the current research focuses on packed bed columns, as they are applied in industrial ion exchange processes for heavy metal removal. Furthermore, since only few articles describe modeling of biosorption breakthrough curves, the present research aims to provide a mechanistically based model for this process. A state of the art description is given here for the modeling of biosorption equilibrium and kinetics in batch and fixed bed reactor.

1.6.2 Batch equilibrium data

In standard biosorption research, a series of batch experiments are conducted by incubating a mixture of aqueous solution containing the target metals and biosorbent for long enough to attain equilibrium with varying biosorbent doses and /or initial metal concentrations. The equilibrium aqueous metal concentration is measured using Atomic Absorption Spectrophotometer AAS and the corresponding equilibrium solid phase concentration is calculated from the integrated form of the mass balance equation for a batch reactor (equation (1.4)) so that a data set comprising of aqueous and solid phase equilibrium concentration ($C\infty$, $q\infty$) can be obtained.

The differential mass balance equation for a batch reactor is

$$V\frac{dC}{dt} + M\frac{dq}{dt} = 0 \tag{1.3}$$

The mass balance equation for a batch reactor (integrated form) is

$$V(C_0 - C) = q\,M \tag{1.4}$$

1.6.3 Equilibrium isotherm

A generic isotherm expression is $q^* = f(C)$ where the function f describes the equilibrium data (C, q^*) generated from batch (C_∞, q_∞) or fixed bed (C_0, q_∞) experiment. An equilibrium isotherm is a function of temperature, ionic strength and pH of the solution. Therefore, either these parameters need to remain constant throughout the experiment, or the isotherm model used needs to include the effect of these parameters. An equilibrium isotherm is classified as concave ($\beta>1$), linear ($\beta = 1$) or convex ($\beta<1$) where the separation factor (β) is defined in equation (1.5) for a sorbent which is initially free of sorbate. The separation factor is analogous to the relative volatility factor, which is the relative volatility (concentration ratio of liquid and vapor at equilibrium) of the more volatile component to the less volatile component. Relative volatility is used in the design of distillation columns to quantify the 'ease of separation' of one component from another. Similarly, the separation factor is the concentration ratio of adsorbate in solid and fluid phase and describes the shape of an isotherm, which in turn determines the feasibility of the adsorption process following that isotherm. Generally, a convex form is considered favorable since relatively high binding is already achieved at low metal concentrations.

$$\beta = \left(\frac{C}{q^*}\right)\left(\frac{q'-q^*}{C'-C}\right) = \left(\frac{X}{Y}\right)\left(\frac{1-Y}{1-X}\right) \tag{1.5}$$

1.6.4 Simple isotherm models

These models are simple mathematical expressions with few adjustable parameters which need to be optimized in order to fit a set of experimental data. The two most frequently used models are the Langmuir (equation (1.6)) and Freundlich models (equation (1.7)).

$$q^* = \frac{q_m b C}{1+bC} \qquad \text{where } b = \frac{k_{ad}}{k_{de}} \tag{1.6}$$

$$q^* = K_F C^{1/\mu} \tag{1.7}$$

While the Freundlich model is purely empirical, the Langmuir model was originally developed for gas adsorption on activated carbon on the basis of assumptions which are typically not valid for biomass-metal interaction:

- The forces exerted by binding sites do not extend further than the diameter of one sorbed molecule and therefore sorption is restricted to a monolayer.
- There is a fixed number of adsorption sites.
- All sorption sites are uniform (i.e., constant heat of adsorption).
- Only one sorbate is present.
- One sorbate species reacts with one active site.
- There is no interaction between the sorbed species.

The Freundlich isotherm (equation (1.7)), unlike the Langmuir isotherm, considers heterogeneity of the adsorbent surface. It assumes that there are always adsorption sites available which require higher activation energy for adsorption to take place and therefore never become saturated. The index μ is a measure of heterogeneity of the surface, an increasing value of μ denotes increasing heterogeneity. In reality, any biomass contains more than one type of binding sites and thus cannot be uniform, and the number or availibility of binding sites usually depends on the pH of the system. The experimental procedure to obtain equilibrium data cannot distinguish among various species of the same metal ion (e.g., metal-ligand complexes), so different metallic species may be adsorbed and there may be electrostatic interaction between them. A Langmuir isotherm, however, may be modified to incorporate the effect of pH /variable binding sites, effect of presence of co-cations and simultaneous binding of more than one sorbate species to a free or occupied site. A mass law type equilibrium expression for equation (1.1), combined with mass balance for the total number of binding sites leads to the derivation of the Langmuir isotherm expression, i.e., equation (1.6). In spite of those shortcomings,

the Langmuir isotherm is the most popularly used isotherm model since it provides a quick way to compare among different biosorbents as shown in Table 1.2.

It may be seen from the general expression of the separation factor (equation (1.5)) that it is concentration-dependent and varies from point to point along an isotherm. However, applying the Langmuir isotherm (equation (1.6)) for q and q^* in the definition of the separation factor β (equation (1.5)), it was found that the separation factor for the Langmuir isotherm β_L (equation (1.9)) only depends on the reference value of C or q used to define X or Y and hence remains constant throughout the isotherm. So it is often referred [9] to as a constant separation factor approximation in the study of fixed bed dynamics. In this context, the reference aqueous concentration C′ for packed bed is chosen as C_0, so that the corresponding q′ becomes q_∞ denoting the change in aqueous and solid phase concentration over the mass transfer zone. The Langmuir equation can also be written in a dimensionless form (equation (1.8)), which is the same as equation (1.5) but with the Langmuir separation factor.

$$Y = \frac{X}{\beta_L + (1-\beta_L)X} \tag{1.8}$$

$$\beta_L = \frac{1}{1+bC'} = 1 - \frac{q'}{q_m} \tag{1.9}$$

For the most favorable condition, β = 0, a special type of isotherm is obtained, which is called the 'irreversible' or 'rectangular' isotherm (equation (1.10))

$$q^* = q_m \tag{1.10}$$

where the curve rises from the origin immediately (at X = 0) to the maximum capacity in the shape of a rectangle. The solid phase metal concentration does not depend on the fluid phase concentration and remains always equal to saturated concentration. Though this behavior is idealized, equilibrium data published in the literature can often be approximated by a rectangular isotherm [10], especially at higher aqueous phase metal concentrations.

Another limiting form of the Langmuir isotherm can be obtained at $\beta = 1$, when the isotherm becomes a linear one (equation (1.11)):

$$q^* = K\,C \qquad (1.11)$$

This approximation can be valid for relatively low aqueous phase metal concentrations. Both of these limiting forms are important for fixed bed modeling since most of the analytical solutions are available for these types of isotherms only. (Table 1.1)

In general, non linear regression is required to obtain parameters for non linear models such as Langmuir and Freundlich isotherm expressions. Alternatively, a non linear equation can be linearized and parameters may be obtained by linear regression. However, this is not a preferred approach since linearization causes violation of some regression assumptions and the most accurate estimation of parameters may not be possible. Regression of Y on X assumes that measurement of X is accurate and all uncertainty is present in Y; the scatter of Y is normal and the standard deviation of the scatter is same for all X. Both of these assumptions are likely to be violated after transforming any non-linear expression into a linear one. This also applies to the Langmuir and Freundlich equations. Still, a huge number of biosorption articles use linear regression since this technique only requires minimum understanding of the data fitting process.

1.7 Fixed bed fundamentals

1.7.1 Basic terminology

A fixed-bed reactor is a vertical column tightly packed with the adsorbent and hence also called packed-bed column reactor. Metal bearing influent solution is passed through the column in an up-flow or down-flow manner. A downflow system may reduce the power consumption but the adsorbent bed tends to be compressed, especially if it is a non-granular material. This may lead to clogging of the column, channelization of flow and other related problems. A downflow system, however, may be recommended for immobilized peels where the bed has a higher porosity. For the purpose of fair

comparison, the present study was done in an upflow manner for both native and immobilized peels.

Initially, the influent saturates the first portion of the sorbent (a very small fraction of total bed height) keeping the remaining bed fresh. The influent solution becomes metal-free by transferring the metal into the solid phase and leaves the column as purified effluent. At later times, the influent metal solution first encounters a saturated zone; and the further it proceeds towards the exit of the column, the fresher sorbent it contacts. This leads to a progressive purification and polishing of the aqueous phase with consequent loading in the solid phase without lowering the driving force (difference in metal concentration between the aqueous phase and solid phase). Initially, effluent coming out from the column is either metal free or may contain very low amounts of metal in the order of ppb. After certain time, the metal concentration in the effluent begins to increase and gradually reaches a predetermined value (usually the discharge limit or other allowable limit) when the column needs to be shut down diverting influent flow into another stand-by fresh column. The first column is then processed for reuse and kept as the new stand-by.

The performance of a packed bed column can be evaluated from breakthrough curves which are plotted as the ratio of effluent concentration (C, mg/L) to influent concentration (C_0) versus process time (t, h). Breakthrough is theoretically defined as the very first appearance of contaminant in the effluent, but for practical purposes, the column can be operated up to a certain concentration (C_b) of the pollutant in the effluent, which is called the breakthrough concentration. This may be defined as a percentage (may be 1-5%) of the feed concentration or may be determined on the basis of local regulations regarding the maximum contaminant level of the pollutant concerned. The time to reach this concentration is called service time, which is the duration for which the column would typically be operated in practice. The service time is theoretically different from the true breakthrough time (t_b) corresponding to the first appearance of the contaminant in the effluent, but this distinction is not made in practice. If the column is continued to operate beyond breakthrough, the concentration of the contaminant in the

effluent rises sharply and eventually becomes equal to inlet concentration, and the corresponding time is called saturation time (t_s). In practice it actually forms a plateau at around 95-98% of the inlet solution, after which no change in concentration is observed. This signifies an equilibrium condition between fluid (C_0) and solid phase (q_∞) concentration of the pollutant, similar to what the end of a batch experiment as explained in the section 1.6.2. An isotherm, in principle, should be independent of the reactor type; it should be the same whether the data is generated from batch (C_∞, q_∞) or from fixed-bed (C_0, q_∞) reactors but there is experimental evidence suggesting different behavior. In a study of Cd biosorption by mineralized peat [11], the metal uptake in the fixed bed reactor was found to be 50% higher than in the batch reactor for a given equilibrium aqueous concentration. For Cu biosorption by *Sargassum* alga [12], isotherms were constructed from both batch and fixed bed data. Both isotherms were found to follow the Langmuir model, but the maximum monolayer capacity (q_m) for the dynamic isotherm (3.57 meq/g) was found to be 64.3% higher than for the batch isotherm (2.17 meq/g). In contrast, when NaX Zeolite was used for Cr removal [13], the uptake capacity found in batch experiments was higher than in fixed bed experiments. Equilibrium data from batch experiments was found to follow an irreversible isotherm with $q_m = 3.61$ meq/g whereas for fixed bed experiments, it was found to match with Freundlich isotherm. For an inlet concentration of 3 meq/L, the uptake was 3.27 meq/L. The pH of the solution was not kept constant during the batch experiment. In another study regarding the removal of Cu by a marine plant [10], batch isotherm experiments were conducted at fixed pH 5 and 6 leading to two different sets of Langmuir model parameters. Model parameters corresponding to pH 6 (Table 1.3) did not match with those obtained from fixed bed experiments, where the influent pH was between 5.8 and 6 but effluent pH was found to rise up to 6.9 during the experiment. For an aqueous phase equilibrium concentration below 10 mg/L, uptake in fixed beds was found to be higher than that in batch. It was argued that ions released from the biosorbents are released from the system for fixed bed process but are retained within the reactor in a batch system, leading to two different isotherms. It was concluded that for fixed bed modeling purposes, a dynamic isotherm

obtained from fixed bed experiments is more reliable than one constructed from batch experimental data. Each of these four articles referred to other articles supporting their findings.

Other than breakthrough and saturation time, breakthrough curves are often compared in terms of equilibrium (maximum) uptake capacity (q_e) at saturation, removal at saturation (Y_s), degree of sorbent used (DoSU), mass transfer zone length (MTZ) and sorbent usage rate (SUR). These parameters are defined and calculated as follows: The amount of metal loaded in the column ($m_{in,t}$, mg) up to time t is the inlet concentration (C_0, mg/L) multiplied by flow rate (Q, L/h) and time (t, h).

$$m_{in,t} = C_0 \times Q \times t \tag{1.12}$$

The amount of unadsorbed metal ($m_{out,t}$, mg) at time t can be obtained from the area under the dimensionless breakthrough curve up to time t multiplied by inlet concentration (C_0, mg/L), and flow rate (Q, ml/min):

$$m_{out,t} = C_0 \times Q \times \int_0^t \left(\frac{C}{C_0} \right) dt \tag{1.13}$$

The amount of metal adsorbed in the column at time t ($m_{ad,t}$, mg) can be determined as:.

$$m_{ad,t} = m_{in,t} - m_{out,t} \tag{1.14}$$

The equilibrium (maximum) uptake capacity (q_∞, mg/g) then can be calculated as the total mass of metal adsorbed at saturation ($m_{ad,ts}$, mg) to the mass of adsorbent in column (M, g)

$$q_\infty = \frac{m_{ad,t_s}}{M} = \frac{C_0 \times Q \times \int_0^{t_s} \left(1 - \frac{C}{C_0} \right) dt}{M} \tag{1.15}$$

Similarly, uptake at breakthrough can be calculated as:

$$q_b = \frac{m_{ad,t_b}}{M} = \frac{C_0 \times Q \times \int_0^{t_b} \left(1 - \frac{C}{C_0} \right) dt}{M} \tag{1.16}$$

Removal at saturation (Y_s) is expressed as the fraction of the total metal loaded in the column ($m_{in,ts}$) that is actually adsorbed in the column at saturation ($m_{ad,ts}$).

$$Y_s = \frac{m_{ad,t_s}}{m_{in,t_s}} = \frac{m_{ad,t_s}}{C_0 \times Q \times t_s} \tag{1.17}$$

Degree of sorbent used (DoSU) is obtained as the ratio of uptake at breakthrough (q_b) to the capacity at equilibrium (q_e).

$$DoSU = \frac{q_b}{q_\infty} = \frac{m_{ad,t_b}}{m_{ad,t_s}} \tag{1.18}$$

Another way to interpret Y and DoSU is as follows: The fraction of $m_{in,ts}$ which is actually adsorbed within the column ($m_{ad,ts}$) is Y, and the fraction of $m_{ad,ts}$ which is adsorbed before breakthrough is DoSU. From that one can calculate the fraction of incoming metal adsorbed at breakthrough as $Y_b = Y_s \cdot DoSU \cdot t_s/t_b$.

SUR signifies the mass of sorbent required for obtaining a unit volume of clean effluent (before breakthrough).

$$SUR = \frac{M}{V_b} = \frac{M}{Q \times t_b} \tag{1.19}$$

where V_b is the breakthrough volume.

MTZ is defined as the mass transfer zone of the column where sorbate is actively adsorbed from fluid phase to solid phase, and where the sorbent is only partially saturated. The fluid and sorbent at any point located downstream of the MTZ is "clean" since the target pollutant has already been sorbed while flowing through the MTZ, and sorbent located upstream of the MTZ is fully saturated. The MTZ moves through the column in the direction of flow and breakthrough is explained as the time when the MTZ reaches the end of the column. At this point, the MTZ contains the sorbent which is only partially saturated, and therefore remains unused. The section of the breakthrough curve between breakthrough time and saturation time actually depicts the process of saturation of this unused sorbent within the MTZ. The shape of the MTZ is an indicator for the rate of the biosorption process (mass transfer and sorption reaction); for an 'ideally' efficient

column with rapid sorption, the length of the MTZ is minimal. In that case, the breakthrough curve follows a step function where breakthrough time is equal to the saturation time, which means 100% utilization of the maximum capacity of the column, i.e., DoSU = 1. The conditions which favor this ideal situation can be derived mathematically (equilibrium non-dispersive model).

For an isothermal packed bed column, where the influent contains a single absorbable solute at low enough concentrations to maintain a constant superficial velocity, the differential mass balance equation for fluid phase is:

$$\frac{\partial c}{\partial t} = -\mathrm{v}\frac{\partial c}{\partial z} + D_L \frac{\partial^2 c}{\partial^2 z} - \rho \frac{(1-\varepsilon)}{\varepsilon}\frac{\partial q}{\partial t} \tag{1.20}$$

The three terms of the right hand side of this equation are respectively flux due to convection, flux due to dispersion, and consumption due to a reaction. For a given set of rate equation and equilibrium isotherm (which determine the 3rd term), two different breakthrough curves are obtained depending on whether the dispersion coefficient is assumed as zero (plug flow) or not.

1.7.2 Ideal situation: Equilibrium non-dispersive model

This assumes that sorbate transfer from the bulk phase to the sorption site and the biosorption reaction are rapid in comparison to the residence time of the fluid in the reactor. That means it can be assumed that a local equilibrium exists at each point of the column. In that case q is a function of C only according to the governing isotherm equation and does not depend on any other variables (z or t) so that it can be written as equation (1.21) where f' denotes the derivative of any isotherm expression f as defined in section 1.6.3.

$$\frac{\partial q}{\partial t} = \frac{dq}{dc}\frac{\partial C}{\partial t} = \frac{\partial C}{\partial t} f'(C) \tag{1.21}$$

Considering axial dispersion as insignificant, the mass balance equation (1.20) can be combined with equation (1.21) as

$$\frac{\partial C}{\partial t} = -\mathrm{v}\frac{\partial C}{\partial z} - \rho\frac{(1-\varepsilon)}{\varepsilon}\frac{\partial C}{\partial t}f'(C) \tag{1.22}$$

Mathematically, the rate at which the mass transfer zone travels through the column is:

$$\left(\frac{dZ}{dt}\right)_C = -\frac{(\partial C/\partial t)_z}{(\partial C/\partial Z)_t} \tag{1.23}$$

This equation may be written as

$$\left(\frac{dZ}{dt}\right)_C = \frac{\varepsilon\ \mathrm{v}}{\varepsilon + (1-\varepsilon)f'(C)} \tag{1.24}$$

This equation (1.24) can be integrated with the condition that z = 0 at t = 0 for any possible C value ($0<C<C_0$), yielding:

$$Z = \frac{\varepsilon\ \mathrm{v}\ t}{\varepsilon + (1-\varepsilon)f'(C)} \text{ at constant C} \tag{1.25}$$

This is the Z value corresponding to a chosen C value at any time t, or in other words, Z is the distance how far MTZ has traveled through the reactor so that Z/t is the velocity of the MTZ, which depends on the C value according to the derivative of the equilibrium relationship $f'(C)$ which increases or decreases or remains constant for concave convex and linear isotherms respectively. A plot of C/C_0 vs. Z at different times will prove that different parts of the MTZ moves with different speeds; a convex isotherm (such as the Langmuir isotherm) causes the downstream points of MTZ to move slower than the upstream points leading to a gradual shrinking of the MTZ, which in turn makes the breakthrough curve as sharp as possible, while reverse occurs in case of concave isotherm. That is why a convex isotherm is also called a favorable isotherm while the concave isotherm is called an unfavorable isotherm. A step function breakthrough curve is only possible when a) equilibrium exists at each point of the MTZ, b) adsorption isotherm is linear or convex and c) velocity profile within reactor follows plug flow.

1.7.3 Causes and effect of non-ideality

In a real system, on the other hand, broadening of the MTZ can be caused by factors such as dispersion and non-equilibrium. Non equilibrium condition occurs due to mass transfer

resistance. However, a favorable (convex) isotherm tends to sharpen the breakthrough curve by shrinking the MTZ. For a long column, these broadening and sharpening effects becomes balanced with each other and a stable MTZ develops whose length no longer changes with distance. The typical S shaped breakthrough curve reflects this MTZ, the length of which can be calculated by equation (1.26).

$$MTZ = h\,(1-\frac{t_b}{t_s}) \tag{1.26}$$

In this situation, which is often termed constant pattern condition, another relationship holds (equation (1.27)), i.e., the dimensionless uptake is equal to the dimensionless concentration, which reduces the mathematical complexity of the modeling since analytical solutions are often possible for this case. The distance required to establish a stable MTZ under dispersive non-equilibrium conditions is discussed elsewhere [9].

$$X = Y \tag{1.27}$$

Another significance of the MTZ is that it defines the critical smallest bed length required to achieve a non-zero breakthrough time; a bed length shorter than the MTZ will produce 'dirty' effluent from the beginning.

Another related term is the stoichiometric time. This signifies the breakthrough or saturation time of the hypothetical "ideal" (vertical) breakthrough curve having the same equilibrium (saturation) capacity as the given breakthrough curve. This is given as equation (1.28)

$$t^* = \int_0^{t_s}(1-\frac{C}{C_0})dt \tag{1.28}$$

For a symmetrical S shaped breakthrough curve, this is equal to the time when the effluent concentration reaches 50% of the inlet concentration.

Since the column cannot be used after breakthrough occurs, only the capacity q_b is used even though the total capacity of bed is q_s. So the fraction of capacity that was utilized is q_b/q_s (which is also equal to t_b/t^*) and the fraction that remains unutilized is $(1-q_b/q_s)$. This fraction of unused capacity of the column is converted into an equivalent length of

the bed which is called Length of Unused Bed (LUB) so that the total length (L) times this unused fraction of capacity becomes the LUB. The LUB does not depend on the total length of the bed, so for scale up purposes one can compute the bed length as the sum of LUB plus the length calculated on the basis of an ideal (vertical) breakthrough curve. This is the simplest and quickest design method, but it works only if the constant pattern assumption is valid. The LUB can be calculated from equation (1.29).

$$LUB = h\left(1 - \frac{q_b}{q_s}\right) = h\left(1 - \frac{t_b}{t^*}\right) \tag{1.29}$$

1.7.4 Simplest non-ideal system: Equilibrium dispersive model

The simplest model to account for non-ideality assumes that the system is in equilibrium and the spreading of the breakthrough curve is only due to the dispersion, even though in reality mass transfer and/or reaction may have an impact on the breakthrough curve. Since equilibrium is assumed at every point of the system, rate equations are not involved here, making the model simpler. Accordingly equations (1.20) and (1.21) are combined to equation (1.30)

$$\frac{\partial c}{\partial t} = -v\frac{\partial c}{\partial z} + D_L\frac{\partial^2 c}{\partial^2 z} - \rho\frac{(1-\varepsilon)}{\varepsilon}\frac{\partial c}{\partial t}f'(c) \tag{1.30}$$

This equation along with the equilibrium isotherm equation needs to be solved simultaneously. For a linear isotherm, $f'(c) = K$ (i.e., constant), this equation can be solved analytically. For non-linear isotherms, a numerical solution is required. Modeling that represents more realistic situations such as mass transfer limitation or surface reaction limitation, will be discussed after presenting those rate equations.

1.8 Rate equations

1.8.1 Anatomy of the biosorption process

A biosorption process may be viewed to consist of the following steps:

1) Movement of adsorbate through the bulk of the solution. This is typically a fast process relative to others, so that the system can be considered as well mixed. For a column, 'well mixed' refers to lateral mixing in the radial direction only. However, if it is not plug flow, some undesired mixing occurs in the axial direction.

2) Film Diffusion (FD) or external mass transfer: There is a fixed layer of liquid surrounding the solid adsorbent. The well mixed zone transitions into this film through a buffer zone, followed by a laminar sublayer with gradual increase in mass transfer resistance due to increasingly restricted lateral mixing. The movement of the adsorbate molecule through these layers is modeled assuming that there is a sharp division between the well mixed zone where there is no mass transfer resistance and a film of stagnant liquid film which the adsorbate molecule penetrates by molecular diffusion.

3) Intraparticle Diffusion (ID): Diffusion of adsorbate through the pore space which is described detail later

4) Intrinsic physisorption or chemisorption reaction where adsorbate from the fluid phase within the pore space is deposited onto the binding site in the solid phase.

Intra-particle diffusion (step 3) can be visualized in two different ways:

Pore diffusion: The biosorbent particle is viewed as a porous particle and the bed volume is divided into three parts: external and internal void fraction and internal solid fraction, whereby the sorption reaction occurs in the internal voids or pores. The mass transfer involves the diffusion of the sorbate into the fluid phase of the pores utilizing the concentration gradient that exists within the pore. Another possibility is that the adsorbate species may be adsorbed to the external surface of the sorbent particle after FD and then may diffuse along the pore surface due to the concentration gradient within the solid, which is then termed as solid diffusion and may be differentiated from pore diffusion and can be included in advanced modeling. Here intra-particle diffusion actually occurs after

the sorption reaction. These two mechanisms (solid and pore diffusion) may act in parallel and depending on the operating condition, one becomes more favorable than the other.

Alternatively, both solid and pore diffusion can be lumped together to create another simplified model called Homogeneous Solid Diffusion Model (HSDM): This assumes the adsorbent is a non-porous solid homogenous sphere. It does not distinguish between diffusion within the pore space, diffusion along the surface of the adsorbent, and diffusion within the solid particle itself. It assumes that the adsorbate molecule has a constant diffusivity D_s at all points in the homogenous adsorbent sphere.

All of these elementary processes (step 1 to 4) may influence the final rate of biosorption, but often it is assumed that one of these steps is much slower than others and controls the overall rate.

In Mass Transfer Modeling (MTM), the intrinsic sorption reaction is assumed to be fast and one (single resistance model) or both (dual resistance model) of the diffusion processes (step 2 and 3) are taken into account. In contrast to MTM, Surface Reaction Modeling (SRM) assumes that mass transfer is instantaneous, but that the reaction at the phase boundary (step 4) is too slow to establish a local equilibrium at the interface and becomes the rate limiting step of the biosorption process. The obvious drawback of either of those types of modeling (MTM/SRM) is that a rate parameter obtained by successful fitting of the model to data may not reflect the intrinsic quality of the parameter; it may be a lumped parameter incorporating the effect of other processes which were not included in the model derivation. This may not reduce the efficiency of the model, if the variation of this lumped parameter with other operating variables is included within the model; for example, in Chapter 2, rate constant of the SRM was found to vary linearly with the inlet concentration. Still, this issue is especially important if the concerned parameter (e.g., diffusion coefficient) needs to be used in other models, which require the intrinsic parameter. Non-applicability of a model, however, conclusively negates the underlying hypothesis.

1.8.2 Batch vs. Fixed-Bed

This general process overview, as discussed above, is same for both batch and fixed bed experiments. The immediate objective of kinetic modeling for both batch and fixed bed is to find a suitable function to represent respective experimental kinetic data, i.e., the change of effluent concentration (for fixed bed) or residual aqueous phase concentration (for batch). The individual rate equation (representing film diffusion, intraparticle diffusion and surface reaction) and an individual isotherm equation (such as Langmuir or Freundlich which describes the equilibrium relationship between solid and aqueous phase concentration of metals) do not depend on the reactor (batch or fixed bed) but the mass balance equation does. The fundamental difference between batch and fixed bed systems is that the mass balance equation for the former (equation (1.3)) can be directly integrated to have an algebraic equation (1.4) which is not possible for the latter (equation (1.20)). As a result, for batch system, it is easy to calculate the corresponding solid phase metal concentration from experimentally obtained aqueous phase metal concentrations. The rate equation, expressed usually in terms of solid phase concentration of metal can again be directly integrated (analytically or numerically), whereas for modeling fixed bed experimental data, two partial differential equations (mass balance equation, rate equation) with proper initial and boundary conditions along with an isotherm equation are required to solve simultaneously.

1.8.3 Rate equations for Mass Transfer Models (MTM)

Different MTM approaches mainly differ in their rate equations which vary in the complexity and detail taken into consideration. A model becomes complex when a lumped parameter is resolved into constituting intrinsic parameters, i.e., an overall process step is resolved into more elementary micro-steps.

1.8.3.1 Rate equations for film diffusion

Film diffusion (FD) is modeled based on a linear driving force (LDF) which assumes that the rate of mass transfer linearly depends on the concentration difference between bulk aqueous phase and external biosorbent surface.

$$\rho \frac{\partial q}{\partial t} = k_f S_0 (C - C_i) \tag{1.31}$$

$$\frac{\partial C}{\partial t} = -k_f S' (C - C_i) \tag{1.32}$$

Many journal articles which focus only on batch systems, express equation (1.31) in terms of the aqueous phase concentration as in equation (1.32). This is obtained by combining equation (1.3) and (1.31). Some studies differentiate between the overall density of the sorbent granule (which is symbolized as ρ here) and the density of the sorbent material itself (ρ_s) when the internal porosity (ε_s) of the sorbent is known; these are related as $\rho = \rho_s(1-\varepsilon_s)$.

1.8.3.2 Rate equations for intra-particle diffusion

Arranged in increasing order of complexity, intra-particle diffusion can be modeled on the basis of LDF, HSDM, pore diffusion, or pore diffusion along with solid diffusion. Another different way of modeling is the shrinking core model (SCM).

a) Linear Driving Force (LDF)

This model assumes that the mass transfer rate is proportional to the concentration difference between the bulk solid phase and the biosorbent surface.

$$\frac{\partial q}{\partial t} = k_s \, S_0 (q_i - q) \tag{1.33}$$

b) Homogeneous Solid Diffusion Model (HSDM)

This model assumes that the adsorbate molecule follows Fick's diffusion equation (1.34), with a constant diffusivity D_s at all points in the homogenous adsorbent sphere and that local equilibrium prevails within the adsorbent particle.

$$\frac{\partial q_r}{\partial t} = \frac{D_s}{r^2}\frac{\partial}{\partial r}\left(r^2 \frac{\partial q_r}{\partial r}\right) \tag{1.34}$$

For a spherical particle, the average uptake is defined according to the equation (1.35)

$$q = \frac{3}{R^3}\int_0^R q_r(r)\, r^2 dr \tag{1.35}$$

It is often assumed that a parabolic concentration profile prevails within the particle which dictates the function $q_r(r)$.

c) Pore diffusion

If intra-particle diffusion within fluid filled pores is considered as the rate determining process, but surface diffusion is neglected, the rate law can be written as equation (1.36)

$$(1-\varepsilon_P)\left(\frac{\partial q}{\partial t}\right) + \varepsilon_P\left(\frac{\partial C}{\partial t}\right) = \frac{\varepsilon_P\, D_P}{r^2}\frac{\partial}{\partial r}\left(r^2 \frac{\partial C}{\partial r}\right) \tag{1.36}$$

d) Pore diffusion with surface diffusion

This approach considers both pore and surface diffusion together:

$$(1-\varepsilon_P)\left(\frac{\partial q}{\partial t}\right) + \varepsilon_P\left(\frac{\partial C}{\partial t}\right) = \frac{1}{r^2}\frac{\partial}{\partial r}\left(r^2 \varepsilon_P\, D_P \frac{\partial C}{\partial r} + r^2 (1-\varepsilon_P) D_S \frac{\partial q}{\partial r}\right) \tag{1.37}$$

e) Shrinking core model

It is often observed that a partially reacted sorbent particle contains a 'reacted' outer shell surrounding an 'untreated' core of material, whereby the reaction takes place only at the interface between shell and core. This is because a metal ion needs to diffuse through the

saturated (no free binding sites are present) shell of the particle into the unreacted core, in order to get adsorbed at the binding site. As a result, as biosorption continues, the core will keep on 'shrinking' and rate of the intra-particle diffusion will be related to the rate of 'shrinking' of the core. For such a system, a rate can be written as in equation (1.38) and the radius of the shrinking core (r_c) is defined in equation (1.39).

$$\frac{\partial q}{\partial t} = \frac{4\pi}{M}\left(\frac{D_s\, C_i}{\frac{1}{r_c} - \frac{1}{R}}\right) \tag{1.38}$$

$$\frac{R}{r_c} = \left(\frac{q_s}{q_s - q}\right)^{1/3} \tag{1.39}$$

1.8.3.3 Rate equations for Surface Reaction Models (SRM)

Here the intrinsic adsorption reaction is expressed in different empirical forms and kinetic rate equations are constructed as mass law type rate equations. As discussed earlier, metal-binding site interaction can be visualized as equation (1.1). The corresponding rate law (1.40), which is 1st order in forward direction and 2nd order in backward direction may be called Langmuir surface reaction since the Langmuir isotherm is based on this rate law and accordingly at equilibrium, when the net rate is zero, the expression can be used to derive the Langmuir isotherm equation. This rate equation is frequently used to model both batch and fixed bed SRM. Another rate equation (1.41) may be developed considering $k_{de} = 0$ in equation (1.40). This rate equation is called a quasi-chemical rate law and is commonly used for fixed bed modeling, forming the basis of the Bohart Adams model, which is further discussed in section 1.10.1. The two other most frequently used empirical rate laws to model batch kinetics are PFO (1.42) and PSO (1.43) rate equations.

The reversible Langmuir rate equation is:

$$\frac{dq}{dt} = k_{ad}\ C(q_m - q) - k_{de}\ q \tag{1.40}$$

The Bohart Adams rate equation is:

$$\frac{dq}{dt} = k_{BA}\ C(q_\infty - q) \tag{1.41}$$

The pseudo first order rate equation is:

$$\frac{dq}{dt} = k_1(q_\infty - q) \tag{1.42}$$

The pseudo second order rate equation is:

$$\frac{dq}{dt} = k_2(q_\infty - q)^2 \tag{1.43}$$

1.9 Kinetic modeling of biosorption in a batch reactor

Different combinations of rate equations and isotherm equations were applied for the construction of MTM and SRM to explain the kinetic profile obtained from batch biosorption experiments.

1.9.1 Surface Reaction Models (SRM)

Application of SRM, especially PFO and PSO rate laws, is the most common practice to model biosorption batch kinetic data as these equations can be directly integrated to simple algebraic expressions (equation (1.44) and (1.45) respectively) for a batch system. A large number of biosorption studies involving different metals and different biomass types, including biosorption of Cd by citrus peels [14], found that PSO and PFO models fit batch kinetic data with great accuracy. Ho et al. [15] reported 70 of such examples.
The integrated rate equation for the pseudo first order model is:

$$\ln(1-F) = -k_1 t \tag{1.44}$$

That for the pseudo second order model is:

$$q = \frac{k_2 q_\infty^{\,2} t}{1 + k_2 q_\infty t} \tag{1.45}$$

It may be noted that a mass law type rate equation based on ion exchange ($A^+ + BR \leftrightarrow B^+ + AR$) and a rate equation considering film diffusion [16] is mathematical analogous to the PFO model, though based on different assumptions for the underlying mechanism. As discussed below, it is easy to observe that the linear relationship between ln(1-F) and t in the PFO model also holds for the Boyd plot (equation (1.49)) which is derived assuming an intra-particle diffusion controlled process. The consequence of this similarity is discussed later in this chapter.
These two rate equations, PFO and PSO, are usually considered as purely empirical. Recently, Azizian [17] showed that when the initial concentration of sorbate in the solution is large enough so that C can be approximated as C_0, the Langmuir kinetic

expression becomes the PFO (equation (1.44)) rate equation. It was also shown in the article that the integrated form of the PSO rate equation (1.45) can be derived from the integrated form of the Langmuir kinetic rate law by using the mathematical approximation of $e^x = 1+x$ for small values of x.

1.9.2 Mass Transfer Models (MTM)

For MTM, a single resistance model assumes that either the external or the internal mass transfer resistance is much higher than other and that resistance is considered as the rate limiting mechanism for the process. Experimental conditions that promote external mass transfer are well mixed reactor, high sorbate concentration, larger particle size and low capacity of biosorbents. Intraparticle mass transfer is likely to be rate limiting at those same conditions. These conditions are often encouraged in an experimental design since one of the common objectives of the batch kinetic modeling is to determine the intrinsic intra-particle diffusion coefficient, to be further used in fixed bed modeling or for other purposes. It may be again mentioned that a model parameter such as the intra-particle diffusion coefficient obtained by fitting a single resistance model to experimental data is always expected to be a lumped parameter incorporating the effect of other resistances.

1.9.2.1 Crank model for intraparticle diffusion with linear isotherm in infinite bath

Without any particular reference to biosorption, Crank [18] derived a number of analytical solutions for diffusion-controlled mass transfer in general. These solutions are often approximated and typically used in biosorption literature, often without considering the limitations imposed by the underlying assumptions.

Crank derived an analytical solution (equation (1.46)) considering a linear isotherm and Fick's law of diffusion (which is also the basis of the HSDM) to describe intra-particle diffusion in a spherical sorbent particle (equation (1.34) and (1.35)). This solution requires a constant concentration of adsorbate species at the biosorbent surface. The ulterior implication of this assumption is that the model does not consider the mass balance equation in the sense that it assumes that the aqueous phase metal concentration

at any time (C) is equal to both the equilibrium concentration (C_e) and the initial concentration of metal (C_0), i.e., the concentration does not change over time. This is a typical approximation often applied to the batch biosorption modeling, which is not realistic unless the free aqueous phase sorbate quantity is much higher than the amount biosorbed so that the aqueous phase concentration does not change appreciably throughout the course of the experiment. This in turn ensures a constant sorbate concentration at interface. This situation can be caused by a combined effect of large (ideally infinite) volume of surrounding medium (which is why this approximation is often referred to as the 'infinite bath case'), high initial concentration of metal, small amount and low equilibrium capacity of biosorbents. The fraction of sorbent saturation can in this case be calculated as:

$$F = 1 - \frac{6}{\pi^2}\sum_{n=1}^{\infty}\frac{1}{n^2}\exp(-n^2 B\, t) \text{ where } B = \frac{\pi^2 D_s}{R^2} \tag{1.46}$$

The corresponding 'short time' approximation of the above equation which is applicable for data with low F at the beginning of the biosorption experiment is given in equation (1.47).

$$F = 6\left(\frac{D_s t}{R^2}\right)^{0.5}\left\{\pi^{-0.5} + 2\sum_{n=1}^{\infty} ierfc\frac{nR}{\sqrt{D_s t}}\right\} - \frac{3D_s t}{R^2} \tag{1.47}$$

For the initial phase when $F < 0.3$, considering the first term only, this equation (1.47) can be reduced to the famous Weber-Morris equation [9] showing the proportionality of F with square root of t.

$$F = 6\sqrt{\frac{D_s}{\pi R^2}}\sqrt{t} \tag{1.48}$$

Though derived for the initial phase, the equation is usually applied for the entire kinetic profile and typically interpreted as follows: A linear plot of F vs. $\sqrt{t}$ passing through the origin means intra-particle diffusion is the sole rate controlling mechanism. A linear plot which does not pass through the origin implies that there is some influence of intra-

particle diffusion in the overall mass transfer process but it may not be the sole rate limiting step and the magnitude of the intercept on Y axis represents the magnitude of external mass transfer resistance. Wu et al. reported 21 articles which showed a multi-linear Weber-Morris plot consisting of a steep sloped portion followed by a linear middle part and a plateau, including Cd biosorption [19]. According to these articles, these three linear segments represent the external mass transfer controlled zone, intraparticle mass transfer controlled zone and equilibrium state respectively. The basis of this interpretation, though not explained in the related literature, may be argued as follows: since equation (1.48) is the approximation of equation (1.46) for brief amount of time (the shorter the time, the better the approximation), the actual curve of the equation (1.46) may be simulated as a number of segments, each of which represents equation (1.48) having different diffusion coefficients. The first segment obviously represents the external mass transfer as it precedes intra-particle mass transfer. The number of segments in the intra-particle mass transfer zone depends on the heterogeneity of the material: sorbent materials with macro-pores, meso-pores and micro-pores should have three segments theoretically.

Boyd [16] also derived this solution (equation (1.46)) and prepared a table of calculated F values for a series of B t values for quick computation of B from this equation (1.46) in that pre computer era. For each experimental F value, the corresponding B t value was read from the table and was divided by the corresponding experimental t value. A constant value of B implied the applicability of the model, and diffusion coefficient D_s was then calculated from B. In order to reduce the errors in B t values found by interpolation from this table for intermediate values of F, Reichenberg [20] obtained a more useful approximation of the equation by expressing B t in terms of F (equation (1.49) and (1.50)) and formed a new tabulation of $B\,t$ values for a series of F values ranging from 0 to 0.99 at increments of 0.01:

$$Bt = -\ln(1-F) - 0.5 \quad (\text{For } F > 0.85) \tag{1.49}$$

$$Bt = 6.28318 - 3.2899F - 6.28318\,(1 - 1.0470F)^{0.5} \quad (\text{For } F \leq 0.85) \tag{1.50}$$

The first one of these (equation (1.49)), which is the 'long time' approximation of equation (1.46), though not introduced by Boyd, is popularly known as the 'Boyd plot' and typically used as the litmus test to determine the rate limiting mechanism: Since B should be a constant value, a linear plot of $B\,t$ vs. t passing through the origin is interpreted as an intraparticle controlled process, whereas external mass transfer is assumed to play a role if a trendline of the data does not pass through the origin. Though originally approximated for long time only (F>0.85), the equation is often applied [21-23] for the initial range of kinetic data to evaluate the rate limiting mechanism at the beginning of the biosorption. Data often follow a linear trend with a negative intercept, which also conforms with the PFO rate law: similarity between the Boyd plot (equation (1.49)) and the PFO equation (equation (1.44)) suggests that application of one equation makes the other redundant. This is further discussed in Chapter 3. Zhu et al. used Reichenberg's table (based on application of both equations (1.49) and (1.50) in the correct range) and found that intra-particle diffusion was the rate controlling mechanism for Cd biosorption on red mud.

The obvious reason for the popular use of Boyd or Weber-Morris plots to determine the rate limiting condition lies in its simplicity: it is easier to check if experimental data fit to a straight line than to a curve.

Helfferich and Plesset [24] showed that for an ion exchange process, the F vs. t plot depends on the ratio of diffusion coefficients of two ions, and a general explicit function was derived which depends on this ratio. Since Crank's solution is a special case when this ratio reduces to one, the whole equation (1.46) can be approximated as (equation (1.51)) which fits all numerical results within an error of ±0.01.

$$F = \sqrt{1 - \exp\left\{\pi^2(-\lambda + 0.96\lambda^2 - 2.92\lambda^3)\right\}} \quad \text{where } \lambda = \frac{D_s t}{R^2} \tag{1.51}$$

Considering only the first term of the equation (1.51), this equation reduces to equation (1.52) which gives a maximum error of 5% for F>0.1 [25]. There is another class of

biosorption literature [25, 26] which applied this equation (1.52) to determine D_s which is often termed Urano solution [27] or Vermeulen's approximation [25]. Incidentally, there are no journal articles which apply Crank's original diffusion model (1.46) instead of its three approximated versions.

$$\ln(1-F^2) = -B\,t \qquad (1.52)$$

The influence of a non-linear isotherm was theoretically discussed in one article [28] which numerically solved Fick's law of diffusion along with the equilibrium isotherm and compared that with Crank's solution by plotting the result in Weber-Morris type representation: F was plotted with square-root of (t/t_f) where t_f is the time F would take to reach F. Since the Weber-Morris equation predicts a linear plot for such a case, the deviation due to a different isotherm was judged on the basis of how the linearity of the Weber-Morris plot was affected by this change. The article considered a Langmuir isotherm with $q_m = 1$ where the b value was varied from a very small number (< 0.1, where it actually reduces to linear isotherm) to a very high number (= 100). It was found that the linear range of the Weber-Morris plot was low initially and then increased when $b>2$. A similar methodology was applied by varying the μvalue of the Freundlich isotherm, revealing that surface heterogeneity did not influence the outcome. Finally the whole procedure was repeated by incorporating a mass balance equation and it was found that increasing the value of b actually increases the range within which the Weber-Morris plot is linear. Overall, it was concluded that the type of equilibrium isotherm may not significantly influence the linearity of the Weber-Morris plot, but the article emphasized the fact that the Weber-Morris approach is only the simpler 'approximate' representation of the original solution.

1.9.2.2 Crank model for intraparticle diffusion with linear isotherm and mass balance

Now, if the infinite bath assumption is not made, but intraparticle diffusion is still assumed as the sole rate controlling step, then Crank gave another analytical solution (equation (1.53)) for a linear isotherm, which is more practical as it did not assume

constant surface concentration and considers the mass balance equation (1.3) along with (1.34).

$$F = 1 - \sum_{n=1}^{\infty} \frac{6\alpha(\alpha+1)\exp\left(\frac{-D_s \gamma_n^2 t}{R^2}\right)}{9+9\alpha+\gamma_n^2\alpha^2}, \quad \tan\gamma_n = \frac{3\gamma_n}{3+\alpha\gamma_n^2}, \quad \alpha = \frac{V C_0}{M q_\infty} - 1 \tag{1.53}$$

It may be noted that this equation (1.53) will be reduced to equation (1.46) for high values of α.

1.9.3 Applications of SRM and MTM for biosorption batch kinetics

Ruiz et al. [29] studied the sorption of Pd on gluteraldehyde cross-linked chitosan in a batch reactor where experimental equilibrium data were represented by Langmuir and Freundlich isotherms. To model the kinetic data, external mass transfer resistance was assumed to be absent and this equation (1.53) was applied without any modification to incorporate the effect of the non-linear isotherm. The intra-particle diffusion coefficient of Pd was optimized by fitting this equation to the batch kinetic data. It was found that the diffusion coefficient continuously increased with increase in the particle size but did not follow any trend with increasing cross-linking ratio. Also, large values of sum of squared residuals (i.e., large errors) were obtained in each case. It was concluded that under the most favorable experimental condition, biosorption is very fast and may not be accurately described by a single resistance model based on intra-particle diffusion controlled mass transfer.

Vilar et al. [30] used an industrial algal waste for Cd biosorption and applied both MTM and SRM. For MTM, it assumed intra-particle diffusion as the rate controlled mechanism but did not use any of Crank equations for modeling kinetic data. Instead, a set of three equations (mass balance (equation (1.3)), HSDM rate law (equation (1.34)) and Langmuir equilibrium isotherm) were solved numerically by applying a finite element method. Equation (1.35), which describes the average uptake for a spherical particle, was modified as biosorbents particles were considered as a one-dimensional thin plate. Finally, an analytical solution was derived by replacing the HSDM by an LDF solid

phase rate law (equation (1.33)) which agreed with the numerical solution. The diffusion coefficient of Cd was found to be in the range of 2.1 to 10.4 x 10^{-8} cm^2s^{-1}.

Similarly, in the biosorption of Cd by *Sargassum* sp., Yang et al. [31] considered the biomass as a one-dimensional thin plate and numerically solved intra-particle diffusion equation based on Fick's law along with the Langmuir isotherm and mass balance equation. The optimized diffusion coefficient of Cd was found to be $3.5x10^{-6}$ cm^2s^{-1}.

For a batch reactor, an analytical solution of the SCM is available from which the diffusion coefficient can be determined. Suzuki [32] modified the model to make it applicable for a flat slab instead of a spherical particle and applied the model for biosorption of Cd and Pb onto brown algal biomass whereby the average diffusion coefficient of Cd was found to be $9x10^{-6}$ cm^2s^{-1}.

Loukidu et al. [33] examined bacterial biosorption of Cd by applying a Linear Absorption Model (LAM) where the sorption process was described by a HSDM based on intra-particle diffusion followed by reaction on binding sites, neglecting any film diffusion. It was assumed that a linear isotherm existed at each point of the biosorbent. This resulted in a very low Cd diffusion coefficient compared to what was obtained by other methods.

Chen et al. [34] compared the LAM with the SCM for Cu biosorption onto calcium alginate gel beads with varying concentration of alginate and concluded that the LAM is the preferred way to explain batch biosorption kinetic data. Under the experimental range of alginate bead densities (2%-5%), the LAM determined a moderately constant diffusion coefficient of Cu (1.19-1.48 x 10^{-9} m^2s^{-1}) which was close to the molecular diffusivity of Cu in water (0.62-0.75 x 10^{-9} m^2s^{-1}) as referred in the article. In contrast, the SCM predicted an exponential increase in the diffusion coefficient (3.62-37.5 x 10^{-9} m^2s^{-1}) with increasing bead density and exceeded the molecular diffusivity of Cu in water by an order of magnitude, which is not plausible. Shortly after that Jang [35] reevaluated the calculation procedure of the SCM (using plotted data from the batch experiment presented by Chen et al.) and found that SCM prediction (1.18-1.56 x 10^{-9} m^2s^{-1}) actually agreed with LAM. Subsequently, Lewandowski et al. [36] recalculated model predictions also using experimental data of Chen et al. The corrected result (0.89-1.84 x 10^{-9} m^2s^{-1})

showed a reduced amount of mismatch between those models, but the SCM still showed a trend of increasing diffusion coefficient with increasing alginate density, however the increase was by a factor of 2, instead of 10.

Any model based solely on intra-particle diffusion is inherently erroneous since the external mass transfer resistance must be dominating at the beginning of the biosorption process, as film diffusion precedes intra-particle diffusion. Also, even in a severely agitated batch reactor, biosorbents particles may move with the fluid at a comparable speed causing diminished shear forces leading to incomplete suppression of this external fluid film.

In order to avoid the dominance of external mass transfer in the initial phase, Yang and Volesky [37] modeled batch desorption kinetic data instead of adsorption kinetic data for Cd biosorption by *Sargassum* biosorbent. This model considered a Langmuir isotherm prepared from desorption data and an intra-particle diffusion rate equation. The corresponding diffusion coefficient of Cd was found to be 1.65 and 3.7×10^{-6} $cm^2 s^{-1}$ at pH 2 and 1, respectively. Theoretical correlations are available to determine the ratio of intra-particle diffusivity and molecular diffusivity as a function of porosity of the biosorbents and these predictions were found to be well correlated with model predictions.

At other extreme, Choy et al. [38] assumed that sorption of Cu, Cd and Zn ions onto bone char was solely controlled by external mass transfer (equation (1.31)). Three different mass transfer models were considered:

1) Equilibrium according to the Langmuir isotherm (equation (1.6)) was combined with the mass balance equation (1.3), and LDF fluid phase mass transfer (1.31), resulting in equation (1.54) which was solved numerically.

$$\frac{d^2C}{dt^2} + \left\{ k_f S' + \left(\frac{k_f S'}{M\, q_m} \right) \left[(1 + bC) + \frac{b}{k_f S'} \frac{dC}{dt} \right]^2 \right\} \frac{dC}{dt} = 0 \qquad (1.54)$$

2) A linear isotherm was considered instead of the Langmuir isotherm for the above mentioned combination. An analytical solution of this combination is possible.

3) The fluid phase mass transfer equation was again simplified by assuming a constant aqueous concentration of metal ions at the interface (C_i) along with mass balance equation and a linear isotherm.

It was found that there was no significant difference in the values of external mass transfer coefficients obtained by these three methods and the average value was in the order of 10^{-4} cm s^{-1} which is an order of magnitude lower than what was obtained by applying an empirical correlation. A steady decrease in the k_f values with increasing metal concentration was observed, which indicated the influence of intra-particle diffusion. Again this was not observed for k_f values obtained from the correlation since this is a simple function of the agitation speed only. The contribution of intra-particle diffusion was evaluated by applying a Weber-Morris plot which finally revealed that intra-particle diffusion was the rate controlling mechanism for systems with large mean particle size. External film diffusion was only dominating for the initial period of time for systems with smaller mean particle size. It was argued that for smaller particles, intra-particle diffusion needs to occur only over small distance and so external film diffusion becomes more important.

Puranik et al. [39] studied the kinetics of lead and zinc biosorption using microbial biomass and followed Choy's 1st approach and used the equation (1.54) for model fitting and to optimize the value of k_f, but the initial assumption of external film diffusion control was never verified by comparing with other models.

McKay [40] applied MTM to different adsorption system by deriving a numerical solution considering both film diffusion and HSDM-based intra-particle diffusion along with a Redlich-Peterson equilibrium isotherm by using a collocation method.

Chu and Hashim [41] took a different approach by combining MTM and SRM for modeling kinetics of Cu biosorption by microalgae. The rate equation (1.31) for film diffusion and the Langmuir surface reaction (1.40) were combined to obtain an analytical solution containing k_f and k_{ad}. There were two variations of this model which described two limiting situations when either of these two rate coefficient (k_f or k_{ad}) becomes too

high to contribute to the overall resistance. All three models were then applied to the experimental data. It was found that both film diffusion and intrinsic adsorption kinetics are required to provide a correct description of the process at high initial concentration, but film diffusion became rate limiting at low initial concentration. It was hypothesized that this change in kinetics (MTM to combined model) with increasing initial metal concentration was due to the heterogeneity of algal biomass i.e., due to the presence of a variety of ligands with different binding affinities towards a metal ion. At low initial concentration, when binding sites are abundant, metals ions are only preferentially adsorbed onto the high affinity binding sites at particle surface with very high k_{ad} so that the rate depends on film diffusion only. At high initial concentration, interaction with low affinity binding sites led to a slower overall rate. Again, the model was derived assuming negligible intra-particle diffusion, which was not verified. It may be the case that at high initial concentration, metal ions required moving further into particle and the process became limited by intra-particle diffusion and hence did not depend on the film diffusion. The k_{ad} found by optimization actually represented a lumped parameter including the effect of surface reaction and intra-particle diffusion.

El-Naas et al. [42] applied the same model for algal biosorption of Pb ions and arrived at the same conclusion. Unlike the previous article, the authors attempted to verify the underlying model assumption by applying the Weber-Morris model, (equation (1.48). A linear Weber-Morris plot was found which did not pass through the origin. This possibly indicated that intra-particle diffusion may have played a role, implying the lumped nature of the external mass transfer coefficient. A better approach would be to apply the original Crank model (equation (1.46)) instead of its approximated form.

A novel approach was taken by Chu et al. [43] to determine the role of intra-particle diffusion mass transfer in a similar situation studying the removal of Cu by prawn shells. It was assumed that intrinsic reaction kinetics was the rate limiting factor. The experimental data was satisfactorily modeled with the Langmuir surface reaction (equation (1.40)). Instead of using the Crank model from which Weber-Morris model can be derived, the one which incorporated mass balance (equation (1.53)) was considered.

But this was derived for a spherical particle whereas the prawn shells had the shape of a plane sheet; so the model was modified accordingly. Now a family of theoretical uptake curve was drawn according to this model considering a practical range of diffusion coefficients (1-4 x 10^7 cm^2min^{-1}). It was found that the shape of the experimental uptake curve was different from the theoretical curves obtained from intra-particle diffusion model. Thus it was concluded that intra-particle diffusion was not rate limiting under the experimental conditions.

1.10 Kinetic modeling of biosorption in a fixed bed reactor

Similar to the modeling of batch kinetic data, SRM rate equations are repeatedly used for modeling of breakthrough curves. Unlike in batch kinetics, these equations cannot be directly integrated, but must be combined with the mass balance equation and a corresponding isotherm equation.

1.10.1 Bohart Adams and Thomas Models

The rate equation (1.41), combined with an irreversible isotherm and the mass balance equation was solved by Bohart and Adams, which is now most frequently used for breakthrough curve modeling (equation (1.55)).

$$\frac{C}{C_0} = \frac{1}{1+\exp\left(\frac{k_{BA}N_0 h}{u} - k_{BA}C_0 t\right)} \tag{1.55}$$

The Langmuir surface reaction rate equation (1.40), combined with a Langmuir isotherm and mass balance equation, was first solved by Thomas [44] resulting in a very complex analytical expression which was later simplified to equation (1.56). This simplified version is now popularly known as "Thomas model", which is a misnomer as it can be showed [Chapter 2] that this so called "Thomas model" is actually identical with the BA model, since the simplification actually implied $k_d = 0$ which is inherent in the BA model. Sorption capacities from two models are related as described in equation (1.57) and rate constants are same ($k_{ad} = k_{BA}$).

$$\frac{C}{C_0} = \frac{1}{1+\exp\left(\frac{k_{Th}\, q_{Th}\, M}{Q} - k_{Th}\, C_0\, t\right)} \tag{1.56}$$

$$q_{Th} = \frac{N_0\, A\, h}{M} \tag{1.57}$$

Unfortunately, in a large number of biosorption articles [Chapter 2] breakthrough data are modeled using both equation (1.55) and (1.56) to determine the best fitting breakthrough model. This approach is fundamentally wrong.

1.10.2 Bed Depth Service Time Model

Another frequently used model to describe column biosorption is the Bed Depth Service Time (BDST). Here BA model is linearized (equation (1.58)) in slope (m) (equation (1.59)) - intercept (I) (equation (1.60)) form and is applied at the breakthrough point so that (C,t) was replaced by (C_b, t_b) [45]. The slope m is related to the reciprocal of the speed of MTZ and the intercept I is the time MTZ takes to progress by MTZ.

$$t_b = m h - I \tag{1.58}$$

$$m = \frac{N_0}{C_0 u} \tag{1.59}$$

$$I = \frac{1}{k_{BA} C_0} \ln\left(\frac{C_0}{C_b} - 1\right) \tag{1.60}$$

As apparent from the equation (1.58), t_b is linearly related to bed depth (h). Experimental work requires generation of a set of (t_b, h) values by running the column at different bed depths at constant feed concentration and flow rate so that a linear plot of t_b vs. h can be constructed to derive the constant parameters (N_0 and k_{BA}) from the slope (m) and intercept (I) of the plot. Using these constants, the critical bed depth (h_0), which is the minimum bed height required to prevent the effluent concentration exceeding C_b at t = 0 can be obtained as I/m. The model is then [45] extended for prediction of a new slope (m') and new intercept (I') for new values of feed concentration (C_0') (equation (1.61) and (1.62)) and flow rate (Q') (equation (1.63) and (1.64)).

$$m' = m\left(\frac{C_0}{C_0'}\right) \tag{1.61}$$

$$I' = I\left(\frac{C_0}{C_b}\right)\frac{\ln\left(\frac{C_0'}{C_b}-1\right)}{\ln\left(\frac{C_0}{C_b}-1\right)} \tag{1.62}$$

$$m' = m\left(\frac{Q}{Q'}\right) \tag{1.63}$$

$$I' = I \tag{1.64}$$

This whole approach may be fundamentally wrong not only because parameter estimation by linearization of an originally non-linear expression usually violates assumptions behind linear regression, but also because it essentially assumes that the model parameters (N_0 and k_{ba}) remain constant for different column runs with varying C, Q and h which is only true under certain limited conditions. A truly intrinsic rate constant may remain constant but if mass transfer limitation is present, which is usually the case, the regressed rate parameter represents a lumped parameter incorporating the effect of mass transfer as well. In that case, either the intrinsic rate parameter has to be determined or the lumped parameter's variation with C, Q and h has to be considered. In fact a sizable portion of articles actually studied the variation of the lumped rate constant with feed concentration, flow rate and bed depth. The sorption capacity, in principle, should vary with C_0 according to the equilibrium isotherm but should in theory not change with the flow rate. Unfortunately, there are several articles which applied the BDST model for Cd biosorption using different agro and microbial biomass types such as rice husk [46], coir pith [47], fungal biosorbent [48] and algal biomass [49] following the procedure discussed above without considering the variability of N_0 and k_{BA}.

A match between experimental data and model, however, is not uncommon when the associated model parameter does not change with varying hydrodynamic condition. For example, Ramesh et al. [47] studied biosorption of Cd by coir pith, another agro based waste product generated in the process of coir fiber separation from coconut husk for

mattress padding. The sorption capacity N_0 was only reduced from 4.09 to 3.66 mg/cm^3 on changing the flow rate from 10 to 15 ml/min, as a result, the slope m′ of the BDST model predicted for 15 ml/min according to equation (1.63), using the old capacity of N_0 = 4.09 mg/cm^3 matches with the experimental slope for one significant digit.

Ko et al. [50] studied Cd sorption using bone char using the BDST model and took a slightly modified approach where an empirical equation (1.65) was proposed to consider the variation of bed N_0 with service time where *a* is a rate parameter depending on mass transfer resistances.

$$N = N_0(1 - \exp(-a * \sqrt{t_e})) \tag{1.65}$$

The best application of the BDST approach was found in a study of Cd biosorption onto a marine alga [51]. Here the column run was not repeated with varying bed heights for a given flow rate, so that variation of k_{BA} and N_0 with bed height was not an issue. Samples were taken from three ports of the same column generating three sets of (t_b, h) values from a single experiment, sufficient to perform a linear regression of $t_b = f(h)$, the slope and intercept of which was used to calculate the sorption capacity (N_0) and critical bed depth (D). The critical bed depth obtained by this method was found to match with the length of the MTZ calculated from t_b and t_s. For changing Q, instead of predicting the new slope using equation (1.63) with BA model parameters from the previous run, the entire experiment was repeated resulting in a different $t_b = f(h)$ for the changed flow rate. Finally, the variation of sorption capacity (N_0) and critical bed depths with Q were plotted. An effectiveness factor was defined as the ratio of the overall sorption rate for the same sorbent in presence and absence of pore diffusion, and expressed as a function of Thiele modulus, the square of which is ratio of sorption rate constant to intra-particle diffusion constant. The effectiveness factor was determined from batch kinetic data using granules (pore diffusion present) and powder (pore diffusion negligible) of the same biomass. The latter was found to follow the first order rate expression and the corresponding sorption rate constant was determined. Film resistance was ignored for both experiments assuming a well mixed batch reactor. The Thiele modulus was

calculated from the effectiveness factor. The diffusion coefficient of Cd was then calculated to be 3.74 x 10^{-3} cm^2/min from the Thiele modulus as rate constant was already known. Finally, the dispersion effect was evaluated from the correlation between Peclet number and Reynolds number and the effect was found to be negligible.
An equilibrium dispersive model based on the Langmuir isotherm was also applied [52] later on the same data when the apparent dispersive coefficient and Langmuir constants (b and q_m) were optimized. It was found that the BA model sorption capacity (N_0) matched the experimental batch capacity which in turn closely corresponded with q_m optimized for the equilibrium dispersive model being equal to 30 mg Cd/g.

1.10.3 Mass Transfer Models

Since fixed bed MTM require simultaneous solution of a mass balance equation, a rate equation and an isotherm equation, a vast number of solutions are theoretically feasible considering the number of combinations possible from the pool of isotherm equations (linear, Langmuir, Freundlich, irreversible) and rate equations ((1.31)-(1.43)) along with assumptions such as plug flow or constant pattern. Those combinations which are included in Table 1.1 are important because either analytical solutions are available and/or these are commonly used in the biosorption literature as mentioned subsequently.
Ko et al. [53] applied the shrinking core model to simulate the breakthrough curve obtained from fixed bed sorption of Cd and Cu by bone char. It was argued that when equilibrium isotherm can be approximated as irreversible, the SCM model is superior to the LDF model.
Since the LDF model is the most frequently used rate equation in MTM, it may be worth to discuss this practice in more detail. Since there cannot be any accumulation at the interface, the rate of external mass transfer is always equal to the rate of internal mass transfer, regardless of the model equation used to represent those rates; but the alluring feature of the LDF modeling is that the individual mass transfer rate can be algebraically combined in a simple way based on the sorbate concentration difference between bulk aqueous phase and the solid phase, retaining the simplicity of the original equations. The

final equation can be expressed in terms of either aqueous (equation (1.66)) or solid phase concentration (equation (1.67)). In each case, the resultant overall rate constant is related to the individual mass transfer coefficients (equation (1.68) and (1.69)). These equations are usually meaningful when the equilibrium isotherm can be expressed or approximated as a linear isotherm so that the slope of the isotherm (K) is constant and known.

$$\rho \frac{\partial q}{\partial t} = K_f S_0 (C - C^*) \tag{1.66}$$

$$\frac{\partial q}{\partial t} = K_s S_0 (q^* - q) \tag{1.67}$$

$$\frac{1}{K_f} = \frac{1}{k_f} + \frac{1}{K \rho k_s} \tag{1.68}$$

$$\frac{1}{K_s} = \frac{K \rho}{k_f} + \frac{1}{k_s} \tag{1.69}$$

The simplicity of either of these representations may lure one to use it as an effortless way to construct a 'two resistance' model only to reveal the shortcoming: the optimized lumped parameter (K_f or K_s) cannot be resolved into its intrinsic components (k_f and k_s) until one of them is supplied from other sources. It must be emphasized that the use of either of these equations is equivalent to a single resistance system: when either external or internal rate is ignored, assuming it to be infinitely higher than the other, the rate coefficient obtained in the course of parameter optimization is the overall fluid or solid phase rate coefficient respectively. The use of equation (1.66) is equivalent to the use of (1.31) ignoring (1.33). Similarly, use of equation (1.67) is equivalent to use equation (1.33) ignoring (1.31) regardless of the type of equilibrium isotherm or other factors considered/neglected in the construction of the final model. The special feature of a linear isotherm is that equation (1.66) and (1.67) are equivalent. Nevertheless, these equations are very useful to calculate the third parameter if two parameters are known: if intrinsic

constants (k_s and k_f) are known, a predictive model can be obtained since overall parameters K_f or K_s can be calculated by using the appropriate equation. Conversely, if the overall coefficient and one intrinsic constant are known, the other intrinsic parameter can be obtained.

When external and intra-particle mass transfer rates are combined as in equation (1.66), an analytical solution is available for a linear system under plug flow condition, commonly called the Klinkenberg solution. In the study of Cr biosorption by baggage fly ash, [54], initially K_f was optimized by applying the Klinkenberg equation, k_f was determined from an engineering correlation and k_s was calculated from equation (1.68), once k_s is known, the same equation (1.68) was used to find out K_f and to predict the breakthrough curve at other experimental conditions.

This procedure can be extended and generalized as follows: for a linear isotherm, all resistances (external film, intra-particle diffusion, dispersion, surface reaction) are serially additive, and the sum is equal to the overall resistance. This equation containing 'n+1' resistances (n individual resistance and one overall resistance) can be applied to determine any one of them when all others are known directly from experiments or from other sources such as engineering correlations and parameter optimization. For a priori prediction of breakthrough curves, however, individual resistances should be determined without any regression on breakthrough data so that the overall resistance may be calculated using this equation. Finally, breakthrough curves may be constructed using the overall resistance. This is done in Chapter 3.

Aksu [55] studied biosorption of copper ions to green alga and ignored intra-particle diffusion. The biosorption process was visualized as film diffusion followed by a surface reaction which was assumed to be first order with respect to the fluid phase concentration. The external mass transfer coefficient was obtained from an engineering correlation and the surface reaction rate was found from experimental data. Another article [26] studying bacterial biosorption of Cr (VI) followed and extended this approach by adding an intraparticle diffusion resistance in series with the surface reaction resistance. The intraparticle diffusion coefficient was obtained from batch experiments by

applying the Urano solution (equation (1.52)) In both examples, the values of individual mass transfer coefficients were obtained independently, without fitting to the breakthrough data but unfortunately the validity of those parameters was not verified by constructing the breakthrough curve using those parameters.

As far as the validity of the linear approximation of the Langmuir isotherm is concerned, Park [56] constructed a model considering axial dispersion, LDF-based external mass transfer and HSDM-based intra-particle mass transfer. The local equilibrium established at the fluid-particle interface was described by the Langmuir isotherm. This model was found to agree excellently with the simpler model where a linear isotherm was used instead of a Langmuir isotherm when b $C_0 << 1$. The higher the affinity of the sorbate (i.e., higher b value), the higher the deviation, as breakthrough curves becomes steeper. It was also showed in the article that HSDM-based intra-particle diffusion coincides with the LDF approximation when the concentration profile within the particle is assumed to be parabolic. In fact, it can be shown [9] that the HSDM (equation (1.34) and (1.35)) is exactly equivalent to LDF approximation equation (1.33) if the following expression (equation (1.70)) is assumed which can be deduced from equation (1.34) and (1.35) by assuming a parabolic concentration profile in a spherical particle, which is generally true unless the bed is too short to develop this profile.

$$k_s = \frac{15 D_s}{R^2} \tag{1.70}$$

For predictive modeling, accurate estimation of model parameters is the most important factor as it directly influences the performance of the model. For batch experiments, experimental conditions may be designed in a way to minimize the external mass transfer resistance, which is not possible for fixed bed experiments because the flow rate cannot be increased too high as it may cause an early breakthrough. External mass transfer coefficient can be determined from various engineering correlations, but a number of correlations exist and k_f values obtained from these correlations vary significantly depending on the power of the void fraction which may be positive, negative or zero.

Also, according to these correlations, k_f mainly varies as a function of the superficial velocity, ignoring all other local effects. In order to avoid those problems, Radcliffe et al. [57] presented a method of experimental determination of the external mass transfer coefficient for a fixed bed reactor. This is based on the same assumption and does not ignore k_f completely in the batch process even at high agitation: at the beginning of the experiment, external film resistance dominates over all other resistances since this is the first step of the mass transfer process. Accordingly, the fluid phase LDF equation was applied with the assumption that $C_i = 0$, and the mass balance equation was modified with $dC/dt = 0$. Combining these two equations, the following equation was derived (equation (1.71)) where C_1 denotes the effluent concentration at the time t_1 equal to the residence time of the column, signifying that the effluent contains the first parcel of the feed. The bed length must be short enough to produce a non-zero C_1 at the desired inlet concentration and flow rate and a C/C_0 vs. t plot can be extrapolated to find C_1. Now this equation (1.71) can be applied to determine k_f if other variables are known.

$$C_1 = C_0 \exp\left\{\frac{Pe}{2} - \sqrt{\left(\frac{Pe^2}{4} + \frac{(1-\varepsilon)k_f SL^2}{\varepsilon D_L}\right)}\right\} \tag{1.71}$$

Later Cooney [58] questioned the validity of the assumption of $C_i = 0$ and showed that this assumption is valid only within a range of Biot number depending on the shape of the isotherm. If the assumption is violated, the external mass transfer coefficient determined from the equation (1.71)will actually represent an overall mass transfer coefficient. Similar to batch kinetics models, single resistance models are often applied for modeling breakthrough curves where either film diffusion (equation (1.31)) or intra-particle diffusion (equation (1.33)) is considered as the rate limiting step, neglecting the other. Gabaldon et al. [11] studied adsorption of Cd onto mineralized peat in a fixed bed reactor. Unlike most other similar studies, the dispersion coefficient for the fixed bed was neither assumed zero nor was it regressed from the MTM, rather it was estimated from a correlation that depends on particle size, bed void fraction and flow rate. The equilibrium was described by a Freundlich isotherm constructed from fixed-bed data and the

dispersive equilibrium model (section 1.7.4) was applied. The predicted breakthrough curve was found to deviate substantially from the experimental data. It was hypothesized that this discrepancy was due to mass transfer limitation. In a second modeling approach, the same authors still ignored external film diffusion and intra-particle diffusion was modeled according to the LDF approximation. This model was then used to fit the experimental data by optimizing the intra-particle mass transfer coefficient. The overall diffusion coefficient of Cd was determined using equation (1.70) as ranging from 2.3 to 3.4 $x10^{-13}$ m^2s^{-1}. This does not prove the hypothesis though. Unlike the dispersion coefficient, the intra-particle mass transfer coefficient was not determined from other sources, but optimized from experimental data. In other words, had the dispersion coefficient been regressed from experimental data, the equilibrium dispersive model could have simulated the breakthrough curves as well.

Izquierdo et al. [10] took a similar modeling approach to study the removal of Cu by biosorption onto algal biomass. The dispersion coefficient was determined experimentally by a tracer study so that it even did not require relying on an engineering correlation. Unlike in previous example, the equilibrium dispersive model (section 1.7.4), was found to simulate the breakthrough curve but only at inlet concentrations below 2 mg/L. Above this concentration, intra-particle diffusion was again hypothesized to be rate limiting and was modeled by a LDF (solid film) rate law. A system of equations comprising of the Langmuir dynamic equilibrium isotherm, mass balance and rate equation was solved by explicit finite difference method. The solid film rate coefficient was regressed by fitting the model to experimental breakthrough data, from which the effective intra-particle diffusion coefficient was determined using equation (1.70). This model matched well with experimental breakthrough curves obtained above 2 mg/L but the same comment that was made for previous example also applies here.

Silva et al. [12] studied biosorption of Cu by *Sargassum* sp. in a fixed bed reactor. Three different single resistance models were considered which obviously differ in their rate equations:

1. Intra-particle diffusion as the limiting factor, rate law based on LDF solid phase (equation (1.31)),

2. Film diffusion as the limiting factor, rate law based on LDF fluid film (equation (1.33))

3. An empirical model involving q, q_i and C

Each of these rate laws was combined with the mass balance equation and the equilibrium equation (Langmuir dynamic isotherm) and solved numerically using DASSL code. In each case, both the dispersion coefficient and the respective rate coefficient were optimized to fit the model to experimental breakthrough data. It was found that the model-1 and model-3 represented the data more satisfactorily than the MTM based on film diffusion. A sensitivity analysis showed that simulated breakthrough curves did not depend on the dispersion coefficient. It must be emphasized that the actual rate limiting mechanism cannot be concluded from this analysis, since the model parameter obtained in each case was a lumped one, incorporating the effect of other factors. If the equilibrium isotherm had been approximated as a linear isotherm, both film and intra-particle diffusion mass transfer models would have become analogous, as described at the beginning of this section.

In contrast, Borba et al.[59] considered a two-resistance model to describe biosorption of Ni where film diffusion and intra-particle diffusion resistances were considered together and represented by respective LDF rate laws and local equilibrium at interface was described by a dynamic Langmuir isotherm. The film mass transfer coefficient typically varies with the flow rate and a number of engineering correlations are available which expresses this coefficient as a function of flow rate. In order to make the model robust, this coefficient is substituted according to a generalized correlation $k_f = AG^n$ where A and n need to be optimized and G is a known function of flow rate. The dispersion coefficient, on the other hand was calculated by using a correlation. These rate equations along with the equilibrium relationship and mass balance equation were simultaneously

solved by using a DASSL algorithm coded in FORTRAN to optimize values of A, n and k_s. It was found that model was able to simulate breakthrough data obtained at different flow rates.

Volesky [60] constructed a MTM to describe the breakthrough data obtained for biosorption of U by *Sargassum* biomass. A plug flow was assumed. Film diffusion and intra-particle diffusion were modeled by LDF and HSDM respectively. The biomass particles were assumed as a one-dimensional thin plate and the concentration profile within the particle was modified accordingly, instead of assuming a parabolic profile as usually done for a spherical particle. The intra-particle diffusion coefficient was obtained from batch experiments, where the same model was used except that film diffusion was assumed to be negligible. The set of PDE's was solved by orthogonal collocation method and a numerical algorithm was developed using FORTRAN. The simulated breakthrough curve matched well with the experimental data in general except for the breakthrough region. The film diffusion coefficient was regressed by fitting experimental data but the model was found not to be sensitive to this coefficient, implying that intra-particle diffusion was the rate-controlling mechanism.

Li et al.[61] examined adsorption of phenol by activated carbon fiber and applied a comprehensive model in which the mass balance equation includes a term for dispersion; the rate equation includes both film diffusion with LDF and intra-particle diffusion described by the HSDM. Equilibrium was described by a Langmuir isotherm which was constructed from fixed bed data. The intra-particle diffusion coefficient was calculated from batch experiments by applying a pore diffusion model and the film diffusion coefficient was obtained by applying an engineering correlation. The set of PDE's was then solved by orthogonal collocation to optimize the dispersion coefficient only, which should be an intrinsic value. A sensitivity analysis showed that there was a threshold value of the intra-particle diffusion coefficient, above which simulated breakthrough curves did not change and this value was lower than the experimentally determined diffusion coefficient. This essentially signifies that intra-particle diffusion was not the rate-controlling mechanism. Similarly, a change in the film diffusion coefficient did not

influence breakthrough curves either, implying that axial dispersion was the only rate-limiting factor for the given experimental condition. Accordingly, in a second modeling approach, the original model was simplified by ignoring the mass transfer parameters and again solved by orthogonal collocation to optimize the dispersion coefficient. It was found that the dispersion coefficient and the breakthrough curve estimated by this simplified model matched with the original model, implying the correct determination of the rate limiting step. This type of elaborated modeling is rare in the biosorption literature.

There are not many articles focusing on more complex models beyond the application of LDF and HSDM. Sulaymon et al. [62] applied a pore diffusion model to describe removal of Pb and Cu ions onto granular activated carbon in both batch and fixed bed reactors. Langmuir isotherm parameters and the pore diffusion coefficient were regressed from a batch kinetic model. The film diffusion coefficient was calculated using an engineering correlation involving the Reynolds number, Sherwood number and Schmidt number. The dispersive coefficient was calculated from another relation involving the Reyolds number and Peclet number. The set of PDEs was solved by reducing them to ordinary differential equations (ODEs) using a finite element method and orthogonal collocation method. Finally ODEs were solved by using MATLAB software. Since none of the model parameters were optimized from fixed bed data, but obtained from other sources, this is an example of predictive modeling; figures showed that predicted breakthrough curves only moderately matched with experimental data though, and no statistical parameter such as variance of error was given to judge the goodness of fit. Under the experimental condition of investigation, the Biot number, which is the ratio of external and internal mass transfer coefficient, ranged between 40 to 50 and 90 to 120 for Pb and Cu respectively. Due to high Biot numbers, it was concluded that intra-particle diffusion was the rate controlling step. In this case, this reasoning was correct due to the intrinsic nature of model parameters.

1.11 Overview of thesis

Chapter 2 focuses on the biosorption of Cd onto protonated citrus peels in a fixed bed reactor under varying conditions of influent concentration, bed height and flow rate. Breakthrough curves were simulated by frequently used mathematical models. These models were then compared to identify the mathematically analogous models and to determine which breakthrough model best fits the experimental data.

Chapter 3 focuses on a-priori prediction of breakthrough curves by deriving the related model parameters from other sources. This includes an exhaustive analysis of different MTM (based on either external resistance or intra-particle diffusion resistance or both) and SRM in both batch and fixed bed reactor. A number of mathematically analogous models were identified. This chapter also investigated different immobilization procedures and compares the biosorption of Cd onto native and immobilized citrus biosorbent.

Chapter 4 focuses on the binary metal biosorption in a batch reactor using protonated citrus peels. It compares the performance of protonated citrus peels for biosorption of Cd and Zn in single and binary systems. A number of isotherm models were considered for modeling single and binary system equilibrium data.

Chapter 5 focuses on binary combinations of Cd, Pb and Zn biosorption in a fixed bed reactor using protonated citrus peels. Biosorption of binary metal systems was compared with corresponding mono-metal systems. The effect of calcium in the influent along with target metal (Pb or Cd) was studied. Finally, the the treatment of real mining effluent collected from Greens Creek, Juneau was investigated.

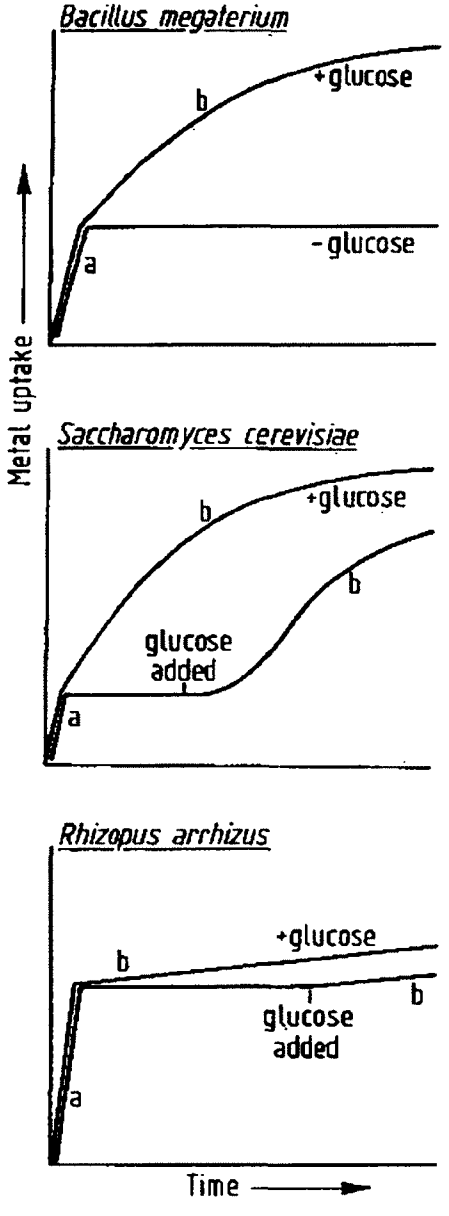

Figure 1.1 Illustration of (a) metabolism-independent and (b) metabolism-dependent metal uptake in suspension of different biomass types. The figure was modified from [63].

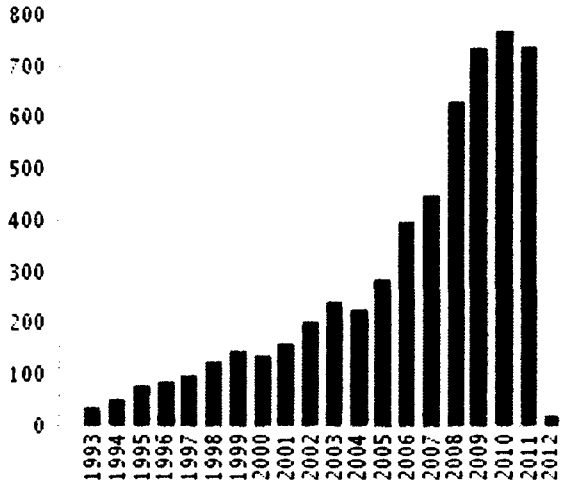

Figure 1.2 Biosorption articles published per year according to ISI web of knowledge.

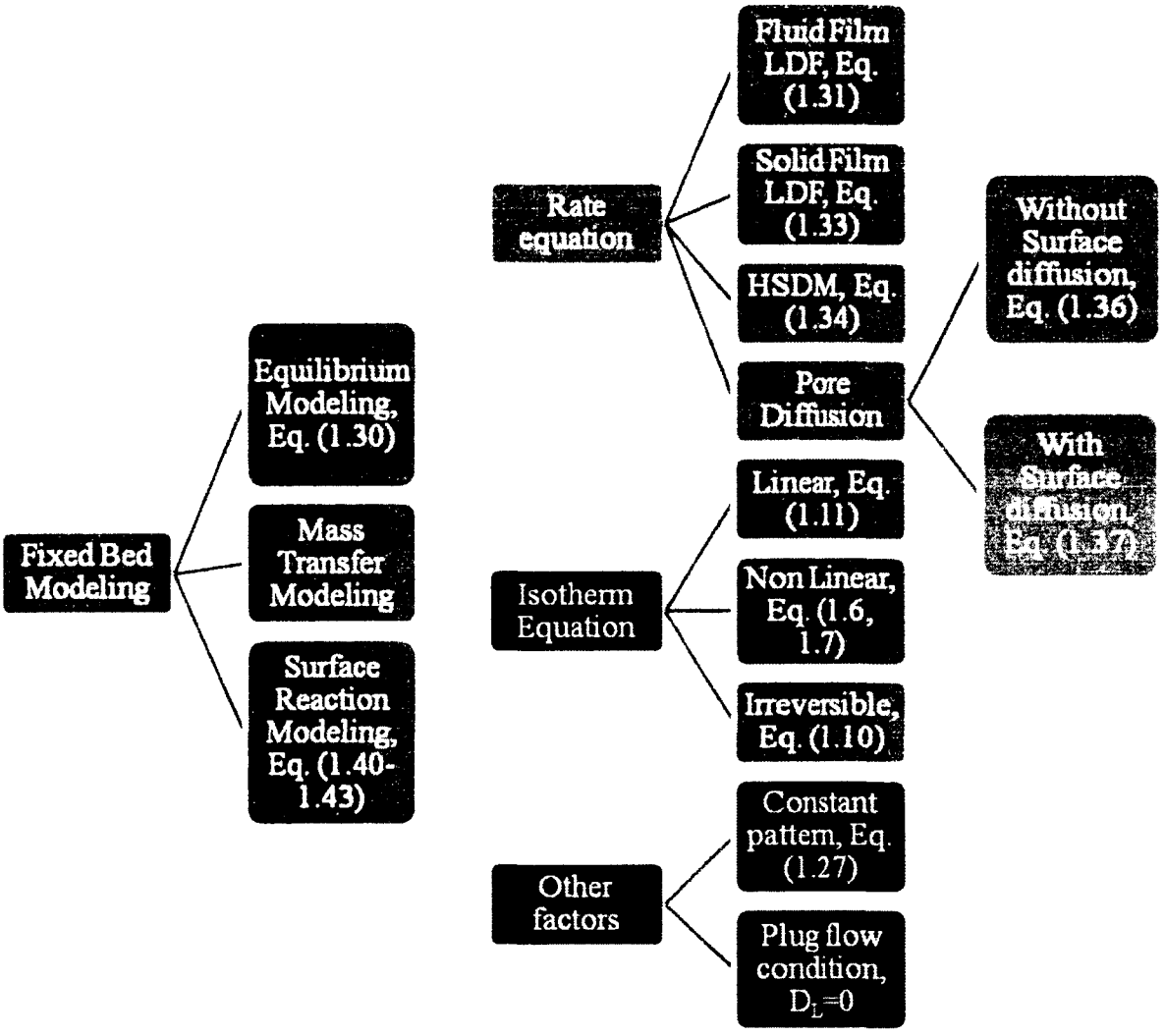

Figure 1.3 Overview of different approaches and mechanisms considered in fixed bed kinetic modeling.

Table 1.1 Fixed bed mass transfer models

Model #	Isotherm	Film diffusion	Intra-particle diffusion	Plug flow?	Constant pattern?	Solution
1[a]	Linear	Overall Fluid film LDF		Y	N	Analytical
2	Linear	LDF	LDF	N	N	Analytical
3	Irreversible	-	HSDM	Y	N	Analytical
4	Irreversible	LDF	LDF	Y	N	Analytical
5[b]	Irreversible	-	LDF	Y	N	Analytical
6[c]	Irreversible	LDF	-	Y	N	Analytical
7[d]	Irreversible	LDF	LDF	Y	Y	Analytical
8	Irreversible	LDF	Pore diffusion	Y	Y	Analytical
9[e]	Irreversible	-	pore	Y	Y	Analytical
10	Irreversible	-	Pore diffusion	N	N	Analytical
11	Langmuir	LDF	-	Y	Y	Analytical
12	Langmuir	-	LDF	Y	Y	Analytical
13	Freundlich	-	LDF	N	N	Numerical
14	Langmuir	-	LDF	N	N	Numerical
15	Langmuir	-	LDF	Y	N	Numerical
16	Langmuir	LDF	-	Y	N	Numerical
17	Langmuir	LDF	LDF	Y	N	Numerical
18	Langmuir	LDF	HSDM	N	N	Numerical
19	Langmuir	LDF	HSDM	Y	N	Numerical

[a] Klinkenberg Model

[b] Can be derived from model #4 with $1/k_f = 0$

[c] Can be derived from #4 with $1/k_s = 0$

[d] Can be derived from #4 by applying constant pattern condition

[e] Can be derived from #9 with $1/k_f = 0$

#13-19 Discussed within chapter

Table 1.2 Biosorption capacity of Cd, Zn and Pb by different plant-based residues

Adsorbent	Metal	q_m mg/g	Ref
Broad bean peel	Cd	148	[64]
Peas peel	Cd	119	
Medlar peel	Cd	98	
Neem leaf powder	Cd	158	
Chestnut shell	Zn	2	[65]
Saw dust	Zn	14	
Neem bark	Zn	13	
Wheat straw	Zn	11	
Mango peel waste	Zn	25	
Black gram husk	Zn	34	
Fig leaves	Pb	37	[66]
Seaweed	Pb	29	
Bagasse fly ash	Pb	3	
Coir	Pb	19	
Groundnut hull	Pb	32	

Table 1.3 Comparison of Langmuir isotherm parameters obtained from batch versus column experiments [10].

	Batch isotherm at pH 5	Batch isotherm at pH 6	Dynamic isotherm at pH 6
b ($L\ mg^{-1}$)	0.10	0.13	2.77
q_m (mg/g)	57	86	57

1.12 References

1. Agency for Toxic Substances and Disease Registry., *Toxicological Profile for Cadmium*. 1999, US Department of Human and Health Services.
2. ACAA, *2008 Coal Combustion Product (CCP) Production and Use Survey Report* 2009a, American Coal Ash Association Aurora, Colorado.
3. Eccles, H., *Treatment of metal-contaminated wastes: why select a biological process?* Trends in Biotechnology, 1999. **17**(12): p. 462-465.
4. Small, H., *The poisoning of ion-exchange resins. Inhibition of cation exchange by cationic surface-active agents.* Journal of the American Chemical Society, 1968. **90**(9): p. 2217-2222.
5. Patil, S.B., *Biosorption of heavy metals by citrus fruit waste materials*, in MS Thesis, *Department of Civil & Environmental Engineering*. 2004, University of Alaska Fairbanks: Fairbanks.
6. Balaria, A., *Biosorption of lead by citrus pectin and peels in aquous solution*, in MS Thesis, *Civil & Environmental Engineering*. 2006, University of Alaska Fairbanks: Fairbanks.
7. Gadd, G.M., *Biosorption: critical review of scientific rationale, environmental importance and significance for pollution treatment*, Journal of Chemical Technology and Biotechnology, 2009. **84**(1): p. 13-28.
8. Pagnanelli, F., *Equilibrium, Kinetic and Dynamic Modelling of Biosorption Process*, in *Microbial Biosorption of Metals*, M.M. Pavel Kotrba, Tomas Macek, Editor. 2011, Springer.
9. Cooney, D.O., *Adsorption Design for Wastewater Treatment*. 1998
10. Izquierdo, M., et al., *Modeling of copper fixed-bed biosorption from wastewater by Posidonia oceanica*. Bioresource Technology, 2010. **101**(2): p. 510-517.
11. Gabaldon, C., P. Marzal, and F.J. Alvarez-Hornos, *Modelling Cd(II) removal from aqueous solutions by adsorption on a highly mineralized peat. Batch and*

fixed-bed column experiments. Journal of Chemical Technology and Biotechnology, 2006. **81**(7): p. 1107-1112.

12. da Silva, E.A., et al., *Modeling of copper(II) biosorption by marine alga Sargassum sp. in fixed-bed column.* Process Biochemistry, 2002. **38**(5): p. 791-799.
13. Barros, M.A.S.D., et al., *Removal of Cr(III) in the fixed bed column and batch reactors using as adsorbent zeolite NaX.* Chemical Engineering Science, 2004. **59**(24): p. 5959-5966.
14. Schiewer, S. and M. Iqbal, *The role of pectin in Cd binding by orange peel biosorbents: A comparison of peels, depectinated peels and pectic acid.* Journal of Hazardous Materials, 2010. **177**(1-3): p. 899-907.
15. Ho, Y.S. and G. McKay, *Pseudo-second order model for sorption processes.* Process Biochemistry, 1999. **34**(5): p. 451-465.
16. Boyd, G.E., A.W. Adamson, and L.S. Myers, *The exchange adsorption of ions from aqueous solutions by organic zeolites. II. Kinetics.* Journal of the American Chemical Society, 1947. **69**(11): p. 2836-2848.
17. Azizian, S., *Kinetic models of sorption: a theoretical analysis.* Journal of Colloid and Interface Science, 2004. **276**(1): p. 47-52.
18. Crank, J., *The Mathematics of Diffusion.* 1980: Oxford University Press.
19. Wu, F.C., R.L. Tseng, and R.S. Juang, *Initial behavior of intraparticle diffusion model used in the description of adsorption kinetics.* Chemical Engineering Journal, 2009. **153**(1-3): p. 1-8.
20. Reichenberg, D., *properties of ion-exchange resin in relation to their structure. III. Kinetics of exchange.* Journal of American Chemical Society, 1953. **75**.
21. Kumar, D. and J.P. Gaur, *Chemical reaction- and particle diffusion-based kinetic modeling of metal biosorption by a Phormidium sp.-dominated cyanobacterial mat.* Bioresource Technology, 2011. **102**(2): p. 633-640.
22. Ofomaja, A.E., E.E. Ukpebor, and S.A. Uzoekwe, *Biosorption of Methyl violet onto palm kernel fiber: Diffusion studies and multistage process design to*

minimize biosorbent mass and contact time. Biomass & Bioenergy, 2011. **35**(10): p. 4112-4123.

23. Ofomaja, A.E., *Biosorption studies of Cu(II) onto Mansonia sawdust: Process design to minimize biosorbent dose and contact time.* Reactive & Functional Polymers, 2010. **70**(11): p. 879-889.
24. Helfferich, F. and M.S. Plesset, *Ion exchange kinetics. a nonlinear diffusion problem.* The Journal of Chemical Physics, 1958. **28**(3).
25. Inglezakis, V.J. and H.P. Grigoropoulou, *Applicability of simplified models for the estimation of ion exchange diffusion coefficients in zeolites.* Journal of Colloid and Interface Science, 2001. **234**(2): p. 434-441.
26. Maiti, S., et al., *Determination of Kinetic Parameters in the Biosorption of Cr (VI) on Immobilized Bacillus cereus[16] in a Continuous Packed Bed Column Reactor.* Applied Biochemistry and Biotechnology, 2009. **159**(2): p. 488-504.
27. Urano, K. and H. Tachikawa, *Process-Development for Removal and Recovery of Phosphorus from Waste-Water by a New Adsorbent .2. Adsorption Rates and Breakthrough Curves.* Industrial & Engineering Chemistry Research, 1991. **30**(8): p. 1897-1899.
28. Plazinski, W. and W. Rudzinski, *Kinetics of Adsorption at Solid/Solution Interfaces Controlled by Intraparticle Diffusion: A Theoretical Analysis.* Journal of Physical Chemistry C, 2009. **113**(28): p. 12495-12501.
29. Ruiz, M., A.M. Sastre, and E. Guibal, *Palladium sorption on glutaraldehyde-crosslinked chitosan.* Reactive and Functional Polymers, 2000. **45**(3): p. 155-173.
30. Vilar, V.t.J.P., C.l.M.S. Botelho, and R.A.R. Boaventura, *Equilibrium and kinetic modelling of Cd(II) biosorption by algae Gelidium and agar extraction algal waste.* Water Research, 2006. **40**(2): p. 291-302.
31. Yang, J.B. and B. Volesky, *Cadmium biosorption rate in protonated Sargassum biomass.* Environmental Science & Technology, 1999. **33**(5): p. 751-757.

32. Seki, H. and A. Suzuki, *Kinetic Study of Metal Biosorption to a Brown Alga, Kjellmaniella crassiforia.* Journal of Colloid and Interface Science, 2002. **246**(2): p. 259-262.

33. Loukidou, M.X., et al., *Diffusion kinetic study of cadmium(II) biosorption by Aeromonas caviae.* Journal of Chemical Technology & Biotechnology, 2004. **79**(7): p. 711-719.

34. Chen, D., et al., *Diffusivity of Cu2+ in calcium alginate gel beads.* Biotechnology and Bioengineering, 1993. **41**(7): p. 755-760.

35. Jang, L.K., *Diffusivity of Cu2+ in calcium alginate gel beads.* Vol. 43. 1994. 183-5.

36. Lewandowski, Z. and F. Roe, *Diffusivity of Cu2+ in Calcium Alginate Gel Beads - Recalculation.* Biotechnology and Bioengineering, 1994. **43**(2): p. 186-187.

37. Yang, J.B. and B. Volesky, *Intraparticle diffusivity of Cd ions in a new biosorbent material.* Journal of Chemical Technology and Biotechnology, 1996. **66**(4): p. 355-364.

38. Choy, K.K.H., et al., *Film and intraparticle mass transfer during the adsorption of metal ions onto bone char.* Journal of Colloid and Interface Science, 2004. **271**(2): p. 284-295.

39. Puranik, P.R., J.M. Modak, and K.M. Paknikar, *A comparative study of the mass transfer kinetics of metal biosorption by microbial biomass.* Hydrometallurgy, 1999. **52**(2): p. 189-197.

40. McKay, G., *Solution to the homogeneous surface diffusion model for batch adsorption systems using orthogonal collocation.* Chemical Engineering Journal, 2001. **81**(1-3): p. 213-221.

41. Chu, K.H. and M.A. Hashim, *Quantitative analysis of copper biosorption by the microalga Chlorella vulgaris.* Environmental Engineering Science, 2004. **21**(2): p. 139-147.

42. Ei-Naas, M.H., et al., *Effect of competitive interference on the biosorption of lead(II) by Chlorella vulgaris.* Chemical Engineering and Processing, 2007. **46**(12): p. 1391-1399.

43. Chu, K.H., *Removal of copper from aqueous solution by chitosan in prawn shell: adsorption equilibrium and kinetics.* Journal of Hazardous Materials, 2002. **90**(1): p. 77-95.

44. Thomas, H.C., *Heterogeneous ion exchange in a flowing system.* J. Am.Chem. Soc., 1944. **66**: p. 1664-1666.

45. McKay, G. and M.J. Bino, *Fixed bed adsorption for the removal of pollutants from water.* Environmental Pollution, 1990. **66**(1): p. 33-53.

46. Kumar, U. and M. Bandyopadhyay, *Fixed bed column study for Cd(II) removal from wastewater using treated rice husk.* Journal of Hazardous Materials, 2006. **129**(1-3): p. 253-259.

47. Ramesh, S.T., et al., *Breakthrough Data analysis of Adsorption of Cd (II) on coir pith column.* Electronic Journal of Environmental, Agricultural and Food Chemistry, 2011. **10**.

48. Zulfadhly, Z., M.D. Mashitah, and S. Bhatia, *Heavy metals removal in fixed-bed column by the macro fungus Pycnoporus sanguineus.* Environmental Pollution, 2001. **112**(3): p. 463-470.

49. Lodeiro, P., R. Herrero, and M.E.S. de Vicente, *The use of protonated Sargassum muticum as biosorbent for cadmium removal in a fixed-bed column.* Journal of Hazardous Materials, 2006. **137**(1): p. 244-253.

50. Ko, D.C.K., J.F. Porter, and G. McKay, *Optimised correlations for the fixed-bed adsorption of metal ions on bone char.* Chemical Engineering Science, 2000. **55**(23): p. 5819-5829.

51. Volesky, B. and I. Prasetyo, *Cadmium Removal in a Biosorption Column.* Biotechnology and Bioengineering, 1994. **43**(11): p. 1010-1015.

52. Hatzikioseyian, A., M. Tsezos, and F. Mavituna, *Application of simplified rapid equilibrium models in simulating experimental breakthrough curves from fixed bed biosorption reactors.* Hydrometallurgy, 2001. **59**(2-3): p. 395-406.

53. Ko, D.C.K., J.F. Porter, and G. McKay, *Film-pore diffusion model for the fixed-bed sorption of copper and cadmium ions onto bone char.* Water Research, 2001. **35**(16): p. 3876-3886.

54. Purnomo, C.W. and A. Prasetya. *The study of adsorption breakthrough curves of Cr(VI) on Bagasse fly ash (BFA).* in *World Congress on Engineering and Computer science.* 2007. San Francisco, US.

55. Aksu, Z. and T. Kutsal, *Determination of kinetic parameters in the biosorption of copper(II) on Cladophora sp., in a packed bed column reactor.* Process Biochemistry, 1998. **33**(1): p. 7-13.

56. Park, I.S., *Numerical analysis of fixed bed adsorption kinetics using orthogonal collocation.* Korean Journal of Chemical Engineering, 2002. **19**(6): p. 1001-1006.

57. Radcliffe, D.F., L.J. Leng, and G. Thomas, *Direct Measurement of External Mass-Transfer in Packed Sorbent Beds.* Aiche Journal, 1982. **28**(2): p. 344-346.

58. Cooney, D.O., *Determining External Film Mass-Transfer Coefficients for Adsorption Columns.* Aiche Journal, 1991. **37**(8): p. 1270-1274.

59. Borba, C.E., et al., *Removal of nickel(II) ions from aqueous' solution by biosorption in a fixed bed column: Experimental and theoretical breakthrough curves.* Biochemical Engineering Journal, 2006. **30**(2): p. 184-191.

60. Volesky, B., *Biosorption process simulation tools.* Hydrometallurgy, 2003. **71**(1-2): p. 179-190.

61. Li, P., G.H. Xiu, and L. Jiang, *Adsorption and desorption of phenol on activated carbon fibers in a fixed bed.* Separation Science and Technology, 2001. **36**(10): p. 2147-2163.

62. Sulaymon, A.H., B.A. Abid, and J.A. Al-Najar, *Removal of lead copper chromium and cobalt ions onto granular activated carbon in batch and fixed-bed adsorbers.* Chemical Engineering Journal, 2009. **155**(3): p. 647-653.

63. Rehm, H.J. and G. Reed, eds. *Biotechnology*. Vol. 6b. 1988.

64. Lodeiro, P., R. Herrero, and M.E.S. de Vicente, *Thermodynamic and kinetic aspects on the biosorption of cadmium by low cost materials: A review.* Environmental Chemistry, 2006. **3**(6): p. 400-418.

65. Kumar, J., C. Balomajumder, and P. Mondal, *Application of Agro-Based Biomasses for Zinc Removal from Wastewater – A Review.* CLEAN – Soil, Air, Water. **39**(7): p. 641-652.

66. Qaiser, S., A.R. Saleemi, and M. Umar, *Biosorption of lead(II) and chromium(VI) on groundnut hull: Equilibrium, kinetics and thermodynamics study.* Electronic Journal of Biotechnology, 2009. **12**(4).

2 Biosorption of cadmium (II) ions by citrus peels in a packed bed column: effect of process parameters and comparison of different breakthrough curve models[1]

2.1 Abstract

The efficiency of low cost citrus peels as biosorbents for removal of cadmium ions from aqueous solution was investigated in a fixed bed column, a process that could be applied to treat industrial wastewaters similar to commonly used ion exchange columns. Effluent concentration versus time profiles (i.e., breakthrough curves) were experimentally determined in a laboratory-scale packed bed column for varying operational parameters such as flow rate (2, 9 and 15.5 ml/min), influent cadmium concentration (5, 10 and 15 mg/L) and bed height (24, 48 and 72 cm) at pH 5.5. Column operation was most efficient for empty bed contact times of at least 10 minutes, which were apparently necessary for mass transfer. While the sorption capacity was largely unaffected by operational variables, the Thomas rate constant increased with the flow rate and slightly decreased with increasing column length. Three widely used semi-mechanistic models (Thomas, Bohart-Adams, and Yoon-Nelson) were shown to be equivalent and the generalized model was compared with a two-parameter empirical model (Dose-Response). The latter was found to be able to better simulate the breakthrough curve in the region of breakthrough and saturation.

Keywords: Biosorption; Cadmium; Citrus peels; Column; Modeling

---

[1] Chatterjee, A., S. Schiewer, Biosorption of cadmium (II) ions by citrus peels in a packed bed column: effect of process parameters and comparison of different breakthrough curve models. Published in Clean – Soil, Air, Water 2011, 39 (9), 874–881.

2.2 Introduction

Cadmium is a priority pollutant and is widely used in industries as an electrode material in nickel-cadmium batteries, stabilizers for PVC, pigments, alloy preparation and metal plating [1, 2]. Waste discharge from these industries may contaminate the aquatic environment and cause harm to the eco system because metals are not degradable and accumulate in living tissues along the food chain, eventually reaching humans. Conventional methods to remove dissolved pollutants from water include chemical precipitation, chemical oxidation-reduction, electrochemical process, membrane filtration, ion exchange and reverse osmosis [3]. These techniques are inefficient for treatment of high volumes of dilute discharge due to high reagent/energy cost, or incomplete metal removal [1, 4]. Biosorption, an adsorptive process which exploits different biomass types to sequester heavy metals from aqueous solution, has recently gained interest as a potential alternative for treating waste water as it offers some advantages over these traditional techniques. The reagent cost is low if the sorbent is a waste product and does not need additional processing such as citrus peels, a waste from fruit processing companies. The process generates minimum amounts of waste when operated in a packed bed column. A significant amount of research has been done and quite a few review articles [1, 3, 5, 6] compile data on biosorption of different heavy metals including Cd [1] using a number of low cost materials which show that the process is efficient in concentrating metals in the order of mg/g from a dilute solution in the range of mg/L. These articles do not provide much information about cadmium biosorption by orange peels, which was found to have an average capacity of about 40-130 mg Cd/g [7-11], which is higher than a number of other agricultural wastes [12] such as peanut hull, castor hull, pine bark, olive pomace, maize bran, coffee husks and other non-citrus peels [13] such as durian and banana peels. A cation exchange resin, e.g., D152 resin, which showed a capacity of 378 mg of Cd/g [14], which is 3-10 times higher than citrus peels, may be 50 times costlier. This makes citrus peels a cost-effective alternative in spite of somewhat lower capacity. Past research also showed that pectin has a higher capacity for Cd removal than other peel constituents [10] , and orange peels are

better biosorbents than other pectin rich fruit materials (grapefruit, lemon and apple peels) [4] considering both Cd uptake capacity and mechanical stability. Other studies focused on the use of the different types of citrus waste, raw and modified, for removal of metal ions such as Zn, Ni, Pb, Cu, Cr, Co [15-20] and other contaminants [21-23] from water. Most of these experiments were done using a batch reactor; indeed a sizable portion of existing biosorption related literature is focused on optimization of biosorption capacity in a batch reactor. On the other hand, a fixed bed column is commercially more viable as this type of reactors is presently used in industries that employ ion exchange resin or other commercial adsorbents. In contrast to a batch reactor or CSTR, where the sorbent is exposed to the low concentration of the effluent and therefore shows low uptake if high effluent purity is to be achieved, in packed bed columns, the driving force (concentration difference between sorbate and sorbent) remains high: the sorbent is efficiently used and shows high metal uptake since it is saturated at the relatively high influent concentration while the metal solution progressively encounters fresher and more powerful sorbent so that effluent becomes virtually metal-free when leaving column contacting the pristine sorbent. The saturated column can be regenerated in situ by eluting the bed with a suitable desorption agent. Research on packed bed columns using citrus biosorbents is very limited [15, 21] and none of them are focused on Cd.

2.3 Materials and methods

2.3.1 Protonation of citrus peels

Dried and ground processed orange peels were obtained from Alarma Consulting Corporation in Florida, USA. After washing and air-drying, 10 g of peels were suspended in 500 ml of 0.1 N nitric acid for 4 hours with constant stirring on an orbital shaker (120 rpm) at 25° C so that peels release naturally occurring light metals such as Na, K and Ca. These so called protonated peels were then filtered, rinsed 4-5 times using about 500 ml distilled water each time until the pH of the washings reached a constant value of 4.0 and dried overnight at 45° C. Enhanced biosorptive capacity was reported for protonated

peels in comparison to raw peels [24]. There was no significant weight loss in this process. Protonated peels were sieved into different size fractions. The peel particles of size 1-2 mm were used for this study. All chemicals and reagents used were of ACS-reagent grade and purchased from VWR.

2.3.2 Column characteristics

The column was made of clear extruded acrylic with a length of 30 cm and an internal diameter of 1.3 cm. The bottom 3 cm of the column was filled with spherical glass beads (diameter = 3 mm) to ensure even distribution of flow across the whole cross-section of the column. A fiber screen was placed at the top of the column to confine the peels within the column.

2.3.3 Continuous flow column system

5 g of protonated peels were 'wet packed' into the column as slurry to give a bed height of 24 cm with a void space of 70%. To increase bed height beyond 30 cm, two or three identical columns, each of 30 cm length, were serially connected (Fig. 2.1). A cadmium solution with a concentration of 5, 10 or 15 mg/L prepared from a 10,000 mg/L cadmium nitrate stock solution (VWR) was pumped from the influent reservoir (20 L) upward through the column with a flow rate of 2, 9 or 15.5 ml/min, using a peristaltic pump (VWR medium flow). The pH of the feed solution was adjusted to 5.5 using nitric acid and sodium hydroxide as this pH was optimal in a batch study [25]. The outlet of the column was attached to a fraction collector (Gilson FC203B) to collect the effluent samples intermittently which were then analyzed for cadmium (II) using an atomic absorption spectrophotometer (Perkin Elmer). All experiments were conducted at 25^0C.

2.4 Theory

2.4.1 Analysis of breakthrough curve

The performance of the packed bed column can be evaluated from breakthrough curves which were plotted as ratio of effluent concentration (C, mg/L) to influent concentration (C_0) versus process time (t, h). Breakthrough and saturation times were defined as the time when the effluent concentration reached 5% and 95% of the inlet solution, respectively. Breakthrough curves were compared in terms of breakthrough time t_b, saturation time t_s, equilibrium (maximum) uptake capacity (q_e) at saturation, removal at saturation (Y), degree of sorbent used (DoSU) and sorbent usage rate (SUR). These parameters are defined and calculated as follows: The amount of metal loaded in the column ($m_{in,t}$, mg) up to time t is the inlet concentration (C_0, mg/L) multiplied by flow rate (Q, L/h) and time (t, h).

$$m_{in,t} = C_0 \times Q \times t \tag{2.1}$$

The amount of unadsorbed metal ($m_{out,t}$, mg) at time t can be obtained from the area under the dimensionless breakthrough curve up to time t multiplied by inlet concentration (C_0, mg/L), and flow rate (Q, ml/min):

$$m_{out,t} = C_0 \times Q \times \int_0^t \left(\frac{C}{C_0}\right) dt \tag{2.2}$$

The amount of metal adsorbed in the column at time t ($m_{ad,t}$, mg) can be determined as:.

$$m_{ad,t} = m_{in,t} - m_{out,t} \tag{2.3}$$

The equilibrium (maximum) uptake capacity (q_e, mg/g) then can be calculated as the total mass of metal adsorbed at saturation ($m_{ad,ts}$ mg) to the mass of adsorbent in column (M, g)

$$q_e = \frac{m_{ad,t_s}}{M} = \frac{C_0 \times Q \times \int_0^{t_s} \left(1 - \frac{C}{C_0}\right) dt}{M} \tag{2.4}$$

Similarly, uptake at breakthrough can be calculated as:

$$q_b = \frac{m_{ad,t_b}}{M} = \frac{C_0 \times Q \times \int_0^{t_b} \left(1 - \frac{C}{C_0}\right) dt}{M} \tag{2.5}$$

Removal at saturation (Y) is expressed as the fraction of the total metal loaded in the column ($m_{in,ts}$) that is actually adsorbed into the column at saturation ($m_{ad,ts}$).

$$Y = \frac{m_{ad,t_s}}{m_{in,t_s}} = \frac{m_{ad,t_s}}{C_0 \times Q \times t_s} \tag{2.6}$$

Degree of sorbent used (DoSU) is obtained as the ratio of uptake at breakthrough (q_b) to the capacity at equilibrium (q_e).

$$DoSU = \frac{q_b}{q_e} \tag{2.7}$$

DoSU is related to the effective use of the column because in an ideal reactor, saturation time would be equal to the breakthrough time signifying 100% utilization of the maximum capacity of the column, i.e., DoSU = 1. SUR signifies the mass of sorbent required for obtaining a unit volume of clean effluent (before breakthrough),

$$SUR = \frac{M}{V_b} = \frac{M}{Q \times t_b} \tag{2.8}$$

where V_b is the breakthrough volume. The shape of the breakthrough curve partially depends on the adsorption equilibrium and the mass transfer factors, which are influenced by the hydrodynamic conditions. Therefore it was hypothesized that some or all of these parameters varied with operational condition such as inlet concentration (C_0, mg/L), flow rate (Q, L/h or ml/min) and bed height (Z, cm).

2.4.2 Mathematical modeling of breakthrough curve

The objective of modeling the breakthrough curve is to derive design parameters, which can be used to describe the breakthrough curve for given experimental conditions or, depending on the 'mechanistic' basis of the model, extrapolate results for scaling up. Developing a fully mechanistic model for column biosorption is inherently difficult

because this is an unsteady state process. A large number of mass transfer parameters are needed to incorporate the effect of axial dispersion, film diffusion resistance and intra-particle diffusion resistance (which includes pore and surface diffusion). These parameters can only be obtained by solving multiple partial differential equations simultaneously which is mathematically challenging. Semi-mechanistic models were derived by making suitable assumptions that simplified the mathematics involved in a mechanistic model, at the cost of limiting its scope of application as some of these assumptions may not be on par with the actual situation. An empirical model, on the other extreme, lacks the physical significance of its parameters and cannot be used to draw any mechanistic conclusion from the good fit of the model. The purpose of this study was to apply both a semi mechanistic and an empirical model to determine which breakthrough model best fits the experimental data.

2.4.2.1 Thomas Model

The model [26] assumes that adsorption kinetics follows pseudo second order rate law, which at equilibrium corresponds to the Langmuir isotherm and a plug flow without dispersion. The model has the following simplified form [27-35]

$$\frac{C}{C_0} = \frac{1}{1+\exp\left(\frac{k_{Th}q_{Th}M}{Q} - k_{Th}C_0 t\right)} \tag{2.9}$$

where q_{th} is the equilibrium uptake capacity (mg/g), k_{Th} is the Thomas rate constant (L $h^{-1}mg^{-1}$).

2.4.2.2 Bohart-Adams Model

The model was derived assuming irreversible adsorption and ideal plug flow [36]. The final form of the model can be expressed as [37]

$$\frac{C}{C_0} = \frac{1}{1+\exp\left(\frac{k_{BA}N_0Z}{u} - k_{BA}C_0t\right)} \tag{2.10}$$

where N_0 is the equilibrium volumetric sorption capacity (mg/L), k_{BA} is Bohart-Adams rate constant (L $h^{-1}mg^{-1}$) and u is the linear flow velocity in cm h^{-1}.

2.4.2.3 Yoon-Nelson Model

The model equation is [38]:

$$\ln\frac{C}{C_0 - C} = k_{YN}t - \tau k_{YN} \tag{2.11}$$

where k_{YN} is the Yoon Nelson rate constant (h^{-1}) and τ is the time when effluent concentration reaches 50% of the influent concentration.

2.4.2.4 Dose-Response Model

The above three models (Eq. 2.9, 2.10, 2.11) predict a non-zero value of C/C_0 at time t = 0 which is not true in reality. This may lead to an underestimation of breakthrough time. To overcome this shortfall, an empirical Dose-Response (DR) model, which is common in the field of pharmacology, was used to model breakthrough curves. The model has the following form [39].

$$\frac{C}{C_0} = 1 - \frac{1}{1+\left(\frac{t}{\beta}\right)^{\alpha}} \tag{2.12}$$

where α, β are the parameters, β can be interpreted as the time when effluent concentration reaches 50% of the influent concentration.

2.5 Results and discussion

2.5.1 Effect of flow rate

To investigate the effect of flow rate, packed bed experiments were conducted at three different flow rates (Table 2.1, Runs # 3, 4, 5) keeping other variables constant. Fig. 2.2 shows that with increasing flow rate, both breakthrough time and saturation time are decreased though not in the same proportion. As a result, breakthrough curves are shifted to the origin and become steeper. This reduction in breakthrough time (107 to 7 h) is related to the efficiency of the process as the uptake capacity before breakthrough is also decreased (25 to 14 mg/g). On the other hand, the maximum cadmium uptake capacity of citrus peels remained nearly constant over the range of flow rates studied. This is expected as the equilibrium solid phase concentration, which was approximately 44 mg/g for all runs (Table 2.1), is determined by the corresponding liquid phase concentration according to the adsorption isotherm and should not be influenced by the flow rate. The steady decrease in the uptake at breakthrough q_b and the constant equilibrium uptake q_e explain the rapid drop in DoSU with increasing flow rate (Table 2.1). This means that the sorbent is not efficiently used at the highest flow rate, which is further discussed in section 4.3.

2.5.2 Effect of inlet concentration

For 5 mg/L influent cadmium concentration (Table 2.1, Run # 1), breakthrough occurred after 36 h. The breakthrough curve (Fig. 2.3) was marked by a very broad trailing edge, related to a broad sorption zone, which means it was difficult to saturate the column completely. Cooney [40] explained similar observations as diffusion-limited mass transfer. The influent cadmium concentration was then doubled (Run # 3) and tripled (Run # 2) in two successive runs keeping all other parameters constant and the corresponding breakthrough time decreased to 19 h and 12 h respectively. Such a decrease is expected since more Cd entered the column. Uptake at breakthrough remained relatively constant (about 19 mg/g, Table 2.1). Variation of equilibrium uptake

was not significant either, possibly the inlet concentration was in the plateau region of the isotherm. For 10 mg/L inlet concentration, removal at saturation was 65.3 % with lower removal at the two other inlet concentrations. Decrease of removal percentage at saturation with increase in inlet concentration was reported earlier [31]. It should be noted however, that though the removal at saturation was 65.3%, it was always close to 100% for operation till breakthrough.

SUR increased with increasing concentration, i.e., more sorbent is necessary to treat a more concentrated feed solution, as expected. Since sorbent mass and flow rate were constant, the decrease in SUR was according to equation 8 due to an increase in breakthrough time with decreasing feed concentration. As SUR is defined on a per volume basis, treating the same mass of cadmium in a larger solution volume leads to decreasing SUR, which would not be the case if the amount of sorbent mass was related to the mass of incoming cadmium till breakthrough. Since nearly all incoming cadmium before breakthrough is removed, the sorbent used per incoming sorbate is approximated by the inverse of the uptake at breakthrough:

$$M/m_{in,tb} \approx M/m_{ad,tb} = 1/q_b \qquad (2.13)$$

Uptake at breakthrough was almost constant for the different feed concentrations. This means, on a mass basis, the same amount of sorbent is needed for a given amount of metal entering the column, be it in a small volume of more concentrated solution or a larger volume of dilute solution.

2.5.2.1 Effect of bed height

The effect of variation of bed height was investigated by conducting experiments at three different bed heights (24, 48 and 72 cm, Run # 5, 6 and 7), keeping flow rate (15.5 ml/min) and inlet concentration (10 mg/L) fixed. Breakthrough curves are shown in Figure 2.4. Longer columns obviously lead to increases in the breakthrough and

saturation times. This influence of column geometry can be accounted for by plotting these curves using the number of bed volumes treated (ratio of the total effluent volume to the empty bed volume) on the x axis (Fig. 2.5). There is almost a linear increase in DoSU with bed height ($R^2 = 0.9478$) (Table 2.1) which is to be expected because a smaller percentage of the column volume is taken up by the mass transfer zone. A broadening of this zone is however noticeable, indicating progressing dispersion with increasing length. At this point it may be worth to consider effect of flow rate and bed height together as the effect of variation of empty bed contact time (EBCT) which is equal to the volume of the empty bed divided by the flow rate, keeping inlet concentration constant. The plot of SUR versus EBCT at 10 mg/L flow rate (Fig. 2.6) shows that for short EBCT, the SUR strongly decreases before leveling off for EBCT around 10 min. This indicates that an EBCT of approximately 10 min, (corresponding to actual residence time of 7 min, void space being 70%), is necessary to allow sufficient time for mass transfer. Run # 7 with an EBCT of 13 min marked an optimized situation after which SUR did not decrease effectively with increase in EBCT. Similarly, the most effective use of the sorbent (maximal DoSU) occurred for Run #7 with an EBCT of 13 min, while the fraction of metal removed (Y) was slightly higher at the longest EBCT of 34 min for Run # 4. When the flow rate was increased from 2 ml/min to 15.5 ml/min, the residence time was decreased from 24 min to 3 min leading to the sharp decrease in breakthrough capacity from 25 mg/g to 14 mg/g. These observations correspond to batch kinetic studies where over 50% of the equilibrium uptake was achieved in 15 min for Pb binding by orange peels [24] or for Ni and Zn binding by grapefruit peels [25]. The early breakthrough at high flow rate was observed in other biosorption studies[41].

2.5.2.2 Application of models

It is important to note that in spite of different assumptions, derivations and simplifications, three models (Eq. 2.9, 2.10 and 2.11) can be expressed by the following equation where a, b are the 'lumped' parameters which are defined in Table 2.2.

$$\frac{C}{C_0} = \frac{1}{1+\exp(b-at)} \tag{2.14}$$

As implied by Eq. (2.14), the Th, BA and YN models are essentially equivalent; breakthrough curve predictions according to Eq. (2.14) represents the breakthrough curve that would otherwise be predicted by any of these three models (Eq. 2.9, 2.10 and 2.11). All three pairs of parameters (k_{Th}, q_{Th}; k_{BA}, N_0; k_{YN}, τ) can be inferred from constants 'a' and 'b' (Table 2.2) and hence are inter-convertible. Both the generalized model (Eq. 2.14) and the DR model (Eq. 2.12) were applied to the experimental breakthrough data and the model parameters were determined by minimization of the root mean square error (RMSE) by using the Excel solver function. All errors (ε) in predicting the breakthrough time in Table 2.3 are calculated as relative % error.

Only one pair of parameters is included for the Th, BA, and YN models to avoid the redundancy. Rather than listing the generalized parameters a and b, the intuitively meaningful and commonly cited Th model parameters are shown to allow easier comparison to other studies. It is notable that the parameter for uptake capacity q_{Th} was approximately constant for all model runs while the rate constant parameter k_{Th} was much lower for Run # 4, which had the lowest flow rate. It is possible that at the lowest flow rate, a thicker stagnant layer was present around the sorbent particles, causing increased film diffusion resistance. Apart from that, the relative stability of the model parameters indicates a broad applicability of the model, whereby the same model parameters could be used for different conditions.

Both models can predict the breakthrough curve well (Figs. 2.2 and 2.3), but the DR model was better able to match experimental data near breakthrough and saturation (Fig. 2.4), which was also reflected in lower RMSE values in most of these runs. Similar results were found by other researchers [39]. Breakthrough times, as expected, were underestimated by the generalized model (Eq. 2.14), but this was found to be overcorrected by DR model which predicted on average too long breakthrough times

though the average magnitude of the absolute error was reduced compared to the generalized model. Parameters from both models agreed well with experimental data, i.e., q_{Th} from Table 2.3 corresponded to q_e from Table 2.1, and the optimized model parameter β corresponds to the half-saturation time β from experiments.

Surprisingly, a huge number of journal articles compare the relative performance of the Th, BA and YN models to find the best fitting breakthrough curve, essentially fitting a set of breakthrough data repeatedly to the same equation expressed in three different forms. Evidently, identical correlation coefficients were obtained for all of these models [28, 31-34] unless redundancy was masked by the use of different regression techniques [29]. The BA model is frequently approximated by disregarding the term "1" in the denominator (Eq. (2.10)) which is valid for low values of C/C_0, causing the model to fit only in the initial segment of the curve [27, 33, 34], and rendering it apparently different from generalized model (Eq. 2.14). Indeed, the simplified Th model (Eq. (2.9)) and BA model (Eq. (2.10)) can be shown to be identical [42] by expressing the mass of the sorbent (M) and volumetric flow rate (Q) in terms of the cross-sectional area (A), superficial flow rate (u) and density of bed (ρ, mass sorbent/volume of bed) in the expression of b in the Th model to calculate $N_0 = q_{Th}\rho$. The model originally developed by Thomas [26] was a complex analytical expression that can only be simplified into this commonly used form under certain conditions [42], which incidentally corresponded to the assumptions underlying Bohart-Adam's model and hence the simplified form is identical with the BA model. Yoon and Nelson derived their model independently but the final form coincided with BA model.

In absence of any other published packed bed column studies for biosorption of cadmium by citrus peels, the present study may be compared with similar studies using either the same metal or similar biosorbents (Table 2.4). In the present study (Table 2.3), the Thomas rate constant was found to increase linearly with an increase in Q ($R^2 = 0.9956$) or decrease in Z ($R^2 = 0.9256$) but it did not follow any trend with variation in C_0. The increase of rate constants with increasing flow rates can be explained by decreasing film transfer resistance. An apparently decreasing rate constant with increasing column length

may be due to dispersion. Dispersion (which is not explicitly accounted for in the models used) leads to broadening of the mass transfer zone, similarly as for increased mass transfer resistance. Increasing Thomas rate constants with increasing Q [43], C_0 [15] or decreasing Z [44] were reported in other studies. The average Thomas rate constant found in this study was higher than that for Zn (Table 2.4) but lower than Cu for pectin rich biosorbents, and maximum values of saturated uptake were almost comparable on a per mole basis (Table 2.4). For removal of cadmium by other biosorbents in packed bed columns, such as wheat straw and chitosan, maximum saturated uptake was found to be much lower than for orange peels but average Thomas rate constants were higher. Overall, orange peels performed as good as other proven biosorbents.

2.6 Conclusions

Citrus peels are a potential alternative to use in a packed bed column for cadmium removal. Breakthrough characteristics depend on parameters such as flow rate, inlet metal concentration and bed height. Increasing feed concentration required increased amounts of sorbent per treated volume (increased SUR), with little effect on DoSU, Y or sorbent mass required per sorbate. With increasing EBCT (due to decreasing flow rate or increasing column length), operation became more efficient (decreasing SUR, increasing Y, increasing DoSU) up to an EBCT around 10 min, a time period which apparently was sufficient for mass transfer. Three widely used semi-mechanistic models (Thomas model, Bohart-Adams model and Yoon-Nelson model) were shown to be mathematically equivalent and use of one of these models renders the use of other models redundant, a fact that is largely unnoticed so far. The capacity q_{Th} was fairly stable for all runs, while the rate constant k_{Th} increased with increasing flow rate, decreased slightly with increasing column length and was largely unaffected by the feed concentration. The above model(s) and the empirical dose response model can predict the breakthrough curves, but the latter performs better near breakthrough and saturation. The kinetics of sorption may be controlled by mass transfer factors, which necessitates use of more mechanistic model in future.

2.7 Acknowledgments

This research was supported in part by the National Research Initiative of the USDA Cooperative State Research, Education, and Extension Service, grant number 2005-35504-16092. Orange peels were provided by Alarma Consulting Corporation in Florida. *The authors have declared no conflict of interest.*

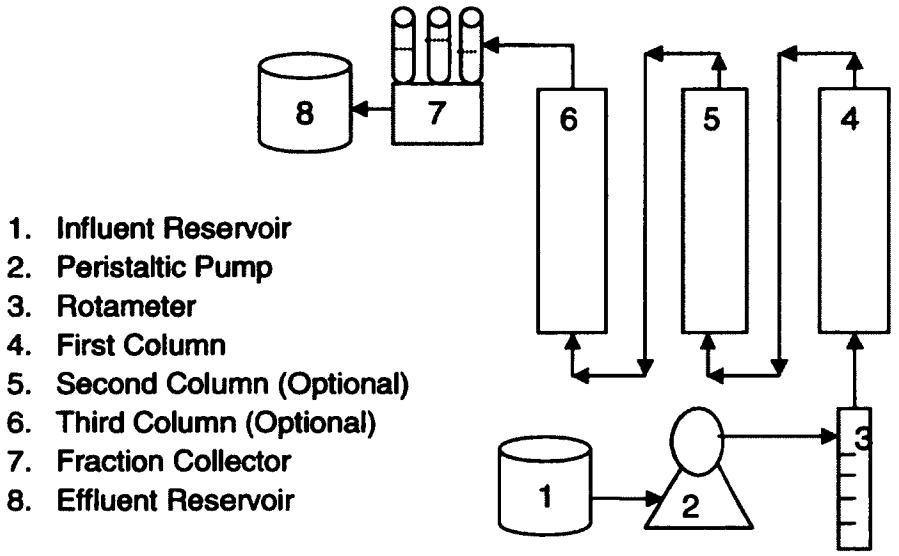

Figure 2.1 Schematic diagram of experimental set-up for packed bed column study

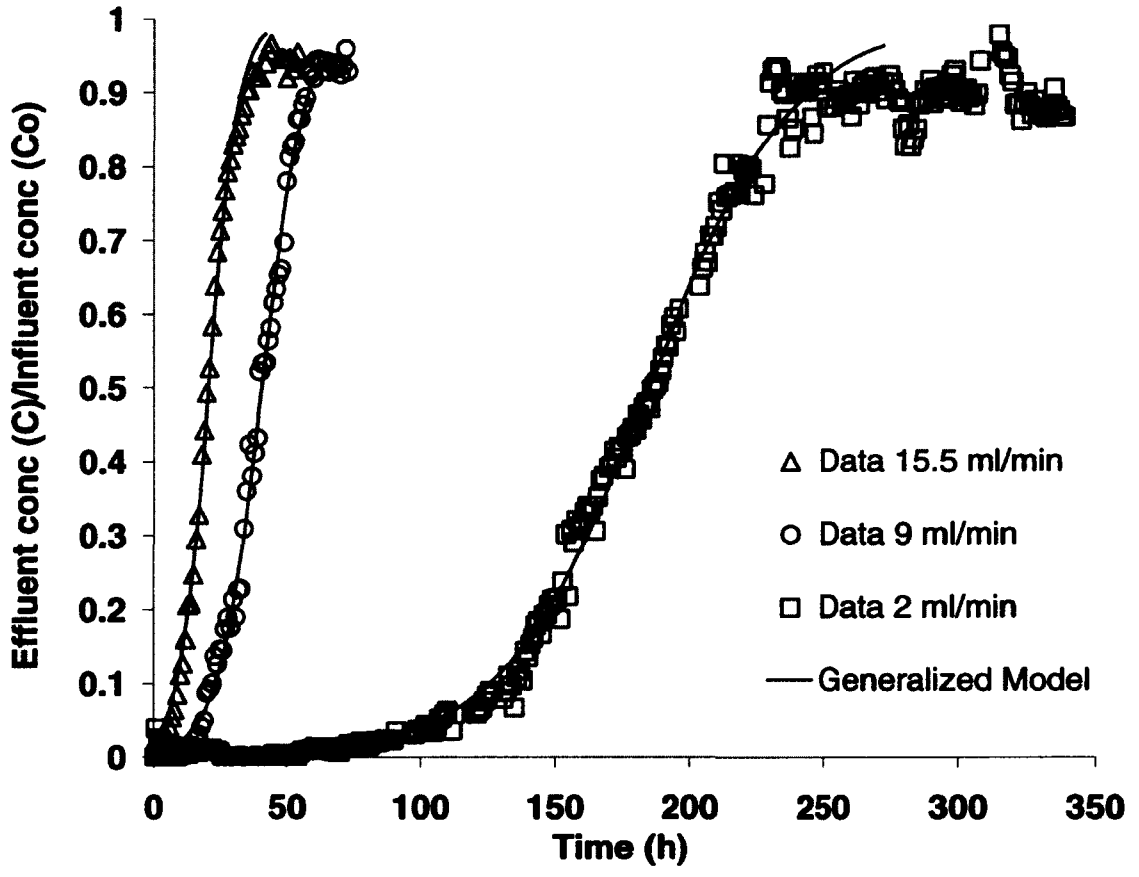

Figure 2.2 Breakthrough curves for biosorption of cadmium onto protonated citrus peels at different flow rates (bed height = 24 cm, inlet cadmium concentration = 10 mg/L, pH 5.5).

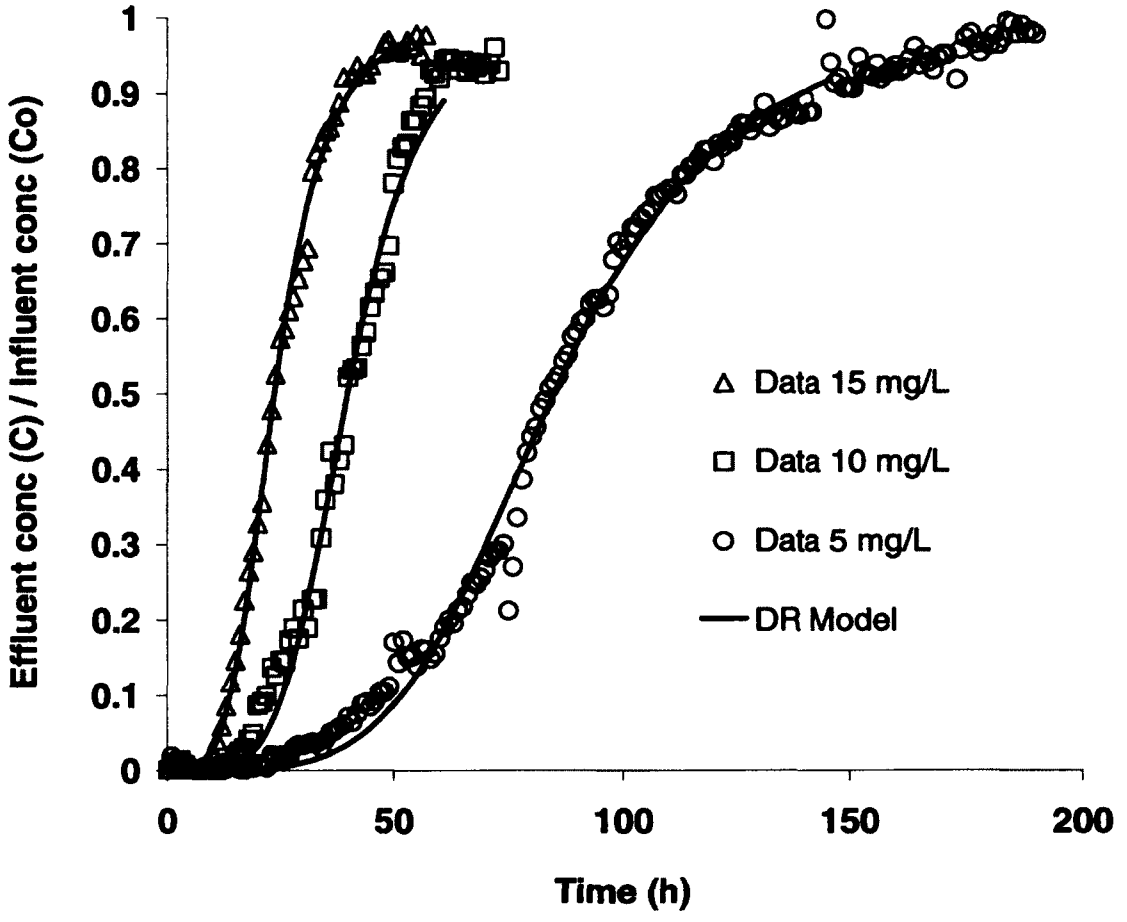

Figure 2.3 Breakthrough curves for biosorption of cadmium onto protonated citrus peels at different inlet cadmium concentrations (flow rate = 9 ml/min, bed height = 24 cm, pH 5.5).

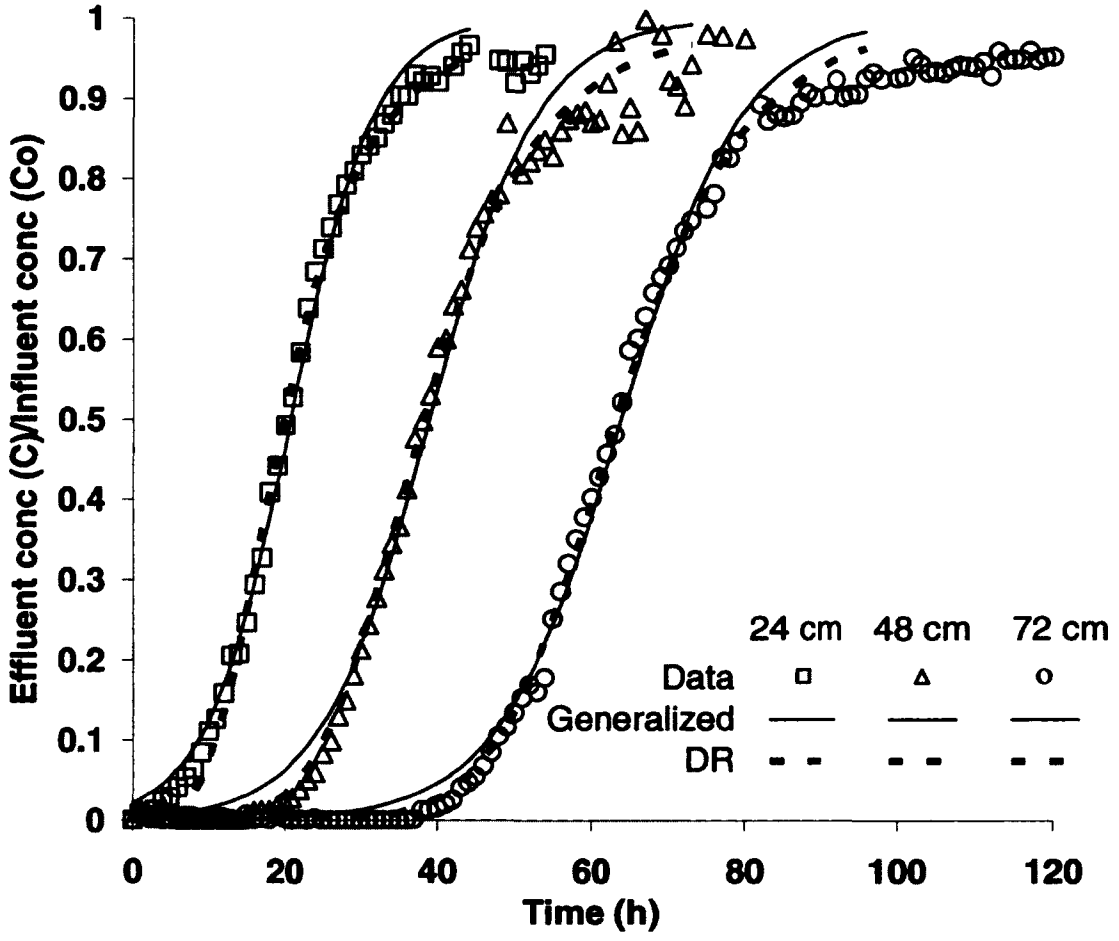

Figure 2.4 Breakthrough curves for biosorption of cadmium onto protonated citrus peels at different bed heights (flow rate = 15.5 ml/min, inlet cadmium concentration = 10 mg/L, pH 5.5).

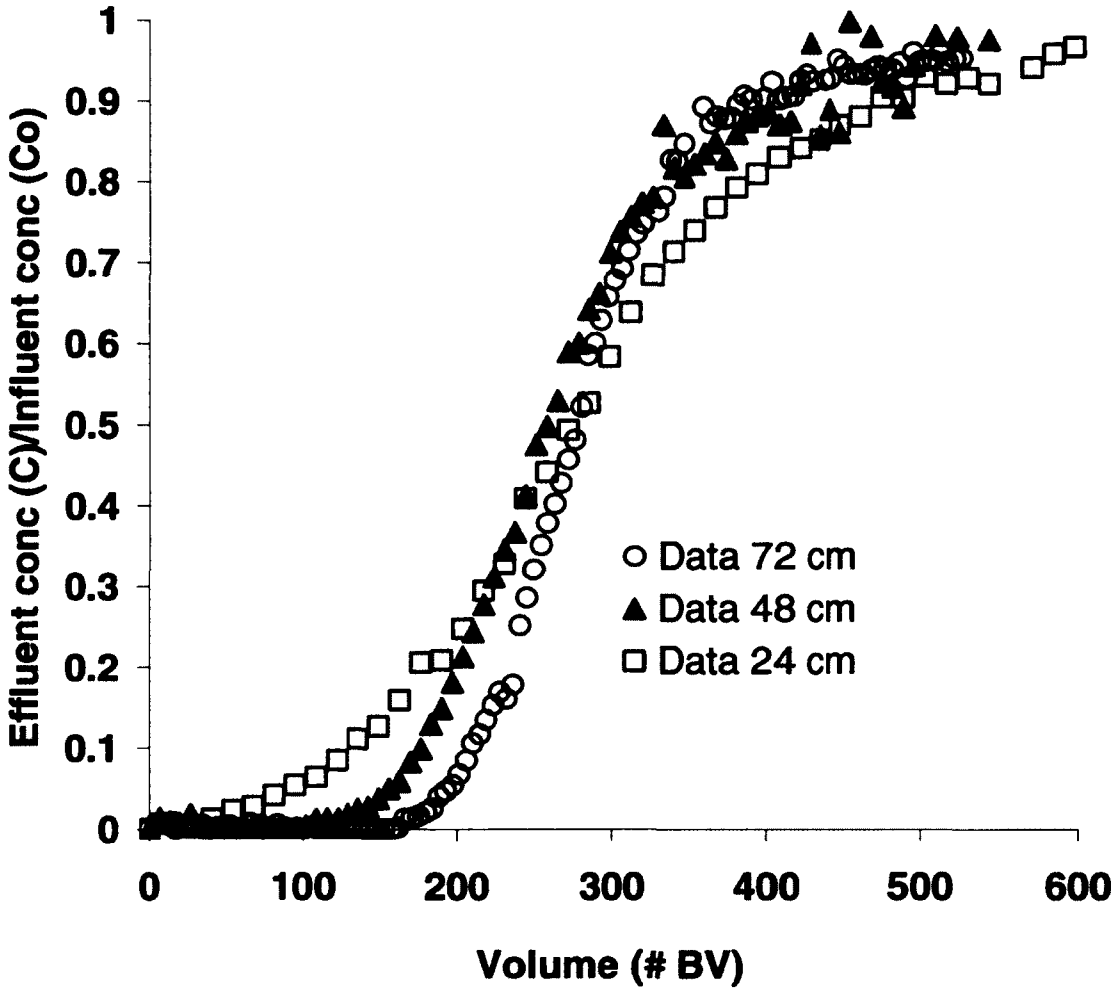

Figure 2.5 Breakthrough curves for biosorption of cadmium onto protonated citrus peels at different bed heights plotted in terms of number of bed volumes treated (flow rate = 15.5 ml/min, inlet cadmium concentration = 10 mg/L, pH 5.5).

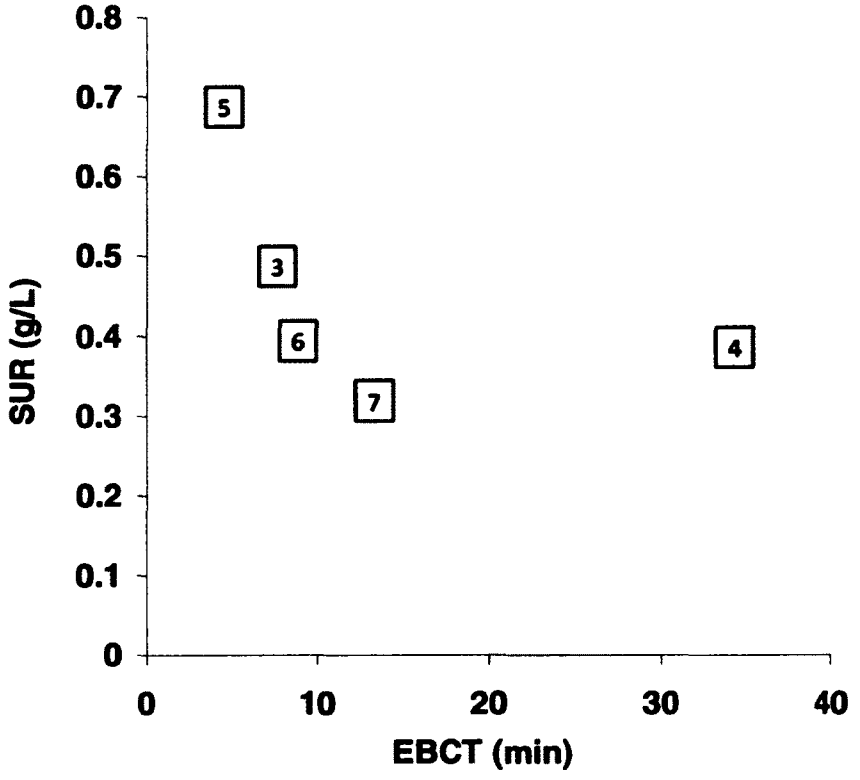

Figure 2.6 Effect of EBCT on SUR at inlet cadmium concentration = 10 mg/L. The number indicating the data point marker refers to the run # specified in Table 2.1.

Table 2.1 Influence of experimental conditions on biosorption of protonated citrus peels for removal of cadmium in a packed bed column

Run #	C_0 (mg/L)	Q (ml/min)	Z (cm)	t_b (h)	t_s (h)	q_e (mg/g)	q_b (mg/g)	Y (%)	DoSU (%)	EBCT (min)	SUR (g/L)
1		9	24	36	146	44	18	60	41	7.6	0.26
2		9	24	12	49	43	19	52	44	7.6	0.77
3			24	19	61	43	21	65	48	7.6	0.49
4	10		24	107	273	45	25	75	55	34	0.39
5	10			7	35	43	14	52	32	4.4	0.77
6	10	15.5		23	73	42	24	63	58	8.8	0.42
7	10	15.5		45	96	43	29	71	68	13	0.32

Table 2.2 Parameters 'a' and 'b' of general model Eq. (2.14) expressed in terms of parameters of different models

	Thomas (Th)	Bohart-Adams (BA)	Yoon-Nelson (YN)
a	$k_{Th}C_0$	$k_{BA}C_0$	k_{YN}
b	$k_{Th}q_{Th}M/Q$	$k_{BA}N_0Z/u$	$k_{YN}\tau$

Table 2.3. Parameters of generalized model and DR Model and deviation from experimental data

	generalized BA/Th/YN model						DR Model					
Run	k_{Th}	q_{Th}	t_b^{model}	$\varepsilon(t_b)$	RMSE		α	β^{model}	β^{exp}	t_b^{model}	$\varepsilon(t_b)$	RMSE
#	ml mg^{-1} min^{-1}	mg g^{-1}	h	%				h	h	h	%	
1	0.19	44	31	-13	0.15		4.43	85	84	44	22	0.13
2	0.20	41	8.9	-26	0.44		4.12	24	24	12	-3.3	0.30
3	0.21	44	17	-8.6	0.23		4.91	40	40	21	11	0.34
4	0.07	43	106	-0.63	0.23		6.75	183	186	119	11	0.23
5	0.32	41	4.6	-35	0.25		3.67	20	21	8.9	27	0.17
6	0.25	41	18	-20	0.37		5.25	38	38	22	-4.1	0.27
7	0.23	40	39	-14	0.23		7.81	63	64	43	-3.4	0.12

Table 2.4 Comparison of equilibrium uptake capacities and Thomas rate constants for removal of Cd by different biosorbents and for removal of other metals by pectin-based biosorbents in packed bed column

Biosorbent	Metal	C	Q	Z	Max q_e	k_{th}	Reference
		mg/L	ml/min	cm	mmol/g	ml/(mmol min)	
Orange peel	Cd	5-15	2-15.5	24-75	0.40	7.8-36	This study
Orange waste	Zn	20-40	8.5	37	0.44	4.3-6.3	[15]
Sugar beet pectin	Cu	25	2	5.25	0.41	31	[43]
Wheat straw	Cd	100	300	50-200	0.15	27-41	[44]
Chitosan	Cd	10	3	9	0.36	34	[45]

2.8 References

[1] P. Lodeiro, R. Herrero, M. E. S. De Vicente, Thermodynamic and Kinetic Aspects on the Biosorption of Cadmium by Low Cost Materials: A Review, *Environ. Chem.* **2006**, 3(*6*), 400.

[2] P. G. C. Campbell, Cadmium - a Priority Pollutant, *Environ. Chem.* **2006**, 3(*6*), 387.

[3] V. O. Arief, K. Trilestari, J. Sunarso, N. Indraswati, S. Ismadji, Recent Progress on Biosorption of Heavy Metals from Liquids Using Low Cost Biosorbents: Characterization, Biosorption Parameters and Mechanism Studies, *Clean-Soil Air Water.* **2008**, 36(*12*), 937.

[4] S. Schiewer, S. B. Patil, Pectin-Rich Fruit Wastes as Biosorbents for Heavy Metal Removal: Equilibrium and Kinetics, *Bioresour. Technol.* **2008**, 99(*6*), 1896.

[5] A. Demirbas, Heavy Metal Adsorption onto Agro-Based Waste Materials: A Review, *J. Hazard. Mater.* **2008**, 157(*2-3*), 220.

[6] K. Vijayaraghavan, Y. S. Yun, Bacterial Biosorbents and Biosorption, *Biotechnol. Adv.* **2008**, 26(*3*), 266.

[7] S. Schiewer, S. B. Patil, Modeling the Effect of Ph on Biosorption of Heavy Metals by Citrus Peels, *J. Hazard. Mater.* **2008**, 157(*1*), 8.

[8] A. B. Perez-Marin, V. M. Zapata, J. F. Ortuno, M. Aguilar, J. Saez, M. Llorens, Removal of Cadmium from Aqueous Solutions by Adsorption onto Orange Waste, *J. Hazard. Mater.* **2007**, 139(*1*), 122.

[9] A. B. Perez-Marin, A. Ballester, F. Gonzalez, M. L. Blazquez, J. A. Munoz, J. Saez, V. M. Zapata, Study of Cadmium, Zinc and Lead Biosorption by Orange Wastes Using the Subsequent Addition Method, *Bioresour. Technol.* **2008**, 99(*17*), 8101.

[10] S. Schiewer, M. Iqbal, The Role of Pectin in Cd Binding by Orange Peel Biosorbents: A Comparison of Peels, Depectinated Peels and Pectic Acid, *J. Hazard. Mater.* **2010**, 177(*1-3*), 899.

[11] X. Li, Y. Tang, Z. Xuan, Y. Liu, F. Luo, Study on the Preparation of Orange Peel Cellulose Adsorbents and Biosorption of Cd2+ from Aqueous Solution, *Sep. Purif. Technol.* **2007**, 55(*1*), 69.

[12] T. K. Sen, M. Mohammod, S. Maitra, B. K. Dutta, Removal of Cadmium from Aqueous Solution Using Castor Seed Hull: A Kinetic and Equilibrium Study, *Clean-Soil Air Water.* **2010**, 38(*9*), 850.

[13] W. Saikaew, P. Kaewsarn, Cadmium Ion Removal Using Biosorbents Derived from Fruit Peel Wastes *Songklanakarin J. Sci. Technol.* **2009**, 31(*5*), 547.

[14] C. H. Xiong, C. P. Yao, Study on the Adsorption of Cadmium(II) from Aqueous Solution by D152 Resin, *J. Hazard. Mater.* **2009**, 166(*2-3*), 815.

[15] A. B. P. Marin, M. I. Aguilar, J. F. Ortuno, V. F. Meseguer, J. Saez, A. Llorens, Biosorption of Zn(II) by Orange Waste in Batch and Packed-Bed Systems, *Journal of Chemical Technology and Biotechnology*. **2010**, 85(*10*), 1310.

[16] M. Ajmal, R. A. K. Rao, R. Ahmad, J. Ahmad, Adsorption Studies on Citrus Reticulata (Fruit Peel of Orange): Removal and Recovery of Ni(II) from Electroplating Wastewater, *J. Hazard. Mater.* **2000**, 79(*1-2*), 117.

[17] A. Balaria, S. Schiewer, Assessment of Biosorption Mechanism for Pb Binding by Citrus Pectin, *Sep. Purif. Technol.* **2008**, 63(*3*), 577.

[18] Z. Xuan, Y. Tang, X. Li, Y. Liu, F. Luo, Study on the Equilibrium, Kinetics and Isotherm of Biosorption of Lead Ions onto Pretreated Chemically Modified Orange Peel, *Biochem. Eng. J.* **2006**, 31(*2*), 160.

[19] G. Annadurai, R. S. Juang, D. J. Lee, Adsorption of Heavy Metals from Water Using Banana and Orange Peels, *Water Sci. Technol.* **2003**, 47(*1*), 185.

[20] F. A. Pavan, I. S. Lima, É. C. Lima, C. Airoldi, Y. Gushikem, Use of Ponkan Mandarin Peels as Biosorbent for Toxic Metals Uptake from Aqueous Solutions, *J. Hazard. Mater.* **2006**, 137(*1*), 527.

[21] B. K. Biswas, K. Inoue, K. N. Ghimire, S. Ohta, H. Harada, K. Ohto, H. Kawakita, The Adsorption of Phosphate from an Aquatic Environment Using Metal-Loaded Orange Waste, *J. Colloid Interface Sci.* **2007**, 312(*2*), 214.

[22] K. N. Ghimire, K. Inoue, H. Yamaguchi, K. Makino, T. Miyajima, Adsorptive Separation of Arsenate and Arsenite Anions from Aqueous Medium by Using Orange Waste, *Water Res.* **2003**, 37(*20*), 4945.

[23] C. Namasivayam, N. Muniasamy, K. Gayatri, M. Rani, K. Ranganathan, Removal of Dyes from Aqueous Solutions by Cellulosic Waste Orange Peel, *Bioresour. Technol.* **1996**, 57(*1*), 37.

[24] S. Schiewer, A. Balaria, Biosorption of Pb2+ by Original and Protonated Citrus Peels: Equilibrium, Kinetics, and Mechanism, *Chem. Eng. J.* **2009**, 146(*2*), 211.

[25] M. Iqbal, S. Schiewer, R. Cameron, Mechanistic Elucidation and Evaluation of Biosorption of Metal Ions by Grapefruit Peel Using FTIR Spectroscopy, Kinetics and Isotherms Modeling, Cations Displacement and EDX Analysis, *Journal of Chemical Technology and Biotechnology*. **2009**, 84(*10*), 1516.

[26] H. C. Thomas, Heterogeneous Ion Exchange in a Flowing System, *J. Am.Chem. Soc.* **1944**, 66, 1664.

[27] Z. Aksu, F. Gonen, Biosorption of Phenol by Immobilized Activated Sludge in a Continuous Packed Bed: Prediction of Breakthrough Curves, *Process Biochem.* **2004**, 39(*5*), 599.

[28] K. Vijayaraghavan, D. Prabu, Potential of Sargassum Wightii Biomass for Copper(II) Removal from Aqueous Solutions: Application of Different Mathematical Models to Batch and Continuous Biosorption Data, *J. Hazard. Mater.* **2006**, 137(*1*), 558.

[29] P. Sivakumar, P. N. Palanisamy, Packed Bed Column Studies for the Removal of Acid Blue 92 and Basic Red 29 Using Non-Conventional Adsorbent, *Indian J. Chem. Technol.* **2009**, 16(*4*), 301.

[30] R. P. Han, Y. Wang, W. H. Zou, Y. F. Wang, H. Shi, Comparison of Linear and Nonlinear Analysis in Estimating the Thomas Model Parameters for Methylene Blue Adsorption onto Natural Zeolite in Fixed-Bed Column, *J. Hazard. Mater.* **2007**, 145(*1-2*), 331.

[31] V. C. Srivastava, B. Prasad, I. M. Mishra, I. D. Mall, M. M. Swamy, Prediction of Breakthrough Curves for Sorptive Removal of Phenol by Bagasse Fly Ash Packed Bed, *Ind. Eng. Chem. Res.* **2008**, 47(*5*), 1603.

[32] S. Singh, V. C. Srivastava, I. D. Mall, Fixed-Bed Study for Adsorptive Removal of Furfural by Activated Carbon, *Colloids Surf., A.* **2009**, 332(*1*), 50.

[33] B. Salamatinia, A. H. Kamaruddin, A. Z. Abdullah, Modeling of the Continuous Copper and Zinc Removal by Sorption onto Sodium Hydroxide-Modified Oil Palm Frond in a Fixed-Bed Column, *Chem. Eng. J.* **2008**, 145(*2*), 259.

[34] M. Calero, F. Hernainz, G. Blazquez, G. Tenorio, M. A. Martin-Lara, Study of Cr (III) Biosorption in a Fixed-Bed Column, *J. Hazard. Mater.* **2009**, 171(*1-3*), 886.

[35] K. Naddafi, R. Nabizadeh, R. Saeedi, A. H. Mahvi, F. Vaezi, K. Yaghmaeian, A. Ghasri, et al., Biosorption of Lead(II) and Cadmium(II) by Protonated Sargassum Glaucescens Biomass in a Continuous Packed Bed Column, *J. Hazard. Mater.* **2007**, 147(*3*), 785.

[36] G. Bohart, E. Q. Adams, Some Aspects of the Behavior of Charcoal with Respect to Chlorine, *J. Am. Chem. Soc.* **1920**, 42, 523.

[37] K. H. Chu, M. A. Hashim, Copper Biosorption on Immobilized Seaweed Biomass: Column Breakthrough Characteristics, *J. Environ. Sci.* **2007**, 19(*8*), 928.

[38] Y. H. Yoon, J. H. Nelson, Application of Gas-Adsorption Kinetics .1. A Theoretical-Model for Respirator Cartridge Service Life, *Am. Ind. Hyg. Assoc. J.* **1984**, 45(*8*), 509.

[39] G. Y. Yan, T. Viraraghavan, M. Chen, A New Model for Heavy Metal Removal in a Biosorption Column, *Adsorpt. Sci. Technol.* **2001**, 19(*1*), 25.

[40] D. O. Cooney, The Importance of Axial-Dispersion in Liquid-Phase Fixed-Bed Adsorption Operations, *Chem. Eng. Commun.* **1991**, 110, 217.

[41] E. Malkoc, Y. Nuhoglu, Y. Abali, Cr(VI) Adsorption by Waste Acorn of Quercus Ithaburensis in Fixed Beds: Prediction of Breakthrough Curves, *Chem. Eng. J.* **2006**, 119(*1*), 61.

[42] K. H. Chu, Fixed Bed Sorption: Setting the Record Straight on the Bohart-Adams and Thomas Models, *J. Hazard. Mater.* **2010**, 177(*1-3*), 1006.

[43] Y. N. Mata, M. L. Blazquez, A. Ballester, F. Gonzalez, J. A. Munoz, Optimization of the Continuous Biosorption of Copper with Sugar-Beet Pectin Gels, *Journal of Environmental Management.* **2009**, 90(*5*), 1737.

[44] H. Muhamad, H. Doan, A. Lohi, Batch and Continuous Fixed-Bed Column Biosorption of Cd2+ and Cu2+, *Chem. Eng. J.* **2010**, 158(*3*), 369.

[45] N. Sankararamakrishnan, P. Kumar, V. S. Chauhan, Modeling Fixed Bed Column for Cadmium Removal from Electroplating Wastewater, *Sep. Purif. Technol.* **2008**, 63(*1*), 213.

3 Multi-resistance kinetic models for biosorption of Cd by raw and immobilized citrus peels in batch and packed bed columns[2]

3.1 Abstract

Biosorbents have to possess suitable size and stability for successful use in packed bed columns, a reactor type commonly used in industrial sorption or ion exchange processes. In the present study, two polymeric materials (calcium alginate and agar) were investigated for immobilization of citrus peels to improve biosorbent properties. Immobilized peels and raw peels pre-saturated with calcium and hydrogen ions were compared for cadmium biosorption in equilibrium and kinetic batch experiments as well as in fixed bed reactors, varying relevant parameters such as initial concentration, flow rate and bed-height. The batch equilibrium was described by Langmuir and Freundlich isotherms, with the affinity sequence being protonated raw peels (PRP)>protonated alginate immobilized peels (PALP)>agar immobilized peels (AGP)>calcinated raw peels (CRP), while the Langmuir uptake capacity followed the order PALP>CRP>PRP>AGP. Batch kinetics were described by three mass transfer models (based on external resistance, intra-particle resistance and both) and three surface reaction models (pseudo first order, pseudo second order and Langmuir kinetics). Frequently used mass transfer models such as Weber-Morris, Boyd, and Urano were reviewed, revealing the fact that these are different approximations of the same parent model. Suitability of using the Weber-Morris and Boyd plots for the purpose of determining dominating mass transfer resistance was evaluated and mathematically analogous models were identified. Breakthrough curves were simulated by a surface reaction model (Bohart-Adams). *A priori* prediction of breakthrough curves was possible by a mass transfer model

[2] Chatterjee, A. and S. Schiewer, 2012. Multi-resistance kinetic models for biosorption of Cd by raw and immobilized citrus peels in batch and packed bed columns. Prepared for submission in Bioresource Technology.

(Klinkenberg) after evaluating the external and intra-particle mass transfer coefficients from engineering correlation and batch kinetic data respectively.

Keywords: Biosorption, Batch kinetics, Film-diffusion model, Intra-particle diffusion model, Predictive breakthrough curve

Symbol	Units	Definition
A	cm^2	Area of cross-section of fixed bed column
b	L/mg	Langmuir affinity constant defined by Equation 3.13
B	min^{-1}	Parameter introduced in Equation 3.20 (= $\pi^2 D_s / R^2$)
Bi	-	The Biot number is a ratio of external film diffusivity to intra-particle diffusivity. ($Bi = R k_f/D_s$)
C	mg/L	Concentration of adsorbate in aqueous phase at time t (min)
C^*	mg/L	Hypothetical adsorbate concentration in equilibrium with q
C_0	mg/L	Initial or influent adsorbate concentration in batch or fixed bed reactor
C_∞	mg/L	Value of C at t_∞ for batch experiment
C_e	mg/L	Equilibrium adsorbate concentration in aqueous phase
C_i	mg/L	Aqueous adsorbate concentration at adsorbate-adsorbent interface
D	cm^2/min	Diffusion coefficient of adsorbate in aqueous phase
D_s	cm^2/min	Diffusion coefficient of adsorbate within the adsorbent
EBCT	min	Empty bed contact time (= V/Q = h/u)
F	-	Saturation fraction (= q/q_∞) introduced in Equation 3.16
h	cm	Bed height
K	L/g	Equilibrium constant for linear isotherm, defined by Equation 3.15
k_1	1/min	Pseudo 1st order rate constant defined by Equation 3.11
k_2	$\frac{g}{mg\ min}$	Pseudo 2nd order rate constant defined by Equation 3.12

k_{ad}	$\frac{L}{mg\ min}$	Second order forward rate constant for Equation 3.10
k_{BA}	$\frac{ml}{mg\ min}$	Rate constant defined by Equation 3.18
k_{de}	1/min	First order reverse rate constant for Equation 3.10
k_f	cm/min	External or film mass transfer coefficient defined in Equation 3.4
K_f	cm/min	Overall fluid phase mass transfer coefficient defined in Equation 3.35
K_F	$L^{1/\mu}/(g\ mg^{1/\mu-1})$	Freundlich isotherm parameter
k_S	cm/min	Intra-particle mass transfer coefficient defined in Equation 3.7
K_S	cm/min	Overall solid phase mass transfer coefficient
M	g	Mass of adsorbent in the reactor (batch/fixed bed)
n	-	Integer used in Equation 3.19, Equation 3.20, Equation 3.25, Equation 3.29, Equation 3.30 to define infinite series
N_0	mg/ml	Bohart Adams Parameter defined by Equation 3.18
q	mg/g	Average concentration of adsorbate within the adsorbent at time t
Q	ml/min	Flow rate
q'	mg/g	Adsorbate concentration within adsorbent at a radius r from adsorbent center
q_∞	mg/g	Value of q at t_∞
q_{BA}	mg/g	Parameter in BA model
q_{bt}	mg/g	Value of q at breakthrough time
q_e	mg/g	Equilibrium adsorbate concentration in adsorbent
q_i	mg/g	Concentration of adsorbate within adsorbent at the adsorbate-adsorbent interface
q_m	mg/g	Maximum concentration of adsorbate within adsorbent at high sorbate conc.
R	cm	Radius of adsorbent particle

Re	-	The Reynolds number is the ratio of inertial forces to viscous forces (= 2 R u/ν)
S'	cm^{-1}	Adsorbent particle surface area per volume of liquid in reactor = $(1-\varepsilon)\, S_0/\varepsilon = S_o M/(V_s \rho)$
S_0	cm^{-1}	Adsorbent particle surface area per unit particle volume (= 3/R)
Sc	-	The Schmidt number signifies the ratio of momentum diffusivity (viscosity) and mass diffusivity. (= ν/D)
Sh	-	The Sherwood number represents the ratio of convective to diffusive mass transport. (= 2 k_f R/D)
t_b	min	Breakthrough time
t_∞	min	Duration of batch experiment or saturation time in fixed bed experiment
u	cm/h	Superficial velocity within column = Q/A
v	cm/h	Interstitial velocity within column = u/ε
V	mL	Volume of reactor (batch or fixed bed)
V_s	mL	Volume of aqueous phase = V ε
Z	cm	Axial distance coordinate, positive in the flow direction (vertically upflow in the present context)
α	-	Ratio of adsorbate remaining in liquid phase to bound, used in Equation 3.26
β	-	Parameter used in Equation 3.31
γ	-	Parameter used in Equation 3.25
δ	-	Tortuosity
ε	-	Void fraction in column
εp	-	Sorbent porosity
λ	-	Constrictivity
ρb	g/mL	Density of packed bed = M/V
ρ	g/mL	Density of adsorbent = M/(V (1-ε))

μ	-	Freundlich isotherm exponent
ν	cm2/min	Kinematic viscosity of water at 25°C
ξ	-	Dimensionless distance defined as $\frac{h K_f S_0}{\varepsilon \nu (1-\varepsilon)}$ used in Equation 3.36
τ	-	Dimensionless time defined as $\frac{S_0 K_f}{K\rho}(t-\frac{h}{\nu})$ used in Equation 3.36

3.2 Introduction

Biosorption is defined as the sequestration of pollutants (especially heavy metals and dye) by biomass from aqueous phase through passive processes. Over the last decades, numerous articles including several reviews, examined biosorption by microbial biomass (bacteria, algae, fungi) or agro-based biomass and established the fact that most biosorbents can concentrate the metal in the order of mg/g from a dilute solution in the range of mg/L. Most of these studies focused on optimization of parameters that influence the biosorption by the investigated biomass type in a batch reactor. However, a fixed bed reactor is more suitable for commercial purposes because it ensures a maximum driving force due to a high solid-liquid concentration difference and avoids the need for subsequent solid-liquid separation. Application in packed bed columns requires the sorbent to be rigid enough to be packed into such a reactor. Unlike microbial slurry, which cannot be used without additional processing, most agro-based products including citrus peels, fulfill these criteria in general. Cost efficiency, which is the most highlighted feature of the biosorption process making it competitive with traditional metal removing processes, can be realized if raw materials in question can be available naturally or supplied as waste product from other industries. Obviously, such sources do not guarantee the physical uniformity of the product. Past research shows citrus peels can be successfully used in packed bed reactor [1], however some types of citrus peels showed problems of clogging and disintegration in packed bed reactors but performed well in batch mode. This necessitates appropriate processing, as done in the present work, to make it suitable for use in a column reactor regardless of its initial shape and size. Immobilization of microbial biomass within a natural or synthetic polymeric matrix has been shown to be effective in this regard; however such processing has not been widely explored for agro-based biomass. The most commonly used immobilization matrices are: alginate [2], agar [2], silica gel [3], polysulfone [4], agarose [5], polyacrylamide [6]; arranged in the order of increasing cost, according to Sigma Chemical Company, 2011. In this study, alginate and agar were chosen as matrix materials because of low cost and

ease of preparation. Polyacrylamide [7] was reported to generate free radicals during the process of immobilization, which are harmful to humans; polysulphone [4] requires dimethylformamide as a solvent. Polyvinyl alcohol beads were reported to be stable in alkaline pH, but its preparation requires repeated freeze-thaw cycles [7], which is time and energy consuming. One of the two main objectives of the present work was to determine a suitable immobilization method for citrus peels, producing a biosorbent that is stable, features a high uptake (affinity and capacity), as well as favorable kinetics. It is important to consider how immobilization influences the biosorption kinetics as it imposes an additional mass transfer barrier. The second main purpose of this article was to evaluate kinetic models for batch and column application to compare the mass transfer kinetics between raw and immobilized peels. The goal was to employ a simple analytically solvable two-parameter-model for *a-priori*-prediction of breakthrough curves without adjusting any parameters, but rather using parameters from other sources, such as batch experiments. A number of published articles focus on different narrow aspects such as modeling biosorption kinetics either in batch or in column mode using either native or processed biosorbents considering either mass transfer or surface reaction as the rate limiting step, but none of them describe an analytical solution for mass transfer in both batch and column as comprehensively as in the present study. There are other articles [8] which consider rigorous mathematical treatment involving a numerical solution of a set of partial differential equations (PDE) using specialized software. Often, the main objective was simply to obtain a best fit of the breakthrough curve, without consideration for the intrinsic nature of the rate constant [9-11]

3.3 Materials and methods

3.3.1 Pretreatment of citrus peels

Dried orange peels with an average size of 1-3 mm were supplied by Alarma Consulting Corporation in Florida, US. After washing and air-drying, 10 g of raw peels (RP) were suspended in 500 ml of 0.1 N nitric acid for 2 hours with constant stirring on an orbital shaker (120 rpm) at 25° C so that binding sites became saturated with hydrogen ions.

These peels will be denoted hereafter as 'protonated raw peels' (PRP). Another 10 g of peels were treated in the same manner using 2.5% calcium chloride solution to saturate binding sites with calcium ions and will be referred as 'calcinated raw peels' (CRP). Both peels types were then filtered, thoroughly washed with distilled water and dried overnight at 45° C, ground and sieved to collect PRPa (size 1-2 mm), PRPb (size < 150 μm) and CRP (size < 150 μm). There was no significant weight loss in this process. All chemicals and reagents used were of ACS-reagent grade.

3.3.2 Scanning Electron Microscopy (SEM)

PRP from two different batches of peels were examined using an ISI SR-50 SEM. To prepare specimens for SEM, PRP samples were dehydrated by using a gradient series of ethanol. The dehydrated samples were dried and sputter coated with gold.

3.3.3 Immobilization

Since the primary purpose of immobilization in this study was to increase the mechanical strength using a minimum amount of matrix material and not maximizing the uptake capacity, a series of preliminary trials was made to determine the minimum amount of supporting material required for granulation. Accordingly, existing methods of immobilization [2] were modified. In similar studies [2, 5, 12], the required amount of matrix material (alginate, agar) was much higher than what was used in this study.

3.3.3.1 Immobilization using Ca-alginate gel

RP of less than 150 μm diameter were used for this purpose. An aqueous suspension of RP (0.05 g/ml) was mixed with a 0.8% sodium alginate solution in a volume ratio of 10:5. This slurry was then dispersed drop-wise into 2.5% calcium chloride solution by a syringe and resultant beads with an average diameter of 3 mm were aged for 2 hr at 4 °C. Then beads were filtered off, and washed thoroughly with distilled water. Alginate immobilized peels (ALP) as produced are saturated with Ca ions and were used in a batch experiment only to compare its capacity with the protonated version (PALP), which were produced from ALP following the same method as used for the preparation of PRP from

RP. Both ALP and PALP were stored temporarily in distilled water until use. These beads contained 7.4% of alginate on a dry basis.

3.3.3.2 Immobilization within agar matrix

A suspension of 0.5 g PRPb in molten agar (0.3 g agar in 12 ml water) was taken in a syringe and added drop-wise into ice cold toluene:chloroform (3:1) mixture. The agar-immobilized beads (AGP) containing 37.5% agar on dry basis were filtered off, air dried to eliminate residual phase and were temporarily stored in distilled water until use.

3.3.4 Batch experiment

All batch experiments were performed at 25 °C for 4 hours in a Metrohm auto-titrator using different citrus biosorbents (0.5 g PRPa, 0.5 g CRP, 0.54 g ALP, 0.54 g PALP and 0.8 g AGP). The amount of sorbent used was always based on 0.5 g of original RP. A constant pH of 5.5 was maintained through the programmed addition of 0.01 N NaOH into the magnetically stirred titrating vessel containing a suspension of the biosorbent in 50 ml of cadmium nitrate solution, prepared from 10,000 ppm AAS standard stock solution purchased from VWR. For the isotherm experiments, the initial Cd concentration ranged from 50 to 1000 mg/L and samples were collected at the end of the experiment. For the kinetic experiments, the initial Cd concentration was 500 ppm, and 0.1 ml samples were collected from the titrating vessel at predefined time intervals. Samples were appropriately diluted, filtered using Whatman 42 filter paper and analyzed for the cadmium concentration using a flame AAS (Perkin Elmer). The metal uptake q was calculated from the mass balance (Equation 3.2) with the mass M referring to the mass of 0.5 g RP contained in each sorbent.

3.3.5 Column characteristics

The column was made of clear extruded acrylic with a length of 30 cm and an internal diameter of 1.3 cm which is large enough (compared to the particle size 1.5 mm) to neglect the edge effect. The bottom 3 cm of the column was filled with spherical glass beads (diameter = 3 mm) to ensure even distribution of flow across the whole cross-

section of the column. A fiber screen was placed at the top of the column to confine the peels within the column.

3.3.6 Fixed bed kinetic experiment

A sample of PRPa or PALP prepared using 1.5 g of RP were 'wet packed' into the column as a slurry yielding an approximate bed height of 26 cm. To increase the bed height, two or three identical columns were serially connected. A cadmium solution with a concentration of 5 or 10 mg/L prepared from a 10,000 mg/L cadmium nitrate stock solution was pumped from the influent reservoir (20 L) upward using a peristaltic pump (VWR) through the column with a flow rate of 2, 9 or 12 ml/min as measured by a rotameter. The pH of the feed solution was adjusted to 5.5 using nitric acid and sodium hydroxide as this pH was found optimal in a batch study [13]. The outlet of the column was attached to a fraction collector (Gilson FC203B) to collect the effluent intermittently. Samples were then analyzed for cadmium (II) using AAS (Perkin Elmer). All experiments were conducted at 25 °C. Calculation of q_∞ for fixed bed was performed as described in prior work by the authors [1].

3.4 Theory: Mathematical modeling

The objective of modeling was to predict or simulate the transient concentration profile of adsorbate in a batch or fixed bed reactor. Biosorption kinetics consist of the following steps: 1) Movement of adsorbate through the bulk of the solution, which is a fast process relative to others 2) Film Diffusion (FD) or external mass transfer: Diffusion of the adsorbate through the fixed layer of a stagnant liquid film surrounding the sorbent particle. 3) Intraparticle Diffusion (ID): Diffusion of adsorbate within the sorbent particle 4) Intrinsic physisorption or chemisorption where adsorbate from the fluid phase within the pore space attaches to the binding site in the solid phase. Alternatively, ID can occur after the reaction: the adsorbate species may be deposited to external surface of the sorbent particle after FD and then may diffuse along the pore surface, which is then termed solid diffusion and may be differentiated from pore diffusion for advanced

modeling. These two mechanisms (solid and pore diffusion) may act in parallel and depending on the operating condition, one may be prevalent. All of these elementary processes may influence the final rate of biosorption, but typically it is assumed that one of these steps is much slower than others and controls the overall rate. In Mass Transfer Modeling (MTM), the intrinsic sorption reaction is assumed to be fast and one (single resistance model) or both (dual resistance model) of the diffusion processes (steps 2 and 3) are taken into account. In contrast to MTM, Surface Reaction Modeling (SRM) assumes that mass transfer is instantaneous, but that the reaction at the phase boundary (step 4) is too slow to establish a local equilibrium at the interface and becomes the rate limiting step of the biosorption process. The obvious drawback of either type of modeling (MTM/SRM) is that the numerical value of a rate parameter, obtained by successful fitting of the model to data, may not reflect the intrinsic value of the parameter; it may be a lumped parameter incorporating the effect of other processes which were not included in the model derivation. Nevertheless, such a model can still be broadly applicable if the variation of this lumped parameter with other operating variables is considered. In prior work of the present authors [1], the SRM rate constant was found to vary linearly with the sorbate inlet concentration. However, this issue is especially important if the parameter in question (e.g., diffusion coefficient) needs to have a general validity so that it can be used under different circumstances. Non-applicability of a model, however, conclusively negates the underlying hypothesis. Both MTM and SRM are considered here, which involves simultaneous solution of mass balance, rate and isotherm equations.

3.4.1 Mass balance equation:

The differential form of the mass balance for batch kinetic operation is Equation 3.1 which can be integrated to Equation 3.2.

$$V_s \frac{dC}{dt} + M \frac{dq}{dt} = 0 \qquad \text{Equation 3.1}$$

$$V_s(C_0\text{-}C) = q\,M \qquad \text{Equation 3.2}$$

To save space, variables used in all equations are explained in the list of symbols above. The mass balance for continuous column operation assuming a plug flow is:

$$\left(\frac{\partial C}{\partial t}\right)_z + v\left(\frac{\partial C}{\partial Z}\right)_t + \rho\frac{(1-\varepsilon)}{\varepsilon}\left(\frac{\partial q}{\partial t}\right)_z = 0 \qquad \text{Equation 3.3}$$

3.4.2 Rate equation for batch/fixed bed:

The rate equation expresses $\frac{\partial q}{\partial t}$ in terms of C or q, and this expression makes the essential difference among different MTM/SRM models.

3.4.2.1 Mass Transfer Modeling (MTM)

1) Film diffusion (FD) is modeled based on a linear driving force (LDF) which assumes that the rate of mass transfer linearly depends on the concentration difference between the bulk aqueous concentration and the concentration at the external surface of the biosorbents:

$$\rho\frac{\partial q}{\partial t} = k_f S_0 (C - C_i) \qquad \text{Equation 3.4}$$

2) Intraparticle diffusion (ID):

a. The Homogenous Solid Diffusion Model (HSDM) assumes the sorbent particle as a non-porous solid homogenous sphere through which adsorbate molecules diffuse after their instantaneous physical attachment at the external surface following the external film diffusion. The concept can be used for porous particle as well; it basically does not distinguish among diffusion within the pore space, diffusion along the surface of the adsorbent and diffusion within the solid particle itself. It assumes that the adsorbate molecule follows Fick's diffusion law Equation 3.5 and has a constant diffusivity of D_s at all points in the homogenous sphere of adsorbent and local equilibrium prevails within the adsorbent particle.

$$\frac{\partial q'}{\partial t} = D_s \frac{\partial}{\partial r}\left(r^2 \frac{\partial q'}{\partial r}\right)$$ Equation 3.5

where the average uptake q and the uptake at any distance from the center q□ are related as

$$q = \frac{3}{R^3}\int_0^R q'(r) r^2 dr$$ Equation 3.6

b. Intraparticle diffusion can also be modeled using the LDF approximation assuming that the mass transfer rate is proportional to the concentration difference between bulk solid phase and surface:

$$\frac{\partial q}{\partial t} = k_s S_0 (q_i - q)$$ Equation 3.7

It can be shown [14] that the HSDM Equation 3.5 is exactly equivalent to the LDF approximation Equation 3.7 if the following expression is assumed:

$$k_s = \frac{15 D_s}{R^2}$$ Equation 3.8

This can be deduced from Equation 3.6 and by assuming a parabolic concentration profile in a spherical particle, which is generally true. The LDF approximation is especially useful for fixed bed mass transfer modeling making an analytical solution possible.

3.4.2.2 Surface Reaction Modeling (SRM)

The intrinsic adsorption reaction is usually expressed as a mass law rate equation. This interaction can be described as (Equation 3.9) a reversible second order adsorption-desorption reaction. The corresponding rate law Equation 3.10 which is mixed 2nd order in the forward direction and 1st order in the backward direction, may be called "Langmuir kinetics" since the rate equation becomes the Langmuir isotherm equation at equilibrium i.e., when the net rate is zero. When the initial concentration of the solution is large

enough so that C can be approximated as constant, e.g., $C = C_0$, the Langmuir kinetic expression becomes the pseudo first order (PFO) rate equation (Equation 3.11), [15] which is commonly used to describe biosorption kinetics. Another widely used rate law is the pseudo second order rate equation (PSO) Equation 3.12, whose integrated form is a mathematical approximation of the integrated form of the Langmuir kinetic rate law [15].

$$\equiv\text{Site} + \text{Metal} \underset{k_{de}}{\overset{k_{ad}}{\leftrightarrow}} \equiv\text{S M} \qquad \text{Equation 3.9}$$

$$\frac{dq}{dt} = k_{ad}C(q_m - q) - k_{de}q \qquad \text{Equation 3.10}$$

$$\frac{dq}{dt} = k_1(q_\infty - q) \qquad \text{Equation 3.11}$$

$$\frac{dq}{dt} = k_2(q_\infty - q)^2 \qquad \text{Equation 3.12}$$

3.4.3 Isotherm equation

A generic expression of an isotherm equation is $q_e = f(C_e)$ where the function f refers to the Langmuir (Equation 3.13) Freundlich (Equation 3.14) or Linear (Equation 3.15) isotherms describing the equilibrium data (C_e, q_e) generated from batch (C_∞, q_∞) or fixed bed (C_0, q_∞) experiments. In MTM, local equilibrium is assumed at the interface (C_i, q_i). The Langmuir isotherm assumes monolayer coverage on a homogenous surface whereas the exponent in the Freundlich isotherm accounts for surface heterogeneity. In dilute solution where $b\,C_e << 1$, the Langmuir isotherm reduces to the linear isotherm with $K = b\,q_m$ (Equation 3.15), which is very powerful from a mathematical point of view, as analytical solutions are rarely available for non-linear isotherms, especially for fixed bed processes.

$$q_e = \frac{q_m b C_e}{1 + bC_e} \text{ where } b = \frac{k_{ad}}{k_{de}} \qquad \text{Equation 3.13}$$

$$q_e = K_F C_e^{1/\mu} \qquad \text{Equation 3.14}$$

$$q_e = K C_e$$ Equation 3.15

3.5 Results and discussion

3.5.1 Batch equilibrium

A set of three isotherms obtained from batch experiments using PRP, CRP and ALP at pH 5.5 and 25°C is shown in Figure 3.1. It shows that the Ca-loaded CRP have a lower Cd uptake than PRP, indicating that the presence of Ca may have an inhibitory effect on Cd biosorption which was also reported by Hashim et al. [16] in a similar study using seaweed. For peels immobilized in calcium alginate without subsequent protonation, Cd uptake was even lower than for CRP. The experimental data were modeled using Langmuir and Freundlich isotherms and model parameters were determined by non linear optimization using the solver function in Excel, minimizing the RMSE values as reported in Table 3.1.

Isotherms for PRP, PALP, and AGP are shown in Figure 3.2. Protonation of ALP increased its capacity substantially; it became even superior to PRP and also surpassed AGP. This proves the requirement of protonation for immobilized peels, similarly as PRP performed superior to RP in past research of the present authors [17]. It was found that both Langmuir and Freundlich models described the experimental data well (Figure 3.1 and Figure 3.2). Uptake by ALP, however, was sufficiently well described by a linear isotherm with $q_e = 0.0554\ C_e$ ($R^2 = 0.9858$) (Figure 3.1). Application of the Langmuir model did not yield meaningful parameter values (Table 3.1). The Langmuir model matched better than the Freundlich model for PALP, AGP and CRP but the reverse was true for PRP (Table 3.1). Since both the capacity q_m and the affinity b of the PALP were larger than for AGP (Table 3.1), required biosorbent doses to remove a certain contaminant percentage will be lower for PALP. Sodium alginate is also cheaper than agar. Therefore alginate was chosen as the best immobilization matrix and AGP was not considered for further study due to its lower effectiveness and higher cost.

3.5.2 Batch kinetics: SRM

The purpose of the batch kinetic study was to determine the time required to reach equilibrium and to determine useful kinetic parameters for modeling fixed bed experiments. Concentration-time profiles of both PRP and PALP from batch kinetic experiments for an initial concentration of 500 ppm are shown in Figure 3.3. Biosorption was fast, being complete within 2 hours, with 80% of q_e reached in about 35 min. It was noted that kinetics for raw peels were faster than those for alginate immobilized peels. This is further discussed in the section 3.5.6. The Langmuir Kinetic model (Equation 3.10) was integrated numerically after combining with the mass balance equation (Equation 3.10) to replace C as a function of q. An analytic solution is also available elsewhere [18]. PFO (Equation 3.16) and PSO (Equation 3.17) models were obtained by integration of the corresponding rate equations (Equation 3.11, Equation 3.12) respectively:

$$\ln(1-F) = -k_1 t \qquad \text{Equation 3.16}$$

$$q = \frac{k_2 q_\infty^{\,2} t}{1 + k_2 q_\infty t} \qquad \text{Equation 3.17}$$

Experimental data were simulated using these three models and rate constants were determined (Table 3.2) by non-linear optimization. For the purpose of fair comparison between MTM and SRM, only one parameter (k_1, k_2, or k) was optimized and the experimental value of q_∞ was used. As seen in Figure 3.3 and from RMSE values (Table 3.2), all models fit similarly well for PALP but for PRP the PSO model matched better than the PFO or Langmuir models. As a second option, a better fit is obviously obtained for any model when q_∞ is optimized along with rate constants. However, such optimized q_∞ values were similar to the experimental ones and introducing this second fitting parameter was not justified based on the slight improvement in model fit. A third option is to calculate q_∞ from other known parameters (C_0, M, V_s, b, q_m) by solving the quadratic equation formed by combining Langmuir isotherm and mass balance for C_∞ and q_∞. This

is done in the Langmuir kinetic model and thus its prediction here does not match with its simplified derivatives, the PFO and PSO.

Irrespective of the wide applicability, a good fit of these equations may not indicate the intrinsic nature of the rate-determining mechanism for different reasons. First, biosorption is actually a combination of mass transfer and surface reaction. For an SRM where the mass transfer resistance is not explicitly accounted for, the apparent "rate constant" actually incorporates the mass transfer resistance, especially since the latter one is often more rate-limiting than the chemical reaction itself. Secondly, it is easy to observe that the linear relationship between ln(1-F) and t in the PFO model (Equation 3.16) also applies for the Boyd plot (Equation 3.23) which is derived assuming intraparticle-diffusion-controlled kinetics. Thirdly, a film diffusion based kinetic model was also found to be mathematically analogous with the PFO model. These points are further discussed in the appropriate sections.

3.5.3 Fixed bed kinetics: SRM

Similar to the application of PFO and PSO models for batch kinetics, models based on surface reaction (SRM) may also be applied to describe fixed bed kinetics. The Thomas (Th) model, which is the analytical solution of Equation 3.3, Equation 3.10 and Equation 3.13 is mathematically unwieldy and often simplified assuming $k_{de} = 0$, in which case it becomes equivalent to the Bohart-Adams (BA) model (Equation 3.18). This is again mathematically analogous with Yoon-Nelson (YN) model, i.e., the BA, simplified Th and YN models all share the same general expression, as explained in a prior article of the present authors [1]. This equation is the most commonly used model for simulating fixed bed breakthrough data, whereby one overall kinetic coefficient is used. Six experimental breakthrough profiles (Figure 3.4), for varying experimental conditions (Table 3.3) using PRP and PALP were modeled by the BA model (Equation 3.18) using a non linear optimization routine for determining the model parameters k_{BA} and N_0. A good fit was obtained in each case. The model uptake, q_{BA}, calculated according to Equation 3.19 [1]

was found to be comparable with the experimental q_∞ value except for run # PRP2 where a large deviation was observed (Table 3.4).

$$\frac{C}{C_0} = \frac{1}{1+\exp\left(\frac{k_{BA}N_0Z}{u} - k_{BA}C_0t\right)}$$ Equation 3.18

$$q_{BA} = \frac{N_0 V}{M}$$ Equation 3.19

It was found that rate constants k_{BA} for a given sorbent were relatively constant within the range of operating conditions averaging 0.32 mL/(mg min) for raw peels, which was almost six times higher than the corresponding average values for immobilized peels of 0.056 mL/(mg min).

3.5.4 Batch kinetics: MTM

One objective of batch kinetics MTM modeling was to determine the diffusion coefficient, which can be used for predictive modeling of fixed bed biosorption as the diffusion coefficient does not depend on the reactor type. The rate limiting mechanism and related parameters, especially the diffusion coefficient, are often determined from a Weber-Morris (WM) plot or a Boyd plot. The origin of these equations needs to be considered before application of these models.

3.5.4.1 Single resistance –intra-particle diffusion models

a) Crank-1 Model (linear isotherm, infinite bath)

Crank derived an analytical solution (Equation 3.20) assuming a linear isotherm Equation 3.15 and intraparticle diffusion (Equation 3.5, Equation 3.6) control, abbreviated as Crank-1 hereafter. The solution also assumes that the liquid phase sorbate concentration at the surface of the sorbent remains constant throughout the experiment, commonly referred to as the "infinite bath case" since this would be the case if the adsorbate solution was 'infinitely' large.

$$F = 1 - \frac{6}{\pi^2}\sum_{1}^{\infty}\frac{1}{n^2}\exp(-n^2Bt)$$ Equation 3.20

The corresponding 'short time' solution is:

$$F = 6\left(\frac{D_s t}{R^2}\right)^{0.5}\left\{\pi^{-0.5} + 2\sum_{n=1}^{\infty} ierfc\frac{nR}{\sqrt{D_s t}}\right\} - \frac{3D_s t}{R^2} \qquad \text{Equation 3.21}$$

(i) For the initial phase, when F < 0.3, considering the first term only, Equation 3.21 can be reduced to Equation 3.22 which is widely known as Weber-Morris (WM) model as it shows the proportionality of F with square root of t.

$$F = \left(6\sqrt{\frac{D_s}{\pi R^2}}\right)\sqrt{t} \qquad \text{Equation 3.22}$$

Application of Equation 3.22 for the entire range of kinetic data obtained from PALP yielded a multi-stage-linear plot (Figure 3.6) consisting of a steep sloped portion followed by a linear middle part and a plateau, which has also been reported in numerous other articles [19] including some on Cd biosorption [20, 21]. Though derived for the initial phase (F<0.3), the equation is applied for the entire data range in many publications. According to these articles, these three linear segments represent an external mass-transfer-controlled phase, an intraparticle-mass-transfer-controlled phase and the equilibrium phase, respectively. This may be interpreted such that more than one resistance should be considered in modeling. However, D_s values calculated from each segment according to Equation 3.22 may or may not be accurate since the equation is approximated from the parent equation for the initial phase only. The parent equation was derived considering a single resistance only. Again, the perception of different phases often depends on the visual judgment, regarded as an indication whether the process can be modeled assuming a single resistance or not. In the present study, parameters obtained from this plot varied widely for different phases, so that they could not be utilized for fixed bed modeling.

(ii) Boyd [22] also derived this solution (Equation 3.20) and prepared a table of calculated F values for a series of B t values for quick computation of B from Equation 3.20 in that pre computer era. For each experimental F value, the corresponding B t value was read from the table and was divided by the corresponding experimental t value. A

constant value of B implied the applicability of the model from which the diffusion coefficient was calculated. In order to reduce the errors in B t values found by interpolation from this table for intermediate values of F, Reichenberg [23] obtained a more useful approximation of the equation by expressing B t in terms of F (Equation 3.23, Equation 3.24) and tabulated those B t values for F values ranging from 0 to 0.99 at increments of 0.01:

$$Bt = -\ln(1-F) - 0.5 \quad (\text{for } F > 0.85) \qquad \text{Equation 3.23}$$

$$Bt = 6.28318 - 3.2899F - 6.28318\,(1-1.0470F)^{0.5} \quad (\text{for } F \leq 0.85) \qquad \text{Equation 3.24}$$

Equation 3.23 is the 'long time' approximation of (Equation 3.20), popularly known as the 'Boyd plot', though not introduced by Boyd, and typically used as the litmus test to determine the rate limiting mechanism: if the regression line in a linear plot of B t vs. t passes through the origin, this is interpreted as intraparticle mass transfer controlling, otherwise external mass transfer is assumed to be rate-limiting, though that may not necessarily be the case, as discussed below. Though originally approximated for long time only (F>0.85), the equation is often applied [21, 24, 25] for the initial range of kinetic data to determine the rate limiting mechanism at the beginning of biosorption. Ofomaja [26] studied biosorption of lead using sawdust and applied Equation 3.23 for the initial biosorption period. It was found that the B t vs. t plot was linear but with an intercept of about -0.4. It was concluded that external mass transfer was the rate limiting mechanism for that period of time. Such a conclusion is not justified for the following reason: it was also found that data matched with a PFO rate equation for that period of time, which means a plot of –ln(1-F) vs. t passes through the origin. Obviously, one can therefore observe an intercept around -0.5 in the plot of –ln(1-F)-0.5 vs. t. A similar negative intercept was also observed in other studies [21]. Had both Equation 3.23 and Equation 3.24 were applied in correct range (as in the Reichenberg table [23]), a different conclusion might be reached. Zhu et al. used this table and found a linear B t vs. t plot passing through the origin for Cd sorption on red mud. The data was not applied to a PFO model though.

(iii) In contrast to the short (Equation 3.22) and long (Equation 3.23) time approximations, which are only valid for a limited data range, Equation 3.20 can be approximated over the entire data range by an equation derived by Helfferich [27] which fits numerical results for any F value within an error of 1%. Considering only the first term of that equation, it reduces to (Equation 3.25) with a maximum error of 5% for F>0.1 [28]. This so called Urano model [29] or Vermeulen approximation [28] is also used in biosorption literature [28, 30] to determine D_s.

$\ln(1-F^2) = -B\,t$ Equation 3.25

As explained above, these equations are not valid over the entire range of the time/surface coverage. All of these equations represent different 'approximations' of the same parent equation which was derived ignoring external mass transfer resistance. For these reasons, application of the original equation (Equation 3.20) is more justified than its different simplified derivatives (Equation 3.22-Equation 3.25) which are, unfortunately, the most frequently used models in related literature and a sizable portion of them [20, 31-33] even consider equation (Equation 3.22 and Equation 3.25) as two 'different' methods to determine the intra-particle diffusion coefficient. None of these, including the parent equation were applied here due to availability of a better model as discussed below.

b) Crank-2 Model (Intraparticle diffusion, linear isotherm, finite volume)

Crank provided another analytical solution, also assuming that intraparticle diffusion is the sole rate-controlling step, referred to as Crank-2 hereafter. This solution is more practical as it does not assume constant sorbate concentration at the interface but instead a finite volume i.e., it is necessary to include the mass balance equation (Equation 3.1) along with Equation 3.5, and Equation 3.6.

$$F = 1 - \sum_{n=1}^{\infty} \frac{6\alpha(\alpha+1)}{9+9\alpha+\gamma_n^2\alpha^2} \exp\left(\frac{-D_s\gamma_n^2 t}{R^2}\right) \qquad \text{Equation 3.26}$$

where $\tan\gamma_n = \frac{3\gamma_n}{3+\alpha\gamma_n^2}$ with $\frac{M\,q_\infty}{V\,C_0} = \frac{1}{1+\alpha}$

This equation was applied for batch kinetic data using PRP and PALP (Figure 3.5) and after determining α based on q_∞ and γ_n based on α, D_s was determined as a fitting parameter.

D_s determined using any of the above equations can be erroneous due to unjustified simplifying assumptions or be a lumped parameter, affected by k_f to different degrees. Therefore, such D_s values cannot be used in fixed bed modeling, where conditions are different from the batch experiment, which entails different external mass transfer resistance.

3.5.4.2 Single resistance –film diffusion models

a) Film diffusion with linear isotherm in infinite bath

Film diffusion is now considered as the sole controlling mechanism (Equation 3.4) under conditions corresponding to the Crank-1 model i.e., with a linear isotherm in an 'infinite bath' where the bulk aqueous concentration is constant and $C_0 \approx C \approx C_\infty$. Applying a linear isotherm (Equation 3.15) for equilibrium ($C \leftrightarrow q_\infty$) and ($C_i \leftrightarrow q$) and substituting C and C_i into Equation 3.4 accordingly, this equation becomes equivalent to the PFO model [22] with a rate constant $k_1 = k_f * S_0/K$ from which k_f can be determined if the data were initially fitted to a PFO model. So without testing the variation of the rate constant with other parameters, a good fit of a PFO model, as such, cannot distinguish between film diffusion and surface reaction actually dominating the kinetics, as mentioned earlier.

b) Film diffusion with linear or Langmuir isotherm in finite volume

Considering a finite volume (equivalent to Crank-2 situation), the mass balance equation (Equation 3.2) along with a linear isotherm ($C_i \leftrightarrow q$) can be applied to substitute C and C_i in Equation 3.4 in terms of C_0 and q respectively to obtain Equation 3.27 which can be integrated yielding Equation 3.28. If alternatively the Langmuir isotherm is used, Equation 3.27 is replaced by Equation 3.29 which can also be solved analytically.

$$\frac{dq}{dt} = \frac{k_f S_0}{\rho}\left(C_0 - q\left(\frac{M}{V_s} + \frac{1}{K}\right)\right) \qquad \text{Equation 3.27}$$

$$F = \left(1 - \exp\left(-\left(\frac{k_f S_0}{\rho}\right)\left(\frac{M K + V_s}{V_s K}\right)t\right)\right)$$ Equation 3.28

$$\frac{dq}{dt} = \frac{k_f S_0}{\rho}(C_0 - q(\frac{M}{V_s} + \frac{1}{b(q_m - q)}))$$ Equation 3.29

The exponential term in Equation 3.28 is constant for any experimental data set, therefore the final expression again becomes equivalent to the PFO model (Equation 3.16) with rate constant being a function of S_0, K, M, ρ, V_s and k_f. The PFO model was previously found to agree with batch kinetic data (section 3.5.2) obtained by using PRP and PALP. However, for the purpose of comparison with the Crank-2 model, this model (Equation 3.28 or Equation 3.16) was included within Figure 3.5 and k_f was calculated (Table 3.2). The equation described the data equally well as the Crank-2 model. Therefore, the assumption of film diffusion as the rate controlling step cannot be rejected either. This necessitates a dual resistance model including both resistances.

3.5.4.3 Dual resistance model (intra-particle and film diffusion)

Even for an intraparticle-diffusion-controlled biosorption process, external mass transfer resistance must be dominating at the beginning since ID cannot occur before the sorbate reaches the particle. For desorption on the other hand, external mass transfer is not necessarily rate-limiting in the initial phase [34]. Assuming a constant liquid phase concentration at the sorbent surface (infinite bath case), Crank derived the most realistic analytically solvable model that includes both external (Equation 3.4) and intraparticle resistance (Equation 3.5, Equation 3.6), denoted as Crank-3 hereafter, application of which, however, is rare [35] in biosorption articles:

$$F = 1 - \sum_{n=1}^{\infty} \frac{6Bi^2 \exp\left(-\beta_n^2 D_s t / R^2\right)}{\beta_n^2 \left\{\beta_n^2 + Bi(Bi-1)\right\}}$$ Equation 3.30

$$\beta_n \cot \beta_n + Bi - 1 = 0$$ Equation 3.31

This equation involves Biot number, which is a function of both D_s and k_f. In order to optimize the diffusion coefficient D_s, k_f needs to be supplied from another source. So Equation 3.1 and Equation 3.4 were combined obtaining Equation 3.32.

$$\frac{dC}{dt} = -k_f S'(C - C_i) \qquad \text{Equation 3.32}$$

Assuming external mass transfer was dominating in the initial period of biosorption and applying the condition that the initial concentration at the interface is zero, ($C_i \rightarrow 0$ as $t \rightarrow 0$), the integrated form of Equation 3.32 is:

$$\ln(C/C_0) = -k_f S' t \qquad \text{Equation 3.33}$$

The k_f value was calculated based on data for the first 10 minutes using Equation 3.33. The initial Biot number was calculated on the basis of this k_f and D_s determined from the Crank-2 plot. Using this Biot number, the solution for Equation 3.31 was calculated using the fzero function in Matlab where the initial guess was supplied from the table given by Crank [36]. Then a new D_s value (and a new Biot number) was optimized by fitting Equation 3.30 to the experimental data. The process was repeated till there was no difference between two successive D_s values for the leading three significant digits. Final optimized values of D_s for PRP and PALP are reported in Table 3.2 and respective plots are shown in Figure 3.5. A comparison among three models (Equation 3.26, Equation 3.28 and Equation 3.30) reveals that the Crank-3 model (Equation 3.30), which includes both internal and external mass transfer, fits better than models assuming either external (Equation 3.28) or internal mass transfer (Equation 3.26) as the sole rate controlling equation. External mass transfer was also considered in algal [37] and bacterial [20] biosorption of Cd(II). In the first example, k_f was determined by Equation 3.27, which was found to be high and hence D_s was determined using Crank-2. This D_s is still an 'effective' one and may not be used for fixed bed modeling. In the second example, Equation 3.32 was further simplified assuming $C = C_0$ along with $C_i = 0$ at $t = 0$ and k_f was determined accordingly. This was found to be small and external mass transfer was

assumed as the rate controlling step, but kinetic data was never modeled using the k_f value as done in the present study. Puranik et al., [38] indeed modeled fungal biosorption of lead and zinc using Equation 3.31 but concluded that film diffusion was the rate limiting factor without considering the fact that another model based on intra-particle diffusion may fit as well.

None of these articles considered conducting fixed bed experiments following the batch experiments, so 'purity' of D_s was not an issue. In a study involving biosorption of Palladium in modified chitosan [39], it was concluded that a single resistance model considering either external (Equation 3.33) or intraparticle (Equation 3.26) resistance may not be adequate to describe a typically "fast" biosorption process under optimized condition but may work for one with "slow" kinetics. The D_s of Palladium obtained from the Crank-2 model was found to be remarkably lower compared to values cited in related literature.

3.5.5 Fixed bed kinetics: MTM

Both external and intraparticle mass transfer resistances were included for modeling the fixed bed reactor. A linear isotherm was assumed, which is reasonable as fixed bed experiments were performed at a very low liquid phase concentrations (5 to 15 ppm). Then, external and intraparticle LDF rate laws (Equation 3.4, Equation 3.7) can be combined as

$$\rho \frac{\partial q}{\partial t} = K_f S_0 (C - C^*) \qquad \text{Equation 3.34}$$

where K_f, the overall fluid phase mass transfer coefficient, is a function of the intrinsic film and intraparticle mass transfer coefficients (k_f, k_s) according to Equation 3.35.

$$\frac{1}{K_f} = \frac{1}{k_f} + \frac{1}{K \rho k_s} \qquad \text{Equation 3.35}$$

This equation (Equation 3.35), along with the fixed bed column mass balance (Equation 3.3), can be solved analytically to express C in terms of dimensionless distance (ξ) and dimensionless time (τ), often referred to as Klinkenberg solution [14].

$$\frac{C}{C_0} = 0.5\left[1 + erf\left(\sqrt{\tau} - \sqrt{\xi} + \frac{1}{8\sqrt{\tau}} + \frac{1}{8\sqrt{\xi}}\right)\right] \qquad \text{Equation 3.36}$$

In order to apply Equation 3.36 to predict breakthrough curves, K_f must be evaluated according to Equation 3.35 which requires K, k_s and k_f. The diffusion coefficient obtained from batch experiments was utilized to calculate k_s using (Equation 3.8). Considering equilibrium between C_0 and q_∞, K can be calculated according to (Equation 3.15). Accordingly, the following equation was obtained:

$$K k_s = \frac{15 D_s q_\infty}{R^2 C_0} \qquad \text{Equation 3.37}$$

The k_f was calculated using engineering correlations involving the Sherwood number, Schmidt number and Reynolds number. Since a number of correlations are available [40], the average of two different correlations (Equation 3.38, Equation 3.39) was used which cover the low range of Reynolds number, as the Reynolds number was varied between 0.3 and 0.9 in the present study.

$$Sh = \frac{1.09}{\varepsilon} \mathrm{Re}^{1/3} Sc^{1/3} (0.0016 < \mathrm{Re} < 55) \qquad \text{Equation 3.38}$$

$$Sh = \frac{1.13}{\varepsilon} \mathrm{Re}^{0.21} Sc^{1/3} (\mathrm{Re} < 10) \qquad \text{Equation 3.39}$$

The Schmidt number involves the diffusivity of Cd^{2+} ions in water (D) which was calculated to be 4.31 E^{-4} cm^2/min according to the Nernst equation [34]. A different value for the diffusivity of Cd^{2+} ions in water (8.64 x10^{-4} cm^2/min) was noted in another article [40]. Diffusion of Cd^{2+} ions was assumed to be accompanied by the diffusion of fast moving H^+ ions and so other ions were not considered. A few articles [30, 41] consider the diffusion coefficient of the Cd-nitrate ion pair for the calculation of Schmidt number.

Equation 3.36 was now evaluated to predict breakthrough curves for both raw and immobilized peels under different experimental condition of C_0, Q, h specified in Table 3.3 for PRP1 to PALP3 using k_f (Table 3.4), D_s (Table 3.2) and q_∞ (Table 3.4) values obtained from the average of two correlations (see above), batch experiments and fixed bed experiments, respectively. It was found that predicted breakthrough curves (KB1 series in Figure 3.4) described the data well except for a moderate deviation for PALP3 and a serious deviation for PRP2, also reflected in higher RMSE values as shown in Table 3.4 (as RMSE2). These curves can be compared with 'optimized' breakthrough curves (KB2 series in Figure 3.4) obtained by applying (Equation 3.36) while using nonlinear optimization for fitting the parameters q_∞ (used in Equation 3.37) and k_f (used in Equation 3.35), specifically for each breakthrough curve.

A comparison between optimized q_∞ and k_f with experimental q_∞ and correlated k_f revealed that high deviations in k_f and q_∞ were found in PALP3 and PRP2 respectively which explains the moderate to serious deviations for these runs. This can be further clarified by plotting those curves using optimized q_∞ and correlated k_f (KB3 series in Figure 3.4), which shows substantial improvement for PRP2 but not for PALP3. The average relative deviation of optimized k_f from the correlated k_f is about 27%. Good correspondence between the values validates the approach used. A difference between $k_{f,corr}$ and $k_{f,opt}$ was also observed in a similar biosorption study [42]. A large number of correlations exist; and k_f values obtained from these correlations vary significantly depending on the power of void fraction which may be positive, negative or zero. Some correlations that were originally derived using the superficial velocity for calculating the Reynolds number, [43] were mistakenly applied [41] using the interstitial velocity or vice versa, which further complicates the situation.

There are articles which use a similar HSDM/LDF based model, but focus on different adsorbents and adsorbates. One article describing biosorption of copper by marine alga [10] considered either film diffusion or intraparticle diffusion as the sole rate controlling mechanism and determined the corresponding mass transfer coefficient (k_f or k_s) by calibrating the LDF based model (Equation 3.4 or Equation 3.7) with experimental data.

It was found that the intra-particle diffusion model represented the breakthrough data better than the film diffusion model. That did not necessarily prove that intra-particle diffusion was the controlling mechanism because when k_f (or k_s) is determined as fitting parameter for the LDF model, it actually represents a lumped parameter (K_f or K_s) incorporating the effect of both resistances which should rather be resolved into corresponding intrinsic parameters using Equation 3.35 or similar relation as done in another article [44] studying dye biosorption: after determining k_f using an engineering correlation, the overall mass transfer coefficient (K_f) was obtained by curve fitting. The diffusion coefficient was obtained by using the relation between k_f and K_f. None of these articles include an *a priori* prediction of breakthrough curves using parameters obtained from other sources.

Aksu [41] studied biosorption of copper ions to green algae and ignored intraparticle diffusion. The biosorption process was conceptualized as film diffusion followed by a surface reaction which was assumed first order with respect to fluid phase concentration. The external mass transfer coefficient (k_f) was obtained from an engineering correlation and the surface reaction rate constant was determined from experimental data. Maiti et al. [30] studying bacterial biosorption of Cr (VI) extended this approach by adding an intraparticle diffusion resistance in series with surface reaction resistance. The intraparticle diffusion coefficient was obtained from batch experiments by applying Urano solution (Equation 3.25). In both examples, the values of mass transfer coefficients were obtained independently, without fitting to the breakthrough data, but unfortunately the validity of those parameters was not verified by modeling breakthrough curves using those parameters.

In the present study, the diffusion coefficient followed the following order: $D > D_{s,PALP} > D_{s,PRP}$. Diffusion of an ion in aqueous phase is always faster than that through a water-filled pore space. This is because free space available for diffusion becomes reduced within the porous sorbent media and the diffusion path becomes tortuous, also reflected in Equation 3.40. Internal porosity and hence water content of immobilized beads are much higher than the native peels, this is reflected in a higher D_s value of the

former. This means immobilization in alginate is advantageous not only because of a higher capacity (Table 3.1), but also because of a higher diffusion coefficient. While the overall rate is also affected by particle size, which was in this case higher for the immobilized sorbents, slowing down their kinetics, immobilized sorbents would outperform the kinetics of raw sorbents if compared at equal size. For large scale packed bed column operation, a certain minimum particle size is desirable to avoid excessive head loss.

$$D_s = \frac{D\varepsilon_P \delta}{\lambda}$$ Equation 3.40

3.5.6 Effect of operating variables and immobilization

The effect C_0, Q and h follows the same trend as discussed in the previous article [1] of the present authors on biosorption using another batch of protonated raw peels. In general, breakthrough and saturation times decreased with increase in Q and C_0 and decrease in h. Uptake at equilibrium (saturation) (q_∞) varied within a very limited range (54 to 66 mg/g for PALP and 17 to 25 mg/g for PRP) without any noticeable trend. For both peel types, doubling the influent concentration lead to a substantial decrease in breakthrough time but uptake capacity at breakthrough remain almost constant or increased marginally. Obviously, breakthrough occurred later when increasing the bed height from 40 to 54 cm. However, both curves (PALP2 and PALP1) overlap with each other when plotting the number of BV treated on the x axis (Figure 3.7), which means both were similarly effective per column volume. A similar result was found for the biosorption of Pd by modified chitosan [45]. The observation that effectiveness was not highly depended on residence time (which is proportional to column length) indicates that the residence time was sufficient to achieve local equilibrium and the process was not critically hindered by intra-particle diffusion under the experimental conditions.
At 40 cm bed height and 2 ml/min flow rate (PALP2), the residence time was about 30 min, after which time about 70% of the equilibrium uptake were reached in batch kinetics for PALP whereas it only took about 15 min for PRP to achieve this uptake. Even though

the diffusion coefficient of PALP is higher than that for PRP, the rate of diffusion is proportional to the square of particle size, and this explains the slower kinetics of former. The breakthrough curve of PRP (Figure 3.4) shows that a preferential flow path exists leading to 'leakage' of contaminant during the first hour of operation. Occasional clogging of the column was also observed for PRP, which is partially attributed to the compact sorbent packing, and partially to the nature of the peels. An SEM picture (Figure 3.8) revealed that surface morphology of this batch of peels (3.8b) was different from another batch of peels for which neither channeling nor clogging occurred (3.8a) in column applications. Immobilization, however, eliminated this problem: 3.8c showed the spherical nature of the bead and 3.8d showed the internal porosity.

3.6 Conclusions

Protonated citrus peels can be used as a potential alternative for cadmium removal in fixed bed columns. Immobilization in calcium alginate followed by protonation significantly increased the removal capacity and ease of handling within the column. Alginate-immobilized peels also featured a higher diffusion coefficient. While in the present case slower kinetics were observed due to a larger particle size of immobilized sorbents, kinetics would generally be faster if raw and immobilized sorbents at equal size were compared. The calcium-saturated form of both original peel particles and the immobilized sorbent had considerably lower uptake capacity than the protonated form. Batch and fixed-bed kinetic data can be simulated using different surface reaction models (pseudo first or second order as well as Langmuir for batch, Bohart-Adams for fixed-bed) where optimized kinetic parameters represented lumped parameters, de facto including the effect of mass transfer and intrinsic reaction kinetics. Two frequently used film diffusion models were shown to be equivalent with the PFO model. Other frequently used intra-particle diffusion models (Weber-Morris, Boyd) were found to be only approximated forms of a parent model (Crank-1) and suffered from other limitations. Instead, a different intra-particle diffusion model, derived using more realistic assumptions, was applied to determine that both resistances merit consideration. Finally,

the only analytical model that includes both diffusion types was applied to determine the intrinsic value of the diffusion coefficient which was then used for *a-priori* prediction of breakthrough curves by the Klinkenberg model.

3.7 Acknowledgements

This research was supported largely by the National Research Initiative of the USDA Cooperative State Research, Education, and Extension Service, grant number 2005-35504-16092 and partly by USGS. Orange peels were provided by Alarma Consulting Corporation in Florida.

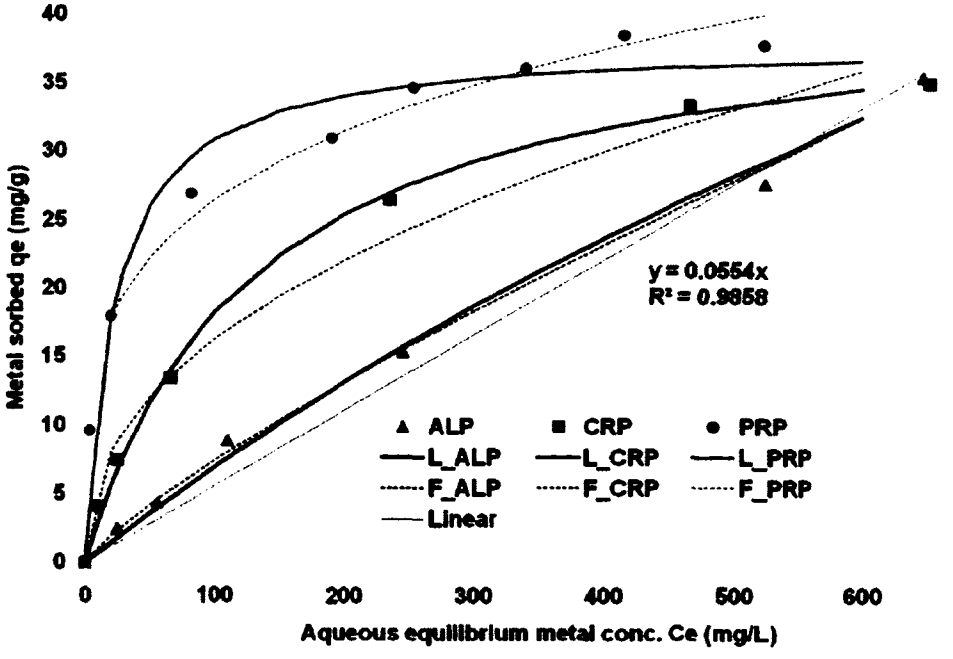

Figure 3.1 Isotherm of Cd (II) biosorption by PRP, PALP and ALP in a batch reactor at pH 5.5

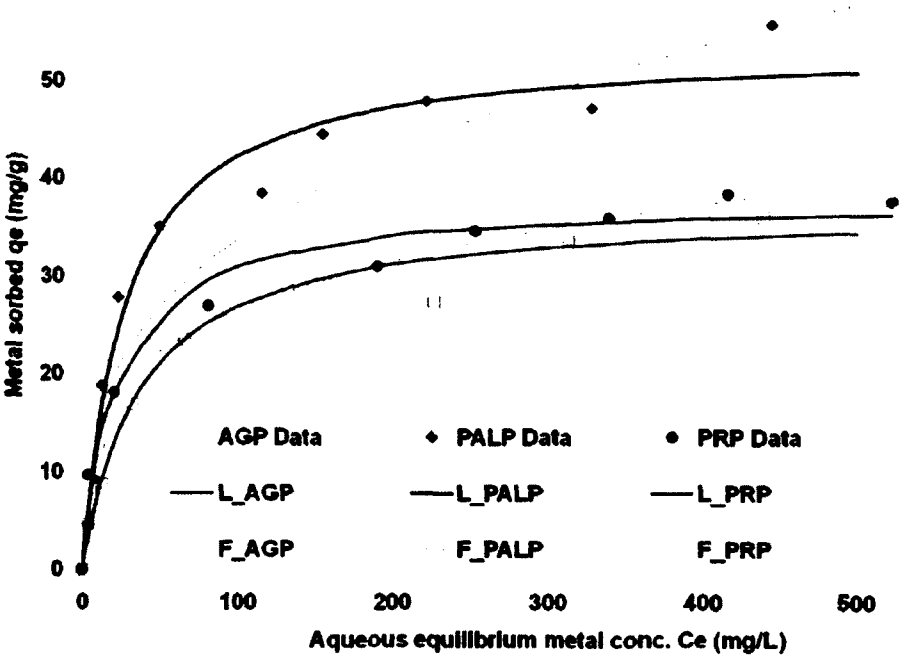

Figure 3.2 Isotherm of Cd (II) biosorption by PRP, PALP and AGP in a batch reactor at pH 5.5

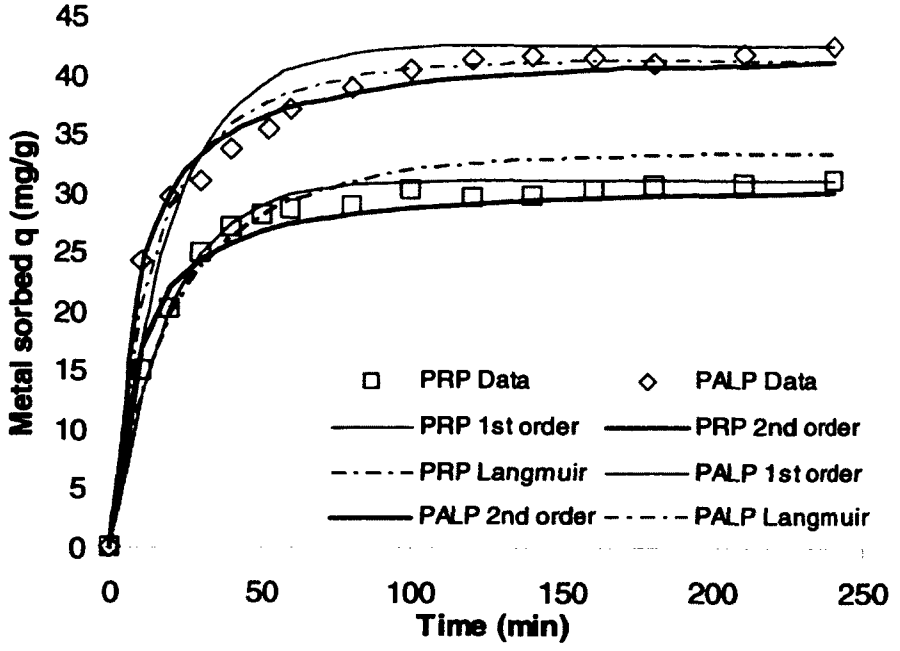

Figure 3.3 Kinetics of Cd (II) biosorption by PRP and PALP in a batch reactor and predictions of different surface reaction models

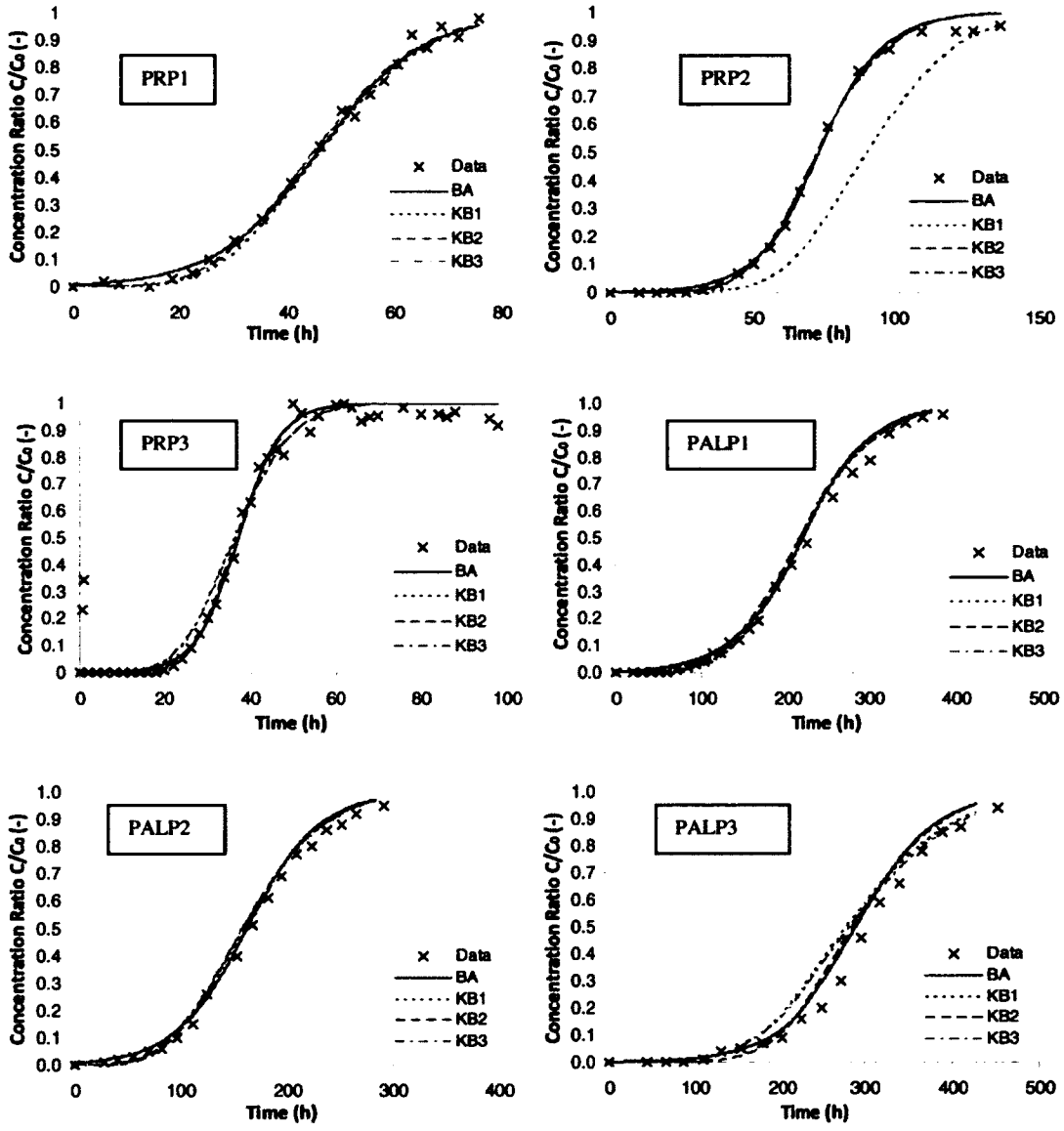

Figure 3.4 Breakthrough curves of Cd (II) biosorption by PRP or PALP in a fixed bed reactor under different conditions as detailed in Table 3.3. Experimental data, simulation by Bohart-Adams model (BA) and Klinkenberg model with parameters either fully predicted (KB1), fully optimized (KB2) or partially optimized (KB3) as detailed in Table 3.4.

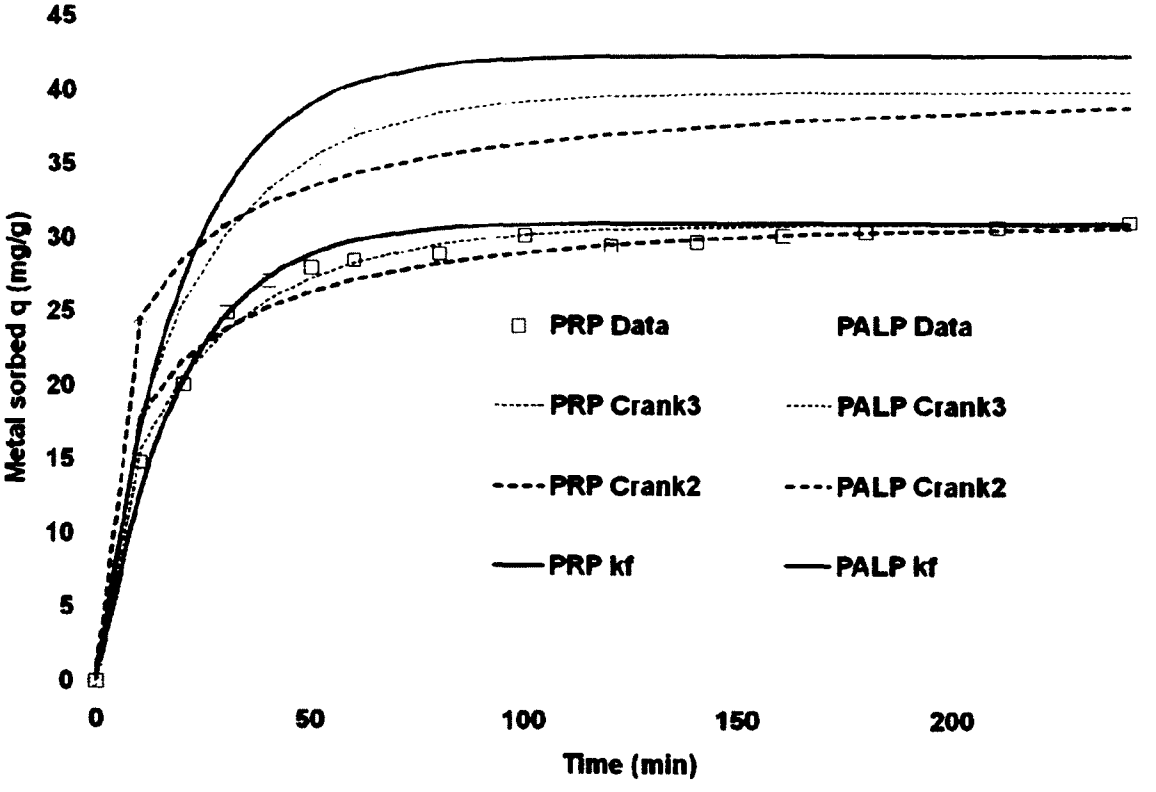

Figure 3.5 Kinetics of Cd (II) biosorption by PRP and PALP in a batch reactor and predictions of different mass transfer models.

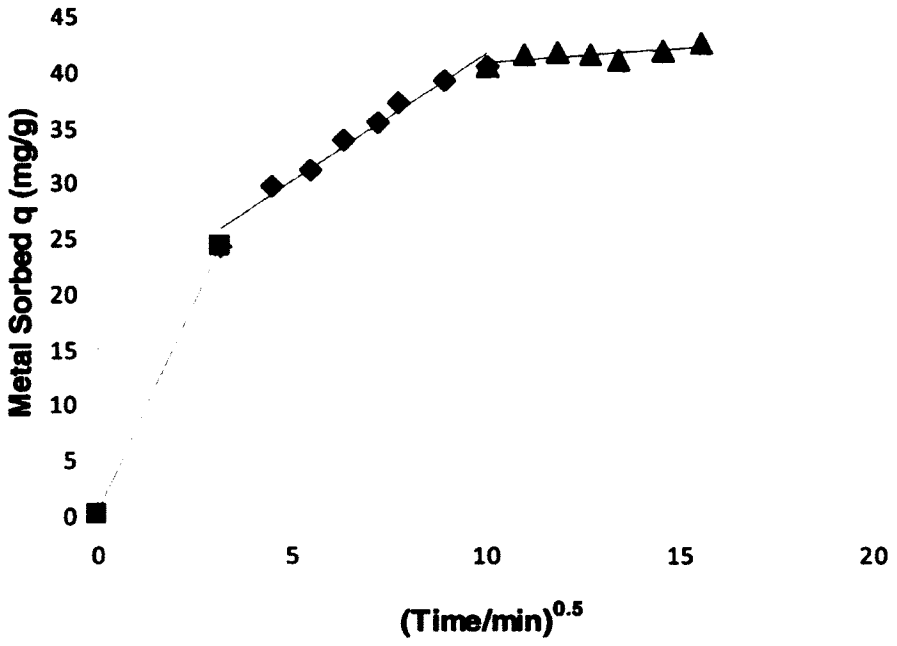

Figure 3.6 Weber-Morris plot for Cd (II) biosorption by PALP.

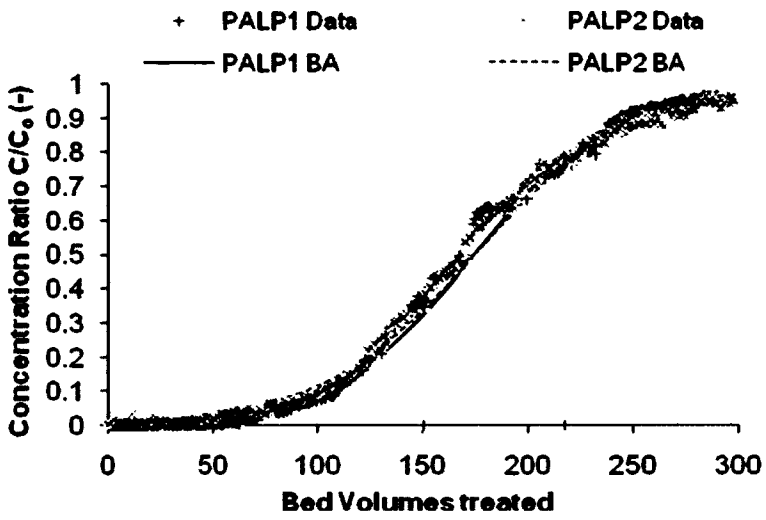

Figure 3.7 Breakthrough curve of Cd (II) biosorption by PALP at different bed heights plotted in terms of bed volumes treated (C_0 = 10 mg/L, Q = 2 ml/min).

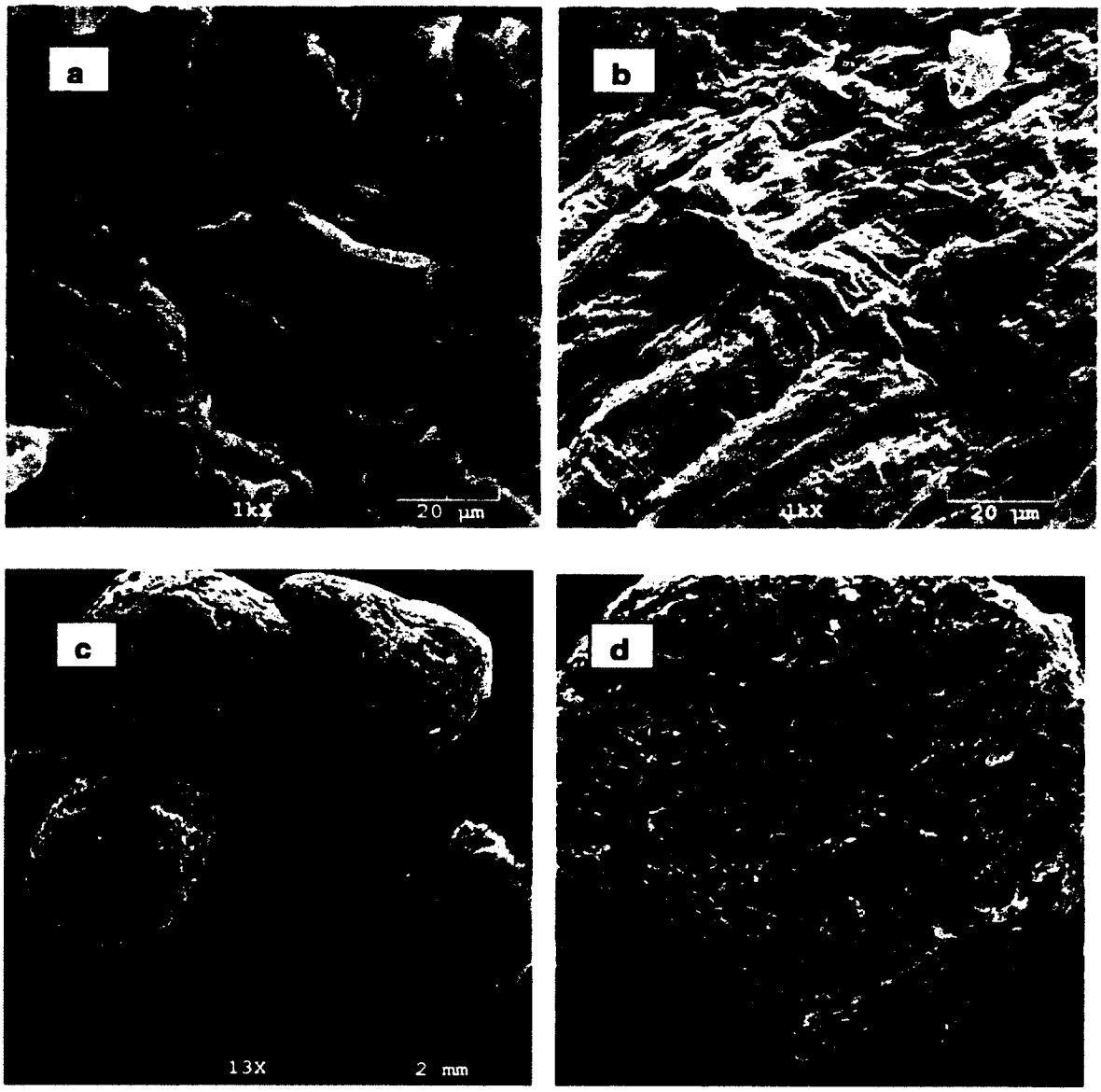

Figure 3.8 SEM pictures of a) raw peels batch 1; b) raw peels batch 2, c) Ca-alginate beads with entrapped peels low magnification, d) Cross-section of Ca-alginate beads at higher magnification.

Table 3.1 Batch Equilibrium: Comparison of isotherm models

	Exp.	Langmuir			Freundlich		
	q_e mg/g	b L/mg	q_m mg/g	RMSE mg/g	μ -	K_F $L^{1/\mu}/(g\ mmol^{1/\mu-1})$	RMSE mg/g
PRP	31	0.04	38	2.2	3.99	8.35	1.4
PALP	43	0.04	54	2.9	3.02	7.39	5.1
AGP	36	0.03	37	2.0	3.09	5.24	2. 9
CRP	35	0.01	42	0.57	2.27	2.13	1.8
ALP	35	6E-4	123	1.0	1.22	0.17	0.75

Table 3.2 Batch Kinetics: Comparison of model parameters (MTM and SRM)

	Model	Parameter		PRP	PALP
SRM1	PFO	k_1	1/min	0.053	0.051
		q_{e1}	mg/g	31	43
		RMSE	mg/g	1.04	2.84
SRM2	PSO	k_2	g/(mg.min)	3.8E-03	2.8E-03
		q_{e2}	mg/g	31	43
		RMSE	mg/g	1.14	1.16
SRM3	Langmuir	k	L/(mg.min)	9.9E-05	1.3E-04
		RMSE	mg/g	1.93	1.53
MTM1	Film Diffusion	k_{f1}	cm/min	1.65E-02	1.08E-02
		RMSE	mg/g	1.04	2.84
MTM2	Crank-2	D_2	cm^2/min	5.9E-06	9.5E-06
		RMSE	mg/g	0.04	0.03
MTM3	Crank-3	k_{f3}	cm/min	2.5E-02	7.5E-03
		D_3	cm^2/min	1.9E-05	1.0E-04
		RMSE	mg/g	0.02	0.05

Table 3.3 Influence of experimental conditions on biosorption of cadmium by PRP and PALP in a fixed-bed column

Run #	experimental conditions							experimental results			
	R	M	h	ε	C_0	Q		q_∞	t_b	t_∞	q_{bt}
	cm	g	cm	-	mg/L	ml/min		mg/g	h	h	mg/g
PRP1	0.08	10	26	0.3	5	12		17	22	67	8
PRP2	0.08	10	26	0.26	5	9		25	40	116	11
PRP3	0.08	10	26	0.26	10	9		20	24	60	13
PALP1	0.15	5	54	0.5	10	2		60	97	356	26
PALP2	0.15	3	40	0.5	10	2		66	74	269	28
PALP3	0.15	3	40	0.45	5	2		54	137	429	26

Table 3.4 Fixed bed kinetics: Comparison of model parameters (MTM and SRM)

Model		Parameter		PRP1	PRP2	PRP3	PALP1	PALP2	PALP3
SRM (Bohart Adams)		k_{BA}	ml / (mg min)	0.348	0.289	0.336	0.040	0.051	0.078
		q_{BA}	mg/g	16	20	20	59	63	55
		error	%	3.6	20.4	-0.1	2.3	5.1	-1.0
		RMSE		0.075	0.062	0.068	0.022	0.022	0.015
MTM (Klinkenberg (KB) model)*	KB1	k_f (cor)	cm/min	0.121	0.129	0.129	0.027	0.027	0.030
		K_{f1}	cm/min	0.106	0.117	0.102	0.026	0.027	0.030
		RMSE1		0.243	0.481	0.209	0.064	0.052	0.089
	KB2	k_f (opt)	cm/min	0.109	0.127	0.236	0.024	0.028	0.046
		q_∞ (opt)	mg/g	17	20	20	59	66	55
		K_{f2}	cm/min	0.096	0.112	0.158	0.024	0.028	0.045
		RMSE2		0.237	0.167	0.193	0.046	0.051	0.044
	KB3	k_f (cor)	cm/min	0.121	0.129	0.129	0.027	0.027	0.030
		q_∞ (opt)	mg/g	17	20	20	59	66	55
		K_{f3}	cm/min	0.106	0.114	0.102	0.026	0.026	0.030
		RMSE3		0.238	0.167	0.208	0.051	0.052	0.082

* k_s = 1.29E-03 cm/min for protonated raw peels (Run # PRP1 to PRP3) and 3.47E-03 cm/min for protonated alginate immobilized peels (Run # PALP1 to PALP3).

3.8 References

1. Chatterjee, A. and S. Schiewer, *Biosorption of Cadmium(II) Ions by Citrus Peels in a Packed Bed Column: Effect of Process Parameters and Comparison of Different Breakthrough Curve Models.* Clean-Soil Air Water, 2011. **39**(9): p. 874-881.
2. Chatterjee, A. and L. Ray, *Biosorption of Cu(II) by immobilized biomass of Bacillus cereus M^{I}_{16} from aqueous solution.* Journal of Scientific & Industrial Research, 2008. **67**(8): p. 629-634.
3. Akar, T., et al., *Enhanced biosorption of nickel(II) ions by silica-gel-immobilized waste biomass: Biosorption characteristics in batch and dynamic flow mode.* Journal of Hazardous Materials, 2009. **163**(2-3): p. 1134-1141.
4. Fu, Y.Z. and T. Viraraghavan, *Column studies for biosorption of dyes from aqueous solutions on immobilised Aspergillus niger fungal biomass.* Water Sa, 2003. **29**(4): p. 465-472.
5. Aksu, Z., G. EÄŸretli, and T. Kutsal, *A comparative study of copper(II) biosorption on Ca-alginate, agarose and immobilized C. vulgaris in a packed-bed column.* Process Biochemistry, 1998. **33**(4): p. 393-400.
6. Vannela, R. and S.K. Verma, *Cu2+ Removal and recovery by SpiSORB: batch stirred and up-flow packed bed columnar reactor systems.* Bioprocess and Biosystems Engineering, 2006. **29**(1): p. 7-17.
7. Khoo, K.M. and Y.P. Ting, *Polyvinyl alcohol as an immobilization matrix - a case of gold biosorption.* Water Science and Technology, 2001. **43**(11): p. 17-23.
8. Volesky, B., *Biosorption process simulation tools.* Hydrometallurgy, 2003. **71**(1-2): p. 179-190.
9. Gabaldon, C., P. Marzal, and F.J. Alvarez-Hornos, *Modelling Cd(II) removal from aqueous solutions by adsorption on a highly mineralized peat. Batch and*

fixed-bed column experiments. Journal of Chemical Technology and Biotechnology, 2006. **81**(7): p. 1107-1112.

10. da Silva, E.A., et al., *Modeling of copper(II) biosorption by marine alga Sargassum sp in fixed-bed column.* Process Biochemistry, 2002. **38**(5): p. 791-799.
11. Izquierdo, M., et al., *Modeling of copper fixed-bed biosorption from wastewater by Posidonia oceanica.* Bioresource Technology, 2010. **101**(2): p. 510-517.
12. Pradhan, S. and L.C. Rai, *Copper removal by immobilized Microcystis aeruginosa in continuous flow columns at different bed heights: study of the adsorption/desorption cycle.* World Journal of Microbiology and Biotechnology, 2001. **17**(9): p. 829-832.
13. Iqbal, M., S. Schiewer, and R. Cameron, *Mechanistic elucidation and evaluation of biosorption of metal ions by grapefruit peel using FTIR spectroscopy, kinetics and isotherms modeling, cations displacement and EDX analysis.* Journal of Chemical Technology and Biotechnology, 2009. **84**(10): p. 1516-1526.
14. Cooney, D.O., *Adsorption Design for Wastewater Treatment.* 1998
15. Azizian, S., *Kinetic models of sorption: a theoretical analysis.* Journal of Colloid and Interface Science, 2004. **276**(1): p. 47-52.
16. Hashim, M.A. and K.H. Chu, *Biosorption of cadmium by brown, green, and red seaweeds.* Chemical Engineering Journal, 2004. **97**(2-3): p. 249-255.
17. Schiewer, S. and A. Balaria, *Biosorption of Pb2+ by original and protonated citrus peels: Equilibrium, kinetics, and mechanism.* Chemical Engineering Journal, 2009. **146**(2): p. 211-219.
18. Chu, K.H., *Removal of copper from aqueous solution by chitosan in prawn shell: adsorption equilibrium and kinetics.* Journal of Hazardous Materials, 2002. **90**(1): p. 77-95.
19. Wu, F.C., R.L. Tseng, and R.S. Juang, *Initial behavior of intraparticle diffusion model used in the description of adsorption kinetics.* Chemical Engineering Journal, 2009. **153**(1-3): p. 1-8.

20. Selatnia, A., et al., *Biosorption of Cd2+ from aqueous solution by a NaOH-treated bacterial dead Streptomyces rimosus biomass.* Hydrometallurgy, 2004. **75**(1-4): p. 11-24.

21. Kumar, D. and J.P. Gaur, *Chemical reaction- and particle diffusion-based kinetic modeling of metal biosorption by a Phormidium sp.-dominated cyanobacterial mat.* Bioresource Technology, 2011. **102**(2): p. 633-640.

22. Boyd, G.E., A.W. Adamson, and L.S. Myers, *The exchange adsorption of ions from aqueous solutions by organic zeolites. II. Kinetics.* Journal of the American Chemical Society, 1947. **69**(11): p. 2836-2848.

23. Reichenberg, D., *properties of ion-exchange resin in relation to their structure. III. Kinetics of exchange.* Journal of American Chemical Society, 1953. **75**.

24. Ofomaja, A.E., E.E. Ukpebor, and S.A. Uzoekwe, *Biosorption of Methyl violet onto palm kernel fiber: Diffusion studies and multistage process design to minimize biosorbent mass and contact time.* Biomass & Bioenergy, 2011. **35**(10): p. 4112-4123.

25. Ofomaja, A.E., *Biosorption studies of Cu(II) onto Mansonia sawdust: Process design to minimize biosorbent dose and contact time.* Reactive & Functional Polymers, 2010. **70**(11): p. 879-889.

26. Ofomaja, A.E., *Intraparticle diffusion process for lead(II) biosorption onto Mansonia wood sawdust.* Bioresource Technology, 2010. **101**(15): p. 5868-5876.

27. Helfferich, F. and M.S. Plesset, *Ion exchange kinetics. a nonlinear diffusion problem.* The Journal of Chemical Physics, 1958. **28**(3).

28. Inglezakis, V.J. and H.P. Grigoropoulou, *Applicability of simplified models for the estimation of ion exchange diffusion coefficients in zeolites.* Journal of Colloid and Interface Science, 2001. **234**(2): p. 434-441.

29. Urano, K. and H. Tachikawa, *Process-Development for Removal and Recovery of Phosphorus from Waste-Water by a New Adsorbent .2. Adsorption Rates and Breakthrough Curves.* Industrial & Engineering Chemistry Research, 1991. **30**(8): p. 1897-1899.

30. Maiti, S., et al., *Determination of Kinetic Parameters in the Biosorption of Cr (VI) on Immobilized Bacillus cereus in a Continuous Packed Bed Column Reactor.* Applied Biochemistry and Biotechnology, 2009. **159**(2): p. 488-504.

31. Gerente, C., et al., *Removal of metal ions from aqueous solution on low cost natural polysaccharides: Sorption mechanism approach.* Reactive and Functional Polymers, 2000. **46**(2): p. 135-144.

32. Guibal, E., et al., *Uranium Sorption by Glutamate Glucan - a Modified Chitosan .2. Kinetic-Studies.* Water Sa, 1993. **19**(2): p. 119-126.

33. Freitas, O.M.M., et al., *Removal of Cd(II), Zn(II) and Pb(II) from aqueous solutions by brown marine macro algae: Kinetic modelling.* Journal of Hazardous Materials, 2008. **153**(1-2): p. 493-501.

34. Yang, J.B. and B. Volesky, *Intraparticle diffusivity of Cd ions in a new biosorbent material.* Journal of Chemical Technology and Biotechnology, 1996. **66**(4): p. 355-364.

35. Choy, K.K.H. and G. McKay, *Sorption of cadmium, copper, and zinc ions onto bone char using Crank diffusion model.* Chemosphere, 2005. **60**(8): p. 1141-1150.

36. Crank, J., *The Mathematics of Diffusion.* 1980: Oxford University Press.

37. Boschi, C., et al., *Cd(II) biosorption using Lessonia kelps.* Journal of Colloid and Interface Science, 2011. **357**(2): p. 487-496.

38. Puranik, P.R., J.M. Modak, and K.M. Paknikar, *A comparative study of the mass transfer kinetics of metal biosorption by microbial biomass.* Hydrometallurgy, 1999. **52**(2): p. 189-197.

39. Ruiz, M., A.M. Sastre, and E. Guibal, *Palladium sorption on glutaraldehyde-crosslinked chitosan.* Reactive & Functional Polymers, 2000. **45**(3): p. 155-173.

40. Ko, D.C.K., J.F. Porter, and G. McKay, *Film-pore diffusion model for the fixed-bed sorption of copper and cadmium ions onto bone char.* Water Research, 2001. **35**(16): p. 3876-3886.

41. Aksu, Z. and T. Kutsal, *Determination of kinetic parameters in the biosorption of copper(II) on Cladophora sp., in a packed bed column reactor.* Process Biochemistry, 1998. **33**(1): p. 7-13.

42. Choy, K.K.H., et al., *Film and intraparticle mass transfer during the adsorption of metal ions onto bone char.* Journal of Colloid and Interface Science, 2004. **271**(2): p. 284-295.

43. Wakao, N. and T. Funazkri, *Effect of fluid dispersion coefficients on particle-to-fluid mass transfer coefficients in packed beds: Correlation of Sherwood numbers.* Chemical Engineering Science, 1978. **33**(10): p. 1375-1384.

44. Murillo, R., et al., *Adsorption of phenanthrene on activated carbons: Breakthrough curve modeling.* Carbon, 2004. **42**(10): p. 2009-2017.

45. JanssonCharrier, M., et al., *Dynamic removal of uranium by chitosan: Influence of operating parameters.* Water Science and Technology, 1996. **34**(10): p. 169-177.

4 Modeling competitive biosorption of cadmium(II) and zinc(II) ions by protonated citrus peels in batch systems[3]

4.1 Abstract

Biosorption by low cost biological sorbent materials can be used as a technique to remove heavy metals from wastewater. Equilibrium batch experiments were performed to investigate the single and binary metal biosorption of cadmium and zinc by protonated citrus peels. Different models were applied to describe the single and binary metal isotherms. The competitive Langmuir model was identified as the best model, providing a good description of the data with a minimum number of model parameters. The influence of different objective functions minimized to optimize model parameters was also considered. Protonated citrus peels showed a preference for Cd over Zn sorption in both single and binary metal systems.

4.2 Introduction

Decades of research established that different inexpensive biomass types can be employed to adsorb metal pollutants from aqueous solution, making it a potential alternative to the traditional metal removal technologies such as membrane processes, ion exchange process, chemical precipitation, solvent extraction, or chemical oxidation/reduction. These operations often require more energy or costly raw materials and/or chemical reagents to meet increasingly stringent regulatory criteria to keep pace with industrial growth which renders them prohibitively expensive for the treatment of large volumes of dilute discharge. Even though a lot of research has been done on the subject of biosorption, little commercial success has been achieved to date. One reason is that biosorption research was more focused on searching novel biosorbents with higher

---

[3] Chatterjee, A. and S. Schiewer. 2012. Modeling competitive biosorption of cadmium(II) and zinc(II) ions by protonated citrus peels. Prepared for submission in CLEAN – Soil, Air, Water.

uptake capacity for a single metal, rather than continuing study on any given biosorbent to investigate features essential for commercial success, such as its behavior in the presence of other heavy and light metals which are likely to be encountered in a real waste. This demands a long-term step by step study focusing on a single biosorbent. Our past research established that citrus peels are more suitable for adsorption of cadmium [1] than other citrus and non citrus fruit waste in a batch reactor and that it can also be used in the commercially preferred fixed bed reactor [2]. Pectin, which consists of galacturonic acid polymers with smaller amounts of other saccharides such as rhamnose, arabinose, is a major peel constituent. Pectin plays an instrumental role in binding heavy metals [3] Metal uptake capacity at equilibrium for single metals at constant pH follows the Langmuir isotherm [4]. Overall batch kinetics follow pseudo first order [1] or pseudo second order rate law [3] and overall fixed bed kinetics can be described by the Bohart Adams model [2]. The obvious next step of this systematic exploration of biosorption by citrus peels is to test its potential in the presence of other toxic metals. The purpose of this article is to study the simultaneous biosorption of cadmium and zinc and to investigate the suitability of different multi-metal sorption isotherm models in explaining the mutual influence of each metal cation on sorption of other. The metals were chosen for their industrial use vis a vis toxic effect on environment. Cadmium is a priority pollutant and released into environment from mining effluent and other industries such as electroplating, Ni-Cd battery and alloy preparation. Zinc is an essential trace element for plants, animals and microorganisms, but becomes toxic for humans at levels of 100-500 mg/day [5]. Zinc is mainly used for galvanization, manufacturing paints and pigments, brass and other alloys including cadmium zinc telluride (CZT) which is used as a semiconductor. Zn and Cd are also found together in mining effluent. The maximum allowable levels of Zn and Cd in safe drinking water, as determined by US EPA are 0.005 and 0.015 mg/L, respectively.

It is obvious that in a binary system, sorption of the primary metal would depend on presence of a second metal in solution. For citrus peels, kinetics were found to be fast and equilibrium was achieved within an hour [3]. The uptake of each cation depends on

the equilibrium concentrations of all metals, which are different from the respective initial concentrations. This presents a fundamental challenge for studying the effect of one metal on the biosorption of other: unlike other parameters such as pH or dose of biosorbent, the equilibrium metal concentration cannot be deliberately adjusted. It is impossible to obtain a desired final concentration in the experiment. Rather, a random set of aqueous (C1, C2) and solid phase (q1, q2) equilibrium concentrations of two metals (M1 and M2) is generated. The problem can be dealt with by generating a smooth surface showing the uptake as a function of c1 and c2, either by interpolating between experimental data or by developing a suitable equilibrium model. Only a small fraction of biosorption publications focused on binary metal biosorption. Incidentally many of them actually analyzed the biosorption of a primary metal as a function of the *initial* co-cation concentration, which can easily be adjusted. However, this is not a meaningful analysis; an isotherm at a particular *initial* co-ion concentration is not 'fixed', but will vary depending on biosorbent dose and other factors which alter the equilibrium concentration of M2 for any given initial concentration.

4.3 Modeling equations

4.3.1 Single metal isotherms

A model describing the equilibrium between solid and liquid phase concentration of the sorbate species is termed 'isotherm'. The reaction at the binding site is often considered as ion-exchange (equation (4.1), (4.2)) though other mechanisms such as chelation, complexation, micro-precipitation and physical adsorption (equation (4.3)) through Van der Waals forces may contribute as well.

Ion exchange:

$$M^{2+} + S\text{-}H \leftrightarrow M\text{-}S^{+} + H^{+} \text{ (1:1 stoichiometry)} \quad (4.1)$$

$$M^{2+} + 2\ S\text{-}H \leftrightarrow 2\ M_{0.5}\text{-}S + 2\ H^{+} \text{ (1:2 stoichiometry)} \quad (4.2)$$

Adsorption:

$$M + S \leftrightarrow M\text{-}S \tag{4.3}$$

Here S denotes the biosorbent surface and M denotes the metal ion as the sorbate species. Two frequently used models to describe the single metal batch biosorption equilibrium are the Langmuir and Freundlich isotherms. The Langmuir model (equation (4.4)) [6], originally developed to describe gas adsorption on activated carbon, views the sorbent as a collection of a finite number of equally efficient binding sites which become saturated when a monolayer of the sorbed species is formed following equation (4.2), which, unlike ion exchange, is not accompanied by the release of another species from sorbent material.

$$q = \frac{q_m b C}{1 + bC} \tag{4.4}$$

Here C denotes the aqueous equilibrium concentration of the concerned metal ion (M1 or M2) in a mono-component system and q is the corresponding equilibrium solid phase concentration, q_m is the saturation or monolayer capacity of the sorbent and b is ratio of adsorption to desorption rate constants for equation 4.3. Higher b values signify a higher affinity for the sorbent.

Since the availability of binding sites may depend on the concentration of the released species, Langmuir isotherm is in general not valid for modeling ion exchange process. But if pH of the solution is kept constant throughout the duration of the experiment and a 1:1 stoichiometry is assumed where one divalent metal binds to one divalent site, it becomes equivalent to an isotherm based on ion exchange [4]. Interestingly, Langmuir isotherm is often used when pH of the solution only intermittently adjusted [7] or not adjusted at all [8]. One reason of the ubiquitous application of Langmuir isotherm in biosorption related study is that isotherm parameters (b, q_m) convey a physical meaning and provides a simple and quick way to compare among different metal-sorbent combination.

The Freundlich isotherm considers heterogeneity of the binding sites. It assumes that there are always adsorption sites available which require a progressively higher energy of activation for adsorption to take place and therefore are never saturated [9].

$$q = K_F C^{1/n} \tag{4.5}$$

Where K_f and n are isotherm parameters. Both Langmuir and Freundlich model can be combined to the Langmuir-Freundlich model:

$$q = \frac{q_m b_{LF} C^{1/n}}{1 + b_{LF} C^{1/n}} \tag{4.6}$$

Where q_m, b_{LF} and n are isotherm parameters. This model with n = 2 also represents the Langmuir isotherm for a 1:2 stoichiometric equation (4.2) [4].

$$q = \frac{q_m b C^{0.5}}{1 + b C^{0.5}} \tag{4.7}$$

4.3.2 Binary metal isotherms

There are three different types of models used to describe the multi-metal batch equilibrium, depending on whether parameters are obtained from a single-component study or multi-metal study.

4.3.2.1 Langmuir Predictive Model (LPM)

This model is a simple extension of the single component model and does not require any additional parameter other than those obtained from single metal isotherms and hence does not require any fitting on binary or multi-metal experimental data.

$$q_i = \frac{q_{mi} b_i C_i}{1 + \sum_{j=1}^{2} b_j C_j} (i = 1, 2) \tag{4.8}$$

4.3.2.2 Semi predictive models

These models incorporate additional corrective parameters into the predictive models making these more flexible for fitting to experimental data from binary system. These additional parameters do not have any physical meaning. These models are not considered in this article, but discussed elsewhere [8].

4.3.2.3 Modified Langmuir type models

Influence of a secondary metal on the biosorption of a target metal may be compared with enzyme inhibition. The Langmuir model for one component is mathematically similar to the Michalis-Menten model used to describe enzyme-substrate kinetics, and can also be extended by hypothesizing a series of reactions similar to those used for describing enzyme inhibition, which is classified as competitive, uncompetitive or partially competitive using modifications of the classical Michalis-Menten Model. Details of the derivation of these equations can be found elsewhere [6].

4.3.2.3.1 Competitive Langmuir Model (CLM)

A competitive model based on the original Langmuir isotherm (equation (4.4)) assumes the following equilibrium relations equation (4.9), (4.10) where b_1 and b_2 denote the respective equilibrium constant. The square bracket represents the concentration of respective species. These equations along with a mass balance for the binding sites lead to the final form of the isotherm, given in equation (4.11). This equation is mathematically analogous to equation (4.8) where it was applied in a predictive way based on monometal parameters i.e., with different q_m and b values for different metals. In CLM, the equation was applied by using the parameters optimized for the binary system so that there was a single optimized q_m value for both M1 and M2 as well as individually optimized b values for each metal.

$$M1+S \leftrightarrow M1S \qquad b_1 = \frac{[M1][S]}{[M1S]} \tag{4.9}$$

$$M2+S \leftrightarrow M2S \qquad b_2 = \frac{[M2][S]}{[M2S]} \tag{4.10}$$

$$q_i = \frac{q_m b_i C_i}{1+\sum_{j=1}^{2} b_j C_j} (i = 1, 2) \tag{4.11}$$

4.3.2.3.2 Uncompetitive Langmuir Model (ULM)

This model considers that two metal ions can simultaneously attach to a single site. Equation (4.9), (4.10), (4.12) and a mass balance for the binding sites can be combined to obtain the final isotherm expression given in equation (4.13):

$$M1+M2+S \leftrightarrow M1M2S \qquad b = \frac{[M1][M2][S]}{[M1M2S]} \tag{4.12}$$

$$q_i = \frac{q_m(b_i C_i + b C_i C_j)}{1+b_i C_i + b_j C_j + 2b C_i C_j} \text{ (for i, j = 1, 2 with } i \neq j) \tag{4.13}$$

4.3.2.3.3 Partially Competitive Langmuir Model (PCM)

This model is derived assuming that a metal cation can attach to a site which is free (equation (4.9), (4.10)) or already occupied by a co cation equation (4.14), (4.15). The final expression of the isotherm is given by equation (4.16) which can be reduced to ULM (equation (4.13)) with $b = b_i b_{ji} = b_j b_{ji}$. This is because the ULM does not consider the order of attachment in the formation of M1M2S (equation (4.12)) which is considered in PCM (equation (4.14), (4.15)).

$$M1+M2S \leftrightarrow M1(M2S) \quad b_{12} = \frac{[M1][M2S]}{[M1(M2S)]} \tag{4.14}$$

$$M2+M1S \leftrightarrow M2(M1S) \quad b_{21} = \frac{[M2][M1S]}{[M2(M1S)]} \tag{4.15}$$

$$q_i = \frac{q_m(b_iC_i + b_jb_{ji}C_iC_j)}{1 + b_iC_i + b_jC_j + C_iC_j(b_ib_{ij} + b_jb_{ji})} \text{ [for i, j = 1, 2 with i} \neq \text{j]} \quad (4.16)$$

4.3.2.3.4 Langmuir-Freundlich Competitive Model (LFCM)

This model is equivalent to the CLM model, but based on the LF isotherm:

$$q_i = \frac{q_m b_i C_i^{ni}}{1 + \sum_{j=1}^{2} b_j C_j^{nj}} (i = 1,2) \quad (4.17)$$

4.4 Materials and methods

4.4.1 Protonation of citrus peels

10 g of dry orange peels were suspended in 500 ml of 0.1 N nitric acid for 4 hours with constant stirring on an orbital shaker (120 rpm) at 25° C so that peels release naturally occurring light metals such as Na, K and Ca. These so called 'protonated peels' were then filtered, thoroughly washed with distilled water, dried overnight at 45° C and sieved into different size fractions. Enhanced biosorptive capacity was reported for protonated peels in comparison to raw peels [10]. There was no significant weight loss in this process.

4.4.2 Batch experiment

All batch experiments were performed at 25 °C for 4 hours in a Metrohm auto-titrator using protonated peels of 1-2 mm size. A constant pH of 5 was maintained through the programmed addition of 0.01 N NaOH into the magnetically stirred titrating vessel containing a suspension of about 0.1 g protonated peels (M) in 100 ml of metal solution (V), prepared from 10,000 mg/L Atomic Absorption Standards stock solution purchased from VWR. The initial Cd and Zn concentration (C_0) ranged from 0 to 500 mg/L. The final equilibrium concentration (C) was measured using a flame AAS (Perkin Elmer). The metal uptake (q) was calculated from the mass balance Equation (4.18).

$$q \times M = V(C_0 - C) \tag{4.18}$$

4.5 Results and discussion

4.5.1 Single metal biosorption

Experimental data obtained from single metal sorption of Zn and Cd were modeled applying Langmuir, Freundlich, LF and Langmuir 1:2 stoichiometry models. Model parameters were obtained by iterative non-linear least square fitting using the solver function in Excel which is based on a generalized reduced gradient method. The following objective function was used for optimization:

$$F_{obj} = \sum_1^N (q_{\text{mod}} - q_{\text{exp}})^2 \tag{4.19}$$

Optimized parameter values along with error variance (s^2) and regression coefficients (R^2) are reported in Table 4.1.

4.5.1.1 Comparison of models

It can be seen from Figure 4.1 that all four models fit well to both Cd and Zn sorption data. A preliminary analysis of these results (Table 4.1) showed that all R^2 were found to be statistically significant. Since the LF model requires one more parameter than the Langmuir, Freundlich, or 1:2 stoichiometry models, these models are now compared with the LF model to determine whether improved model fit justifies introduction of an additional parameter. This was done by performing an F test [11], where the F statistic is calculated as equation (4.20) and the corresponding probability P (F, df1-df2, df2) was evaluated using MS Excel.

$$F = \frac{(SS1 - SS2)/SS1}{(df1 - df2)/df2} \tag{4.20}$$

Here *SSi* denotes square sum of error for i^{th} model, *df* is the degrees of freedom calculated as the number of data points less the number of parameters. This test answers the following question: When replacing model 1 by model 2, is the improved fit, measured as

a decrease in the sum square of errors *((SS1-SS2)/SS1)*, greater than the increase in complexity by introduction of a new parameter *((df1-df2)/df2)*? The result is shown in Table 4.2. This confirmed that the better fit of the LF model is not significant (P>0.05) for either of other three models for Zn and Cd sorption data, except that the LF model fits significantly better than the Langmuir model for Cd as the P value in this instance is lower than the traditional threshold value of 0.05. Overall, use of a third model parameter is not justified for the present data. Therefore the Langmuir model with 1:2 stoichiometry, which fits better than the other 2-parameter models, is considered the best model in this case.

4.5.1.2 Comparison of metals

The Langmuir equilibrium constant of Cd was found to be 50% higher than that for Zn, which can be explained by considering the related physiochemical properties of those metal ions which are shown in Table 4.3. Several related articles [12, 13] compared the Langmuir affinity of metals on the basis of similarity between the biosorption reaction (equation (4.1)-(4.3)) and the hydrolysis reaction (equation (4.21)), which suggest that metals with a lower hydrolysis constant (-log K for Zn>Cd) are more acidic, leading to easier interaction with a protonated site and hence higher affinity. Accordingly, a higher affinity is expected for Zn.

$$HO\text{-}H + M^{2+} \leftrightarrow M\text{-}OH^{+} + H^{+} \qquad (4.21)$$

On the other hand, ions with smaller crystal radii usually have stronger hydration shells and larger hydrated radius. A Cd ion, having a slightly lower hydrated radius compared to Zn, would have a little stronger electrostatic interaction with a negatively charged binding site, which would imply a higher affinity of Cd.

A further factor contributing to overall affinity is that an ion in aqueous solution needs to break the hydration sphere by providing hydration energy before being bound at the binding site. If sorption affinity is driven by the hydration enthalpy the higher absolute value of hydration enthalpy of Zn due to its lower ionic radius implies a higher energy requirement, leading to lower affinity.

Either of these reasons may explain the affinity sequence noted in an individual study, however such trends cannot be generalized since the order of affinity for Zn and Cd varies depending on the biosorbent used (Table 4.6). Earlier, Schiewer explained higher affinity of Cd than Zn for an algal biosorbent as the combined effect of a decrease in covalent and electrostatic binding and increase in hydration strength [14]. Since most of the physicochemical characteristics of these two metals are not widely different from each other, the biosorption performance depends on the experimental condition and biosorbents. Different affinity sequences were even reported for the same biosorbent in two different studies [8, 15].

Finally, the equilibrium uptake capacity for Zn was found to be higher than that for Cd when expressed in molar units. A similar result was reported in another related study [15]. It may also be noted that a different conclusion can be reached if mass units are used instead of molar units. As shown in Table 4.6, the uptake capacity of citrus peels is comparable with other biosorbents.

4.5.2 Binary metal biosorption

4.5.2.1 Model fitting

The LPM, along with CLM, ULM, PCM and LFCM are applied to the experimental data obtained from simultaneous sorption of Cd and Zn. Model parameters for all models were obtained by applying the same numerical method as for single metal sorption. Two different objective functions, one based on the absolute error and another based on the relative error were employed for the purpose of optimization. The results are reported in Table 4.4.

$$F_{rel} = F1 + F2 = \sum_{i=1}^{N}\left(\frac{q1_{i,\exp} - q1_{i,\mathrm{mod}}}{q1_{i,\exp}}\right)^2 + \sum_{i=1}^{N}\left(\frac{q2_{i,\exp} - q2_{i,\mathrm{mod}}}{q2_{i,\exp}}\right)^2 \tag{4.22}$$

$$F_{abs} = F1 + F2 = \sum_{i=1}^{N}\left(q1_{i,\exp} - q1_{i,\mathrm{mod}}\right)^2 + \sum_{i=1}^{N}\left(q2_{i,\exp} - q2_{i,\mathrm{mod}}\right)^2 \tag{4.23}$$

An objective function based on the absolute error does not differentiate between uptake data obtained from different metals having low or high average experimental uptake capacity. For a given absolute error, the relative error would be higher for the data point showing a lower experimental uptake capacity. For two metals with large differences in their respective average uptake, fraction of error contributed by individual metals (F1/F or F2/F) would be very different for F_{rel} and F_{abs} and the impact of each metal on goodness of fit would be different: the optimization algorithm tends to give a undue weight to the points with larger q_{exp} values associated with a larger average scatter and ignores points with lower q_{exp} values when F_{abs} is used. An objective function based on the relative error F_{rel} removed this bias by scaling the error with the factor $(1/q_{exp}^2)$, but the relative error becomes larger for very low q_{exp} values and a reverse bias may occur: points with lower q values will receive more weight due to having more scatter in their relative error. The final choice of the objective function would then depend on whether both metals are equally important and have similar uptake or not. This choice becomes important if the optimal set of parameters vary with the objective function used.

A plot of residuals against predicted uptake (q_{mod}) for each of the 8 regression models (4 models for each objective function) did not follow any pattern (plot not shown). The normal probability plot of residuals in each case confirmed an approximate normal distribution of errors. These observations justified that regression assumptions are not violated and each model adequately represents the data. This analysis, however, cannot compare the predictive capability among models.

To compare among models, scatter plots (Figure 4.8) showing regressed value of the dependent variable q_{mod} vs. the independent variable q_{exp} were prepared. For scatter plots, all data points should ideally lie on the squared diagonal (slope = 1 and intercept = 0) with minimum deviations. The parameters (slope (m) and intercept (c)) for these scatter plots, along with squared regression coefficient (R^2) and error variance (s^2) are reported for each objective function in Table 4.5. The LPM did not fit as good as other four models (not included in figure) which is not surprising because model parameters were derived from a different experimental data set, namely the single-metal systems of each

metal. Even then, the regression coefficient value is statistically significant, which means the influence of one metal on other metal in a binary system may be qualitatively predicted from this model based on mono-metal data. Based on the high regression coefficient and a tight fitting of points around squared diagonal in a scatter plot (Figure 4.8) (which is also evident from near zero intercept and slope close to unity), the other models perform equally well.

For the ULM, an extremely low and negative b value, obtained by using F_{rel} signifies that formation of a M1-M2-S complex is very unlikely. This was also observed in biosorption of other binary combination of metals (Pb/Cu, Pb/Cd, Cd/Cu) using a macro-alga [6]. Similarly, b_{12} and b_{21} for the PCM were found orders of magnitude lower than b_1 and b_2, implying that cations were reluctant to bind to an already occupied site.

Since the CLM was found to fit the experimental data satisfactorily, having lower or equal error variance as other models with more parameters, this model was chosen for as the best one for this study. According to the CLM, the b values follow the same trend as found in single metal systems which means that Cd was able to retain its higher affinity in presence of Zn. This was also reported in another Zn-Cd binary sorption study with orange waste (Table 4.6). The CLM was used in other binary metal sorption studies, most of which were done using seaweed based biomass.

Both similar and reverse affinity order was noticed for Zn-Cd systems even using the same biomass (algal) species (Table 4.6). Similar to what was discussed in the single metal section (4.5.1), b values for Zn and Cd do not follow a strict order. In yet another study, individual b values of single component systems were almost same as those for the binary solution. In other combination of binary metals including either Zn or Cd with a third metal, it was found [16] that the order of affinity (Zn<Cd) found in single component systems was reversed in the presence of Cu.

4.5.2.2 3D Biosorption surface

One way to illustrate binary bisorption data is the construction of a surface plot where x and y axes represent the equilibrium concentrations of two metals and the z axis shows

either the combined uptake or the uptake of individual metals. Accordingly three such plots are required for the complete description. Matlab provides a tool to interpolate randomly generated experimental uptake data to create a surface plot. An interpolated surface is not preferred; as shown in Figure 4.2, it is not smooth, but creates ups and downs since the surface honors all experimental points. For a smooth surface, uptake needs to be calculated using a suitable model.

The LC model obtained from F_{rel} may be used to generate such a smooth surface and experimental data can be plotted along with the model surface, enabling a visual judgment of the model quality which is shown in Figure 4.3 and Figure 4.4. The total uptake (Figure 4.5) is calculated by adding individual uptake values for Zn and Cd. While such a 3D plot is effective for illustration purposes, a more quantitative assessment of inhibition can be obtained by "cutting" the 3D surface plot at suitable x or y values, resulting in a series of 2D plots, which can be constructed from the model equation (4.11).

4.5.2.3 Influence of co-cation on biosorption of primary metal

Figure 4.6 and Figure 4.7 were produced from the CLM using model parameters obtained by minimizing F_{rel} (Table 4.4). Figure 4.6 describes the effect on the uptake of one metal at a fixed concentration of the other metal. It compares the Langmuir isotherm of the single-component system using parameters from Table 4.1 with the binary system (Zn and Cd) using parameters from Table 4.4, at high (2 mmol/L) and low (0.2 mmol/L) Cd concentration. It can be observed that the presence of a co cation always lowers the uptake the primary metal, but extent of inhibition differs from metal to metal. Biosorption of Zn in the presence of Cd was found to be affected more severely than vice versa. Presence of 0.2 mmol/L of Cd lowers the isotherm of pure Zn substantially while the effect was not so pronounced for Cd binding at the same Zn concentration. Increase in the co-cation concentration from 0.2 to 2 mmol/L depressed the metal uptake more heavily and that reduction was more pronounced for Zn binding in the presence of Cd. The

reason for Cd being more competitive than Zn is that its b value (affinity) is almost three times higher than that of Zn.

This situation is further illustrated in Figure 4.7 which demonstrates how the uptake of metal M1 (as percent of the uptake in the mono-metal system) is influenced by progressively increasing concentrations of metal M2 at a fixed residual concentration of metal M1. At higher residual concentration of Cd (curve a), its uptake is gradually dropped to about 40 percent of its original value (Zn concentration = 0) when the Zn equilibrium concentration is gradually increased to 2 mmol/L. In the same situation, (curve b, Zn concentration is 2 mmol/L), Zn was able to retain only about 15 percent of its original uptake when the Cd concentration is progressively increased to 2 mmol/L. Also, curve b lies below a, which means, at any co-cation concentration, Zn uptake is more strongly reduced than that of Cd, implying stronger inhibition power of Cd. A similar extent of Cd sorption inhibition only occurs when the Cd concentration is an order of magnitude lower, 0.2 mmol/L which is shown in curve c. At this low concentration of 0.2 mmol/L, Zn uptake is reduced to less than 5% of its original value.

In a similar study using orange waste, both Zn and Cd sorption were found to be moderately affected by the co-cation. In that study isotherms were compared by varying the initial concentration and not the equilibrium concentration of co-cation. Sorption of Cd was found to be competitively preferred to Zn by one seaweed species and also by a peat based biosorbent [17].

It may be noted that CLM model parameters may depend on the objective function chosen. Figure 4.3 to Figure 4.8, which were prepared using model parameters from F_{rel}, do not vary significantly when F_{abs} was considered. This consideration is vital because the influence of a co-cation on uptake of a primary metal, as predicted by CLM, cannot be verified by experimental data since the equilibrium concentration of co-cations cannot be controlled experimentally.

4.6 Conclusions

Protonated citrus peels show a higher affinity for Cd compared to Zn sorption in both mono-component and binary metal systems. Cd had the higher uptake capacity on a mass basis and Zn on a molar basis. For monocomponent systems, the Langmuir model based on a 1:2 stochiometry fits the isotherm data better than other two parameter models (1:1 Langmuir and Freundlich). Models with more than two parameters improved fitting only slightly but introduction of a third parameter was not justifiable based on an F test considering the degrees of freedom. A two parameter model (competitive Langmuir model) was also sufficient to explain binary biosorption i.e., to describe the isotherm in presence of another metal. Metals-peels interaction in binary biosorption is likely to be competitive in nature with no or negligible formation of M1-M2-S and M1-(M2-S) type complexes. CLM model parameters depend on whether the absolute or relative error is minimized during parameter optimization. Physicochemical properties of Zn and Cd are only moderately different and the order of preference for Zn vs. Cd in binary systems is highly dependent on the biosorbents' characteristics and other related factors.

Table 4.1 Single metal isotherm

Model	Zn			Cd		
	Parameters	s^2	R^2	Parameters	s^2	R^2
Langmuir	q_m = 0.51 mmol/g	1.49E-03	0.968	q_m = 0.34 mmol/g	6.15E-04	0.972
	b = 1.66 L/mmol			b = 4.90 L/mmol		
Freundlich	K_F = 0.27 $L^{1/n}/(g\ mmol^{1/n-1})$	1.15E-03	0.973	K_F = 0.24 $L^{1/n}/(g\ mmol^{1/n-1})$	2.69E-04	0.977
	n = 3.07			n = 4		
Langmuir (1:2)	q_m = 0.90 mmol/g b = 0.47 $(L/mmol)^{0.5}$	8.59E-04	0.995	q_m = 0.48 mmol/g b = 1.15 $(L/mmol)^{0.5}$	6.58E-05	0.991
Langmuir-Freundlich	q_m = 0.74 mmol/g	9.97E-04	0.981	q_m = 0.50 mmol/g	8.08E-05	0.997
	b = 0.66 L/mmol			b = 1.04 L/mmol		
	n = 1.73			n = 2.09		

Table 4.2 Comparison of 2 parameter models with LF model

Model compared with LF	Cd		Zn	
	F	P	F	P
Langmuir	34	0.01	3.99	0.14
Freundlich	9.31	0.06	1.94	0.26
1:2 stoichiometry	0.07	0.80	0.17	0.70

Table 4.3 Physicochemical properties of Cd and Zn [18]

	Zn	Cd
Crystal radius (pm)	88	109
Hydrated radius (pm)	430	426
Hydration enthalpy (-KJ/mol)	2044	1806
Hydrolysis constant (-log K)	8.96	10.08
Electronegativity	1.65	1.69
HSAB category	borderline	soft, close to borderline

Table 4.4 Modeling parameters for binary metal sorption (i = 1 for Zn, 2 for Cd)

Model	Model parameters	Using F_{rel}	Using F_{abs}
CLM Eq. 6 3 parameters	b_1	7.69	6.06
	b_2	21.06	16.15
	q_m	0.230	0.288
ULM Eq. 10 4 parameters	b	-0.24	1.01
	b_1	7.54	5.99
	b_2	20.65	16.38
	q_m	0.232	0.293
PCM Eq. 13 5 parameters	b_{12}	0.09	0.36
	b_{21}	-0.01	0.08
	b_1	8.52	6.71
	b_2	17.66	11.84
	q_m	0.23	0.29
LFCM Eq. 14 5 parameters	n_1	1.41	1.16
	n_2	0.91	1.05
	b_1	4.62	4.00
	b_2	7.75	9.19
	q_m	0.23	0.25

Table 4.5 Goodness of fit analysis for binary metal sorption models

F_{rel}						F_{abs}			
	R^2	m	c	s^2		R^2	m	c	s^2
LPM	0.70	1.49	0.02	0.44		0.70	1.49	0.02	0.44
CLM	0.88	0.88	0.01	0.0008		0.88	0.93	0.01	0.0007
ULM	0.88	0.89	0	0.0390		0.88	0.91	0.01	0.0007
PCM	0.88	0.89	0	0.0395		0.88	0.90	0.01	0.0007
LFCM	0.87	0.89	0	0.0008		0.88	0.90	0.01	0.0006

Table 4.6 Comparison of LM and CLM parameters with related studies

Biosorbent	Single metal system				Binary metal system			Ref
	$q_{m,Zn}$ (mmol/g)	$q_{m,Cd}$ (mmol/g)	b_{Zn} (L/mmol)	b_{Cd} (L/mmol)	q_m (mmol/g)	b_{Zn} (L/mmol)	b_{Cd} (L/mmol)	
Citrus peels	0.51	0.34	1.66	4.90	0.22	4.76	4.41	this study
Orange waste					0.26	5.04	6.06	[19]
Sargassum sp.	2.56	2.52	12.2	8.4	2.14	4.78	2.28	[15]
Ascophyllum sp.	0.68	0.75	2.27	4.98	0.67	2.27	6.67	[7]
Sargassum sp.	0.69	1.03	3.07	8.4	0.68	10.40	19.34	[8]
Moss sp.	0.16	0.14	8	18	0.18	9	12	[20]
Rice husk ash	0.09	0.05	12.4	21.3				[21]
Zeolite 4A	0.65	0.46	19.6	61.8				[21]

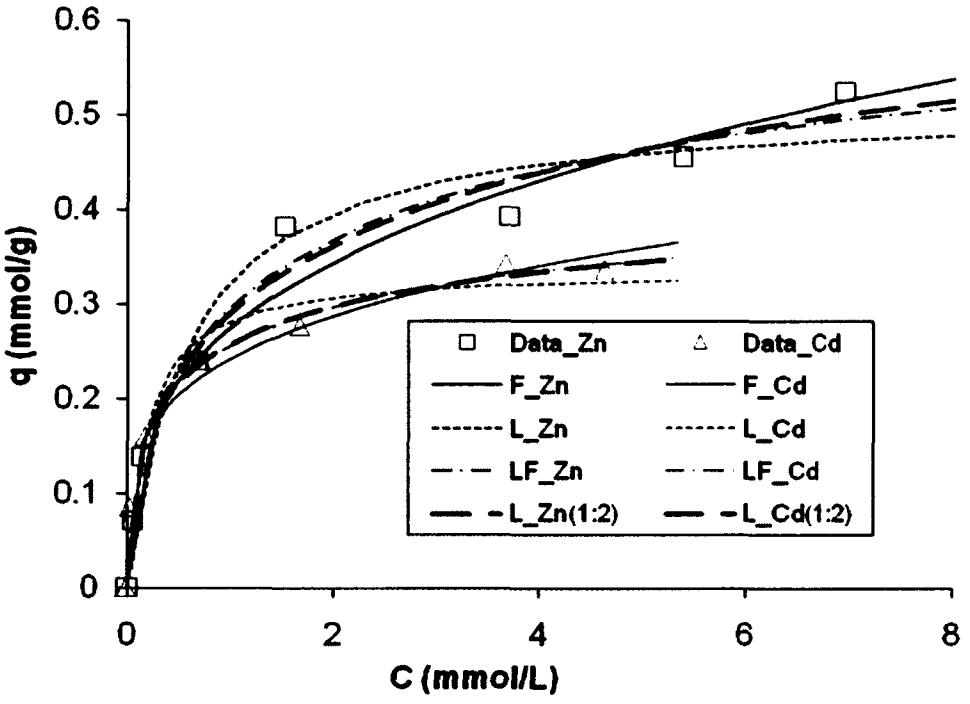

Figure 4.1 Single metal isotherms for Zn and Cd using citrus peels

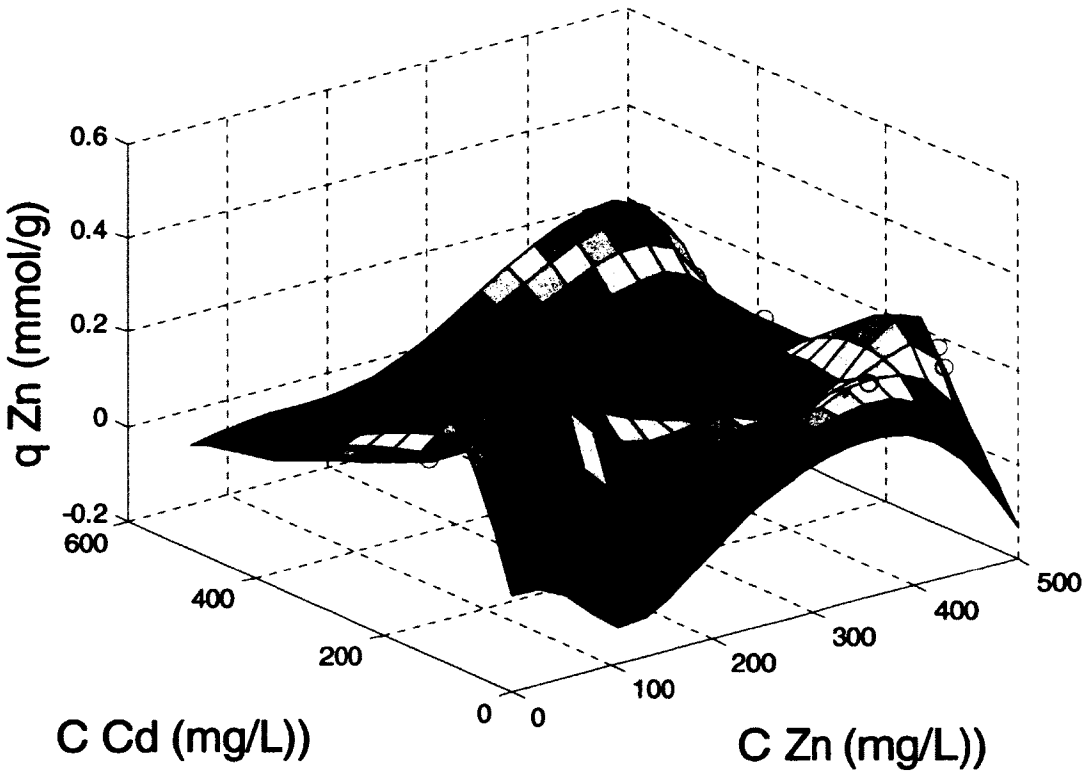

Figure 4.2 3D biosorption surface (interpolated) for Zn in binary system

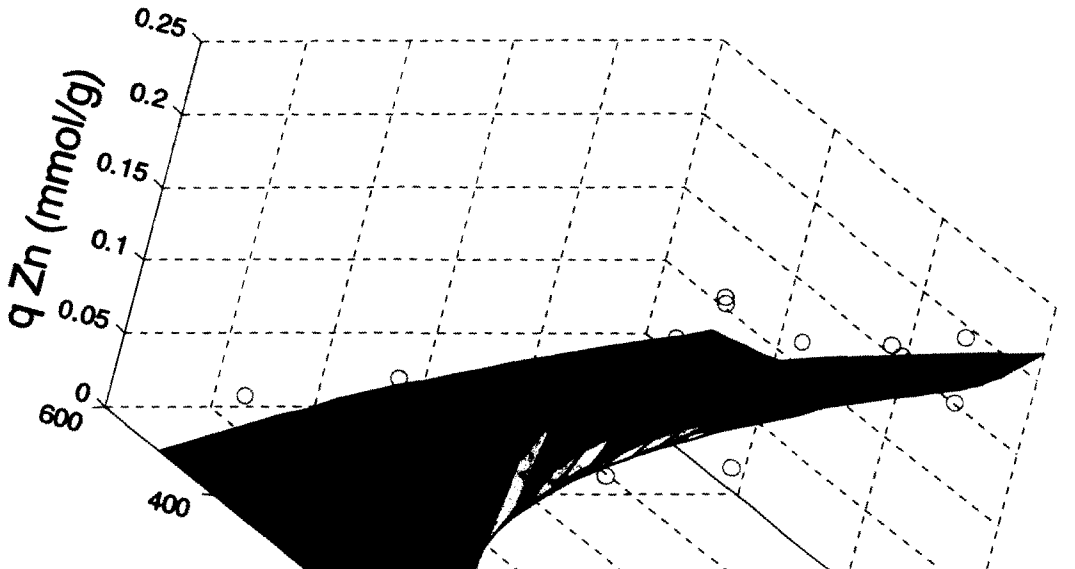
q Zn (mmol/g)
0.25
0.2
0.15
0.1
0.05
0
600
400

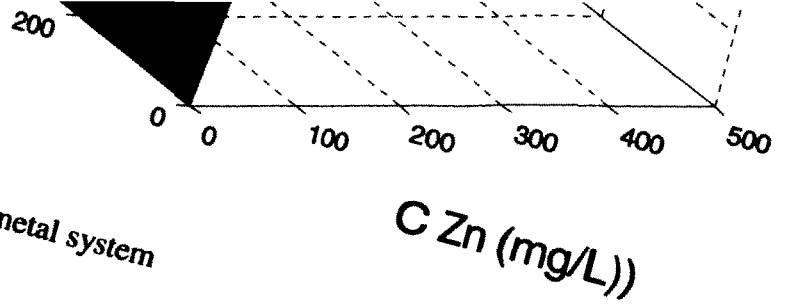

Figure 4.3 Uptake of Zn in bimetal system

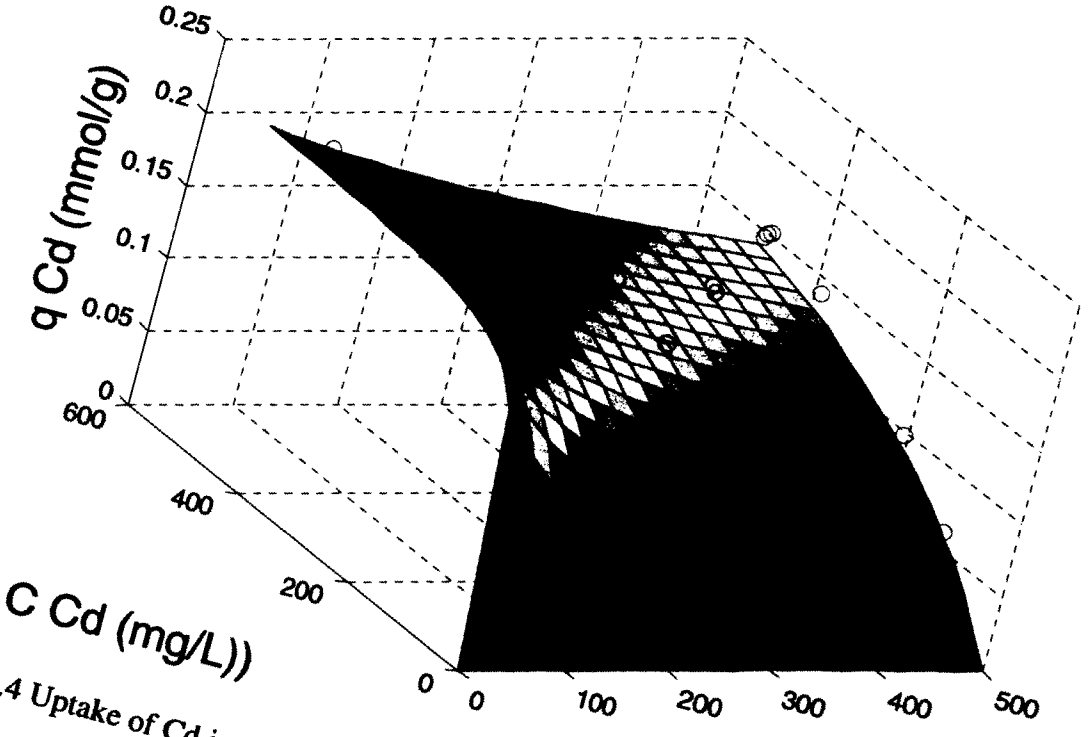

Figure 4.4 Uptake of Cd in bimetal system

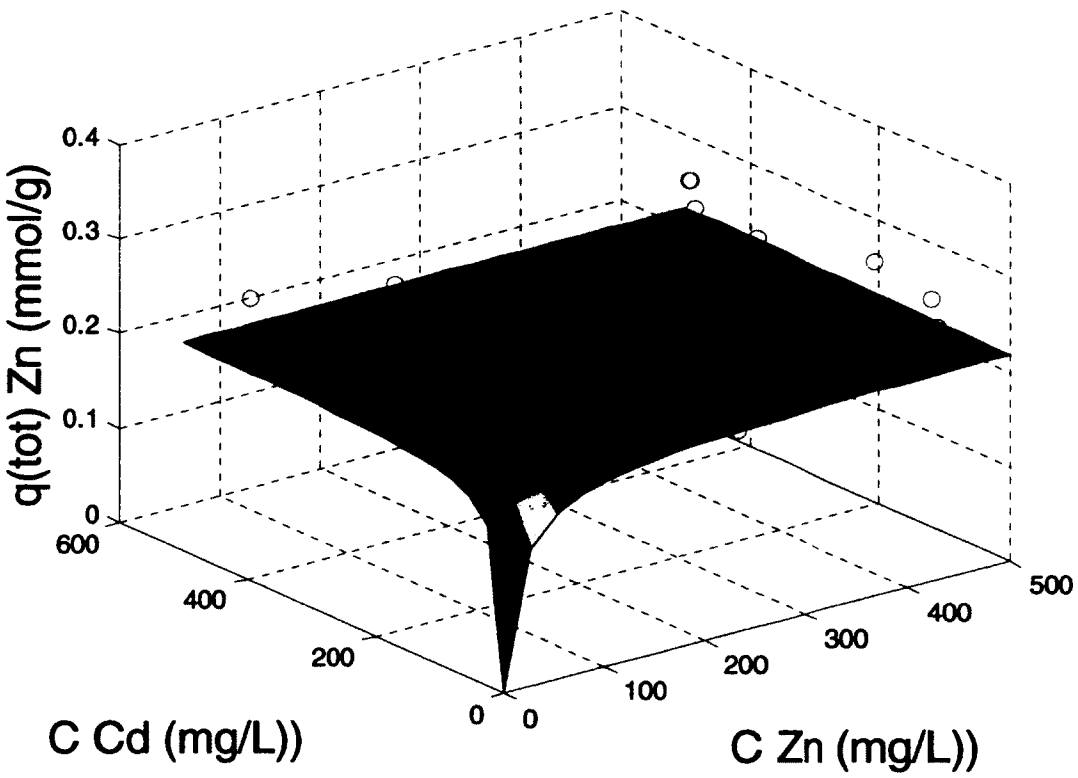

Figure 4.5 Total uptake (Cd and Zn) in bimetal system

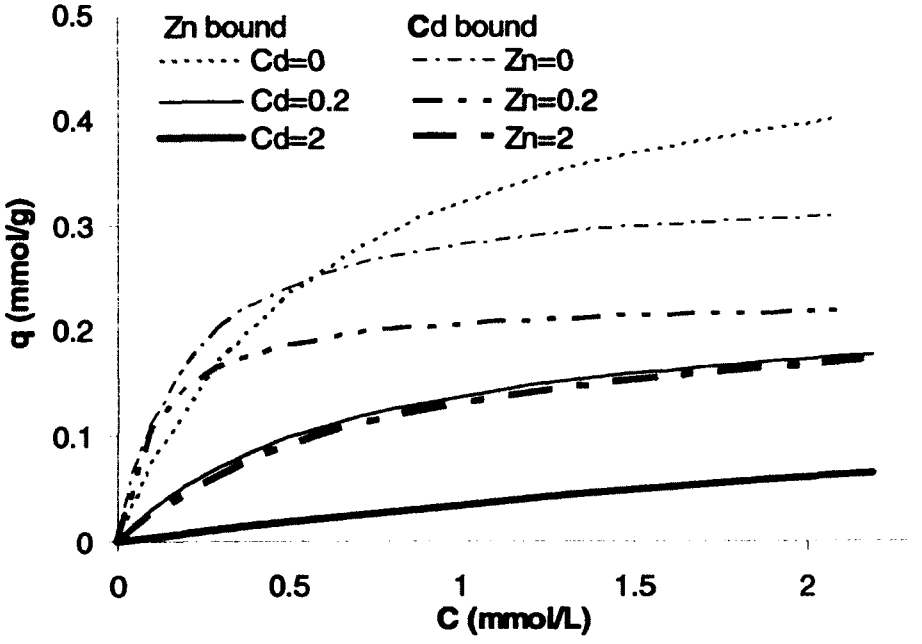

Figure 4.6 Cd and Zn isotherm at 0.2 and 2 mmol/L co-cation concentration

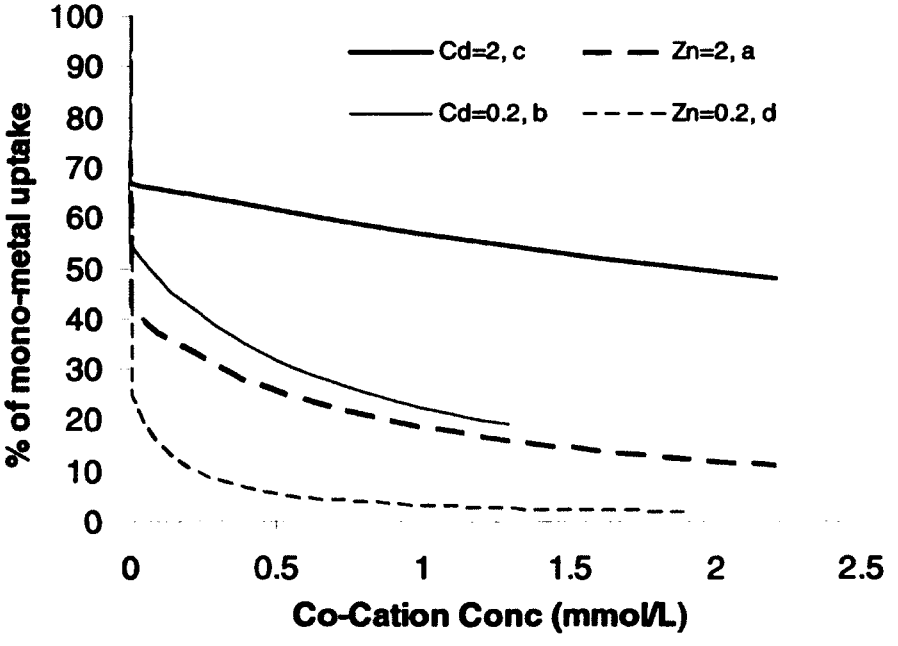

Figure 4.7 Reduction of Cd and Zn uptake with increasing co-cation concentration

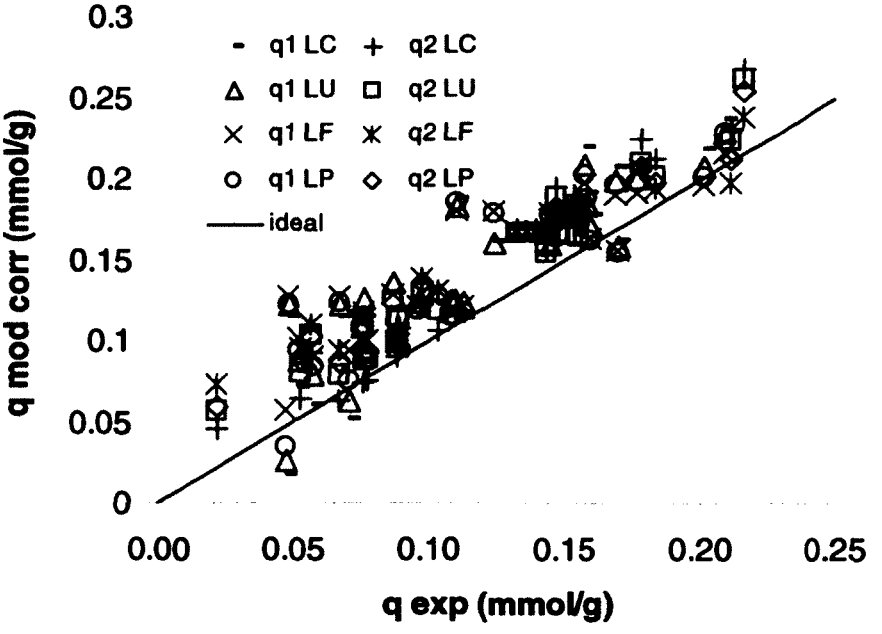

Figure 4.8 Scatter plots of 4 Langmuir type competitive models using F_{rel}

4.7 References

1. Schiewer, S. and S.B. Patil, *Pectin-rich fruit wastes as biosorbents for heavy metal removal: Equilibrium and kinetics.* Bioresource Technology, 2008. **99**(6): p. 1896-1903.
2. Chatterjee, A. and S. Schiewer, *Biosorption of Cadmium(II) Ions by Citrus Peels in a Packed Bed Column: Effect of Process Parameters and Comparison of Different Breakthrough Curve Models.* Clean-Soil Air Water, 2011. **39**(9): p. 874-881.
3. Schiewer, S. and M. Iqbal, *The role of pectin in Cd binding by orange peel biosorbents: A comparison of peels, depectinated peels and pectic acid.* Journal of Hazardous Materials, 2010. **177**(1-3): p. 899-907.
4. Schiewer, S. and S.B. Patil, *Modeling the effect of pH on biosorption of heavy metals by citrus peels.* Journal of Hazardous Materials, 2008. **157**(1): p. 8-17.
5. Volesky, B. and Z.R. Holan, *Biosorption of Heavy-Metals.* Biotechnology Progress, 1995. **11**(3): p. 235-250.
6. Apiratikul, R. and P. Pavasant, *Sorption isotherm model for binary component sorption of copper, cadmium, and lead ions using dried green macroalga, Caulerpa lentillifera.* Chemical Engineering Journal, 2006. **119**(2-3): p. 135-145.
7. Chong, K.H. and B. Volesky, *Description of 2-Metal Biosorption Equilibria by Langmuir-Type Models.* Biotechnology and Bioengineering, 1995. **47**(4): p. 451-460.
8. Luna, A.S., et al., *Competitive biosorption of cadmium(II) and zinc(II) ions from binary systems by Sargassum filipendula.* Bioresource Technology, 2010. **101**(14): p. 5104-5111.
9. Stumm, W. and J.J. Morgan, *Aquatic Chemistry.* 1970, New York: John Wiley & Sons.

10. Schiewer, S. and A. Balaria, *Biosorption of Pb2+ by original and protonated citrus peels: Equilibrium, kinetics, and mechanism.* Chemical Engineering Journal, 2009. **146**(2): p. 211-219.

11. Motulsky, H. and A. Christopoulos, *Fitting Models to Biological Data Using Linear and Nonlinear Regression: A Practical Guide to Curve Fitting*. 2004: Oxford University Press.

12. Hawari, A.H. and C.N. Mulligan, *Effect of the presence of lead on the biosorption of copper, cadmium and nickel by anaerobic biomass.* Process Biochemistry, 2007. **42**(11): p. 1546-1552.

13. Zhang, Y. and C. Banks, *The interaction between Cu, Pb, Zn and Ni in their biosorption onto polyurethane-immobilised Sphagnum moss.* Journal of Chemical Technology and Biotechnology, 2005. **80**(11): p. 1297-1305.

14. Volesky, B. and S. Schiewer, *Biosorption, Metal*, in *Biosorption technology: fermentation, biocatalysis and bioseparation*, M.C. Flickinger and S.W. Drew, Editors. 1999, John Wiley & Sons, Inc.

15. Fagundes-Klen, M.R., et al., *Equilibrium study of the binary mixture of cadmium-zinc ions biosorption by the Sargassum filipendula species using adsorption isotherms models and neural network.* Biochemical Engineering Journal, 2007. **34**(2): p. 136-146.

16. Pagnanelli, F., A. Esposito, and F. Veglio, *Multi-metallic modelling for biosorption of binary systems.* Water Research, 2002. **36**(16): p. 4095-4105.

17. Balasubramanian, R., S.V. Perumal, and K. Vijayaraghavan, *Equilibrium Isotherm Studies for the Multicomponent Adsorption of Lead, Zinc, and Cadmium onto Indonesian Peat.* Industrial & Engineering Chemistry Research, 2009. **48**(4): p. 2093-2099.

18. Wulfsberg, G., *Principles of Descriptive Inorganic Chemistry*. 1992: Univ Science Books.

19. Perez-Marin, A.B., et al., *Study of cadmium, zinc and lead biosorption by orange wastes using the subsequent addition method.* Bioresource Technology, 2008. **99**(17): p. 8101-8106.

20. Pipiska, M., et al., *Biosorption of Cadmium, Cobalt and Zinc by Moss Rhytidiadelphus squarrosus in the Single and Binary Component Systems.* Acta Chimica Slovenica, 2010. **57**(1): p. 163-172.

21. Srivastava, V.C., I.D. Mall, and I.M. Mishra, *Removal of cadmium(II) and zinc(II) metal ions from binary aqueous solution by rice husk ash.* Colloids and Surfaces a-Physicochemical and Engineering Aspects, 2008. **312**(2-3): p. 172-184.

5 Effect of competing cations (Pb, Cd, Zn and Ca) in fixed bed column biosorption and desorption from citrus peels [4]

5.1 Abstract

Biosorption of Pb, Cd and Zn from mono- and bi-component solutions at feed concentrations of 0.1 meq/L was investigated using a fixed bed column (length 30 cm, diameter 3 cm) packed with 5g protonated citrus peels. Uptake at breakthrough and saturation was found to follow the order Zn<Cd<Pb in single metal biosorption. Uptake of each ion was affected by co-ion presence in binary metal systems (Pb-Cd, Pb-Zn, Zn-Cd). An overshoot of the Zn or Cd effluent concentration was observed in Pb-Zn and Pb-Cd systems due to the high affinity of Pb. The efficiency of desorption of the saturated column using 0.1 N nitric acid was 74 to 100% whereby a concentration factor, based on average concentration of desorbed metal solution, of 34 to 129 was achieved. The common practice of defining the concentration factor on the basis of peak concentration is misleading and may lead to an overestimated value. Fixed bed experiments with varying Ca concentrations in Pb-Ca and Cd-Ca systems revealed that Ca as a co-ion inhibited the biosorption of target metal less strongly compared to other regulated metals (Pb, Zn, Cd). The extent of inhibition (i.e., reduction in target metal uptake at breakthrough and saturation) increased with Ca concentration especially for target metals with lower affinity (Cd vs. Pb). Finally, a sample of mining effluent was treated using this column.

5.2 Introduction

Mining activities may lead to contamination of surface waters with toxic metals from mine tailings through different pathways. This can cause problems to the ecosystem

---

[4] Chatterjee, A. and S. Schiewer. 2012. Effect of competing cations (Pb, Cd, Zn and Ca) in fixed bed column biosorption and desorption from citrus peels. Prepared for submission in CLEAN – Soil, Air, Water.

because metals are not degradable but bioaccumulate in the living tissues throughout the food chain. Conventional methods for treating metal bearing waste water such as chemical precipitation, ion exchange and membrane filtration become costly for high volumes of dilute discharge such as mining effluent. Alternatively, biosorption, which utilizes the metal-sequestering capacity of certain natural organic materials, becomes cost-effective if a cheap and abundant source of raw material with reasonable capacity can be identified. Decades of research identified different biomass types to concentrate metals from a large volume of dilute waste streams [1-3]. However, a major fraction of published biosorption articles primarily focused on two issues: 1) search for a novel biosorbents and the optimization of its uptake in a batch reactor containing a single target metal [1], 2) increasing the uptake capacity by suitable processing [3] even by genetic modification (e.g., insertion of a metalloregulatory protein MerR onto the surface of *Escherichia coli* to provide high specificity and affinity for mercury biosorption [4]) without considering the economic viability of the resultant system.

In contrast to such batch studies, a fixed bed reactor is preferred for commercial application due to better mass transfer kinetics and is typically used for the same purpose with commercially available ion exchange resins or for activated carbon sorbents. Also, a mining effluent is likely to contain several regulated and non-regulated metals. Therefore, multi-metal biosorption and desorption studies are more important than the search for a novel biosorbent or processing of existing biosorbents to achieve high capacity; use of higher amounts of minimally processed biosorbents may still be cost efficient for a cheap and abundant source, especially if the saturated biomass can be desorbed and reused. Desorption is also important to minimize waste generation.

Past research of the present authors identified citrus peels as a promising biosorbents for the removal of priority pollutants such as cadmium[5] and lead [6] using batch reactors. Being an underutilized waste material, a cheap and abundant availability of the raw material can be ensured. Citrus peels are mechanically rigid and stable enough to be used in a fixed-bed reactor [7] A mechanistic study confirmed ion exchange as the main biosorption mechanism and identified the concerned functional groups as carboxyl and

hydroxyl [6, 8]. A preliminary study has shown the effect of additional metals on the biosorption of a target metal in a batch reactor [Chapter 4]. The main objective of this article is to continue this systematic study to explore biosorption by citrus peels using a fixed bed reactor in the presence of several regulated and non regulated metals likely encountered in a real mining effluent.

5.3 Materials and methods

5.3.1 "Protonation" of citrus peels

Dried and ground processed orange peels were obtained from Alarma Consulting Corporation in Florida, USA. After washing and air-drying, 10 g of peels were suspended in 500 ml of 0.1 N nitric acid for 4 hours with constant stirring on an orbital shaker (120 rpm) at 25° C so that peels release naturally occurring light metals such as Na, K and Ca. These so called protonated peels were then filtered, rinsed 4-5 times using about 500 ml distilled deionized water each time till the pH of the washings reached a constant value of 4.0 and dried overnight at 45° C. Enhanced biosorptive capacity was reported for protonated peels in comparison to raw peels [9]. There was no significant weight loss in this process. Protonated peels were sieved into different size fractions. The peel particles of size 1-2 mm were used for this study. All chemicals and reagents used were of ACS-reagent grade and purchased from VWR.

5.3.2 Column characteristics

The column was made of clear extruded acrylic with a length of 30 cm and an internal diameter of 1.3 cm. The bottom 3 cm of the column was filled with spherical glass beads (diameter = 3 mm) to ensure even distribution of flow across the whole cross-section of the column. A fiber screen was placed at the top of the column to confine the peels within the column.

5.3.3 Continuous flow column system

5 g of protonated peels were 'wet packed' into the column (Figure 5.1) as slurry to give a bed height of 24 cm with a void space of 70%. Influent metal solution was pumped upward through the column at flow rate 9 ml/min by a peristaltic pump (VWR medium flow) from a reservoir (20 L) till the column became saturated. Four different types of influent solutions were used: 1) single metal solution of 0.1 meq/L of Cd, Zn, Pb; 2) all possible binary combinations of those metals, each with a concentration of 0.1 meq/L; 3) single regulated metal (Pb or Cd) in presence of varying amounts of Ca as a non-regulated alkali metal; 4) mining effluent. A real effluent sample was collected from Wet Well 3, Greens Creek Mine, Juneau, Alaska, USA. The effluent contained Zn (2 mg/L), Cd (0.5 mg/L), Pb (5 μg/L), Ca (180 mg/L) and other non-regulated alkali and alkaline earth metals at pH 4.0. Details of quantitative chemical analysis and seasonal variation of Wet-Well 3 effluent sample can be found elsewhere [10]. The effluent sample was loaded to the column without any pretreatment.

The feed solution was always adjusted to pH 5 except when it contained mining effluent. All metal solutions were prepared by diluting 10,000 mg/L stock solution (VWR). After saturation, the column was prepared for desorption by passing distilled water through the column at flow rate 9 ml/min for 45 minutes to expel any unbound metal. The influent reservoir was then filled with 0.1 N nitric acid as the desorption agent and pumped into the system at flow rate 9 ml/min until the desorption effluent concentration became constant or lower than 0.1 mg/L. Effluent samples during sorption and desorption were collected intermittently using a programmed fraction collector (Gilson FC203B) attached to the outlet of the column (Figure 5.1). Samples were then analyzed for the target metal concentration (C, mg/L or mmol/L) using an atomic absorption spectrophotometer (Perkin Elmer). All experiments were conducted at 25°C.

5.4 Analysis of breakthrough and desorption curve

The performance of a packed bed column can be evaluated from breakthrough curves which are typically plotted as the ratio of effluent concentration (C, mg/L) to influent

concentration (C_0, mg/L) versus process time (t, h). Breakthrough and saturation times are defined as the time when the effluent concentration reaches 5% and 95% of the inlet solution, respectively. Breakthrough (V_t, L) and saturation (V_s, L) volume correspond to the volume of solution passed through the column at these times respectively. Breakthrough curves were compared in terms of breakthrough time, t_b, saturation time, t_s, uptake capacity at breakthrough (q_b, mg/g) and saturation (q_e, mg/g) and the length of mass transfer zone (MTZ, cm). These parameters are defined and calculated as follows: The amount of metal adsorbed in the column at time t ($m_{ad,t}$, mg) can be determined from equation (5.1) which requires the amount of metal loaded in the column ($m_{in,t}$, mg) and the amount of unadsorbed metal ($m_{out,t}$, mg) up to time t (h). These can be obtained from equation (5.2) and (5.3):

$$m_{ad,t} = m_{in,t} - m_{out,t} \tag{5.1}$$

$$m_{in,t} = C_0 \times Q \times t \tag{5.2}$$

$$m_{out,t} = C_0 \times Q \times \int_0^t \left(\frac{C}{C_0} \right) dt \tag{5.3}$$

The equilibrium (maximum) uptake capacity (q_e, mg/g) then can be calculated as the total mass of metal adsorbed at saturation ($m_{ad,ts}$ mg) to the mass of adsorbent in column (M, g):

$$q_e = \frac{m_{ad,t_s}}{M} = \frac{C_0 \times Q \times \int_0^{t_s} \left(1 - \frac{C}{C_0} \right) dt}{M} \tag{5.4}$$

Similarly, uptake at breakthrough can be calculated as:

$$q_b = \frac{m_{ad,t_b}}{M} = \frac{C_0 \times Q \times \int_0^{t_b} \left(1 - \frac{C}{C_0} \right) dt}{M} \tag{5.5}$$

MTZ is defined as the mass transfer zone of the column where sorbate is actively adsorbed from fluid phase to solid phase, and where the sorbent is only partially

saturated. The MTZ moves through the column in the direction of flow and breakthrough is the time when the MTZ reaches the end of the column.

$$MTZ = (1 - \frac{t_b}{t_s}) \times L \tag{5.6}$$

Here L denotes the length of the bed. The desorption curve is usually plotted as C vs. t and the total mass of metal desorbed at any time t ($m_{de,t}$) can be found from equation (5.7).

$$m_{de,t} = Q \times \int_0^t C dt \tag{5.7}$$

The desorption efficiency (E) is defined as the ratio of metal desorbed ($m_{de,t}$) and the metal bound ($m_{ad,\,ts}$) during the sorption cycle.

$$E = \frac{m_{de,t}}{m_{ad,t_s}} x\,100\% \tag{5.8}$$

To calculate the maximum desorption efficiency possible, i.e., E_{max}, the function $m_{de,t}$ was evaluated at the time t_d, when the concentration in the effluent from desorption reaches less than 1 mg/L. For efficient use of the desorption agent, desorption can be terminated at the time $t_{0.9}$ when 90% of the maximum desorption has been achieved, i.e., $E = 0.9\ E_{max}$. The reagent requirement for the process (i.e., corresponding eluent volume at $t_{0.9}$) is denoted as $V_{0.9}$.

The average concentration of the eluent ($C_{av,de}$) at the outlet from the beginning (i.e., t = 0) to this time $t_{0.9}$ can be calculated from equation (5.8).

$$C_{av,de} = \frac{\int_0^{t_{0.9}} C\,dt}{t} \tag{5.9}$$

The concentration factor (CF) is the ratio of concentration of desorbed metal to the influent stream and can be calculated according to equation (5.10). It signifies the effectiveness of metal pre-concentration from the dilute influent stream and is a measure for the overall effectiveness of the adsorption/desorption cycle.

$$CF = \frac{C_{av,de}}{C_0} \tag{5.10}$$

A higher CF implies a higher recovery ratio ($R = V_s/V_{0.9}$), leading to a lower required eluent volume ($V_{0.9}$) and therefore lower reagent cost. It is easy to prove that these three key terms (E, R, CF) are related as follows, provided each of them is calculated for the same time period (up to t_d or $t_{0.9}$ or any other time t):

$$\frac{1}{R} = E\left(\frac{1}{CF} - \frac{C_{av,ad}}{C_{av,de}}\right) = E\,\frac{C_0 - C_{av,ad}}{C_{av,de}} \tag{5.11}$$

Here $C_{av,ad}$ denotes the average concentration in the effluent during the sorption cycle and can be calculated using equation (5.12) up to t_s or any other time t.

$$C_{av,ad} = \frac{\int_0^t C\,dt}{t} \tag{5.12}$$

For most practical situations, if the sorption cycle is terminated at breakthrough, then $C_{av,ad} = 0$, and equation (5.11) leads to the following elegant relationship:

$$E = \frac{CF}{R} \tag{5.13}$$

5.5 Results and discussion

5.5.1 Single metal biosorption

Breakthrough curves of Cd, Zn and Pb at 0.1 meq/L inlet concentration and 9 ml/min flow rate are shown in Figure 5.2. It was found (Table 5.1, run# 1-3) that Zn breaks through the column first followed by Cd and Pb respectively at 30, 36 and 50 hours. Uptake at breakthrough and saturation also followed this same order (Zn<Cd<Pb) in both molar and mass units, but molar uptake of Zn and Cd at breakthrough was similar, being close to 0.2 mmol/g. There are only few studies which compare mono-metal capacities of these three metals in fixed bed, but a relatively larger database is available for comparison between two of them in batch reactors. For most biosorbents, metal uptake (on a mass basis) follows the order Zn<Cd<Pb, as in this study (Table 5.2). Though it is

preferable to compare metal binding at equal molar concentrations of each metal, as done in the present study, most other studies compared metal uptake at equal mass concentration. When uptake values are converted from mass to molar units, no general trend in uptake could be discerned, with different metals featuring the highest uptake in different studies. The sequence was in some cases (Table 5.2) even reversed since the molecular weight also increases in the order Zn<Cd<Pb. In the present study, however, the uptake sequence Pb>Cd>Zn was maintained also on a molar basis though uptakes were quite similar.

Selectivity of lead over other metals can be explained by its favorable hard-hard interaction with hard ligands such as carboxylate and hydroxyl groups and other relevant properties (smaller hydrated ion radius, lower hydrolysis constant and higher covalent character of bonding) (Table 5.3). Two commercial resins, however, showed a different sequence (Cd>Pb) due to a different mechanism of adsorption, i.e., formation of chelate complexes with iminodiacetate groups [11] involving both O and N as donor atoms. Cd has smaller crystal radius but higher hydrated radius than Pb (Table 5.3). A smaller crystal radius is favorable to minimize the steric inhibition of chelate formation. The additional stability gained due to chelate formation makes the whole process favorable by overcoming the apparent disadvantage of breaking a larger hydration sphere.

The metal uptake of citrus peels for each of these three metals is comparable or higher than for other established biosorbents (Table 5.2) and commercially available ion exchange resins. This is especially remarkable since the metal concentrations used here were much lower than those used in most other studies. Since metal binding typically increases with increasing metal concentration, and since at the low concentrations used here do not yet lead to saturation of all binding sites, citrus peels are even more advantageous compared to other sorbents when the maximal binding capacities are compared, which were about 400, 70, 100 mg/g for Pb [9], Cd [Chapter 4] and Zn [Chapter 4], respectively, based on isotherm studies.

5.5.2 Binary metal biosorption

5.5.2.1 Effect on individual uptake

Other studies have shown that uptake of any one metal from a binary system was lower than the uptake of that metal from the single component system. For better comparison, all binary metal experiments of the current study were done at 1:1 molar ratio since relative uptake of either metal of a pair is obviously increased as its concentration ratio is increased with respect to the other. For example, Sag et al. [12] found that as the ratio of Cu at the inlet feed (Cu+Cr) was increased from 1 to 2.5, uptake onto a fungal biosorbent was respectively decreased for Cr (20 to 14 mg/g) and increased for Cu (20 to 30 mg/g).

5.5.2.1.1 Effect of presence of other metals (Pb, Zn) on Cd biosorption

A comparison of run# 2, 4 and 6 in Table 5.1 and Figure 5.3a shows that the concentration in the effluent approached that in the influent more quickly (higher C/C_0) than for the single-metal system. This means that the uptake of Cd was negatively influenced by the addition of a second metal. For the single-metal system, breakthrough occurs after 37 hours with a breakthrough capacity of 22 mg/g. The column becomes saturated after 120 h showing a capacity of 44 mg/g. When 0.1 M Zn was added to the influent, Cd shows an early breakthrough after only 10 h with a 67% reduction in its breakthrough capacity. Saturation capacity was decreased by 55% in this Cd-Zn system. When Pb was added, the breakthrough capacity was 5 mg/g which is a 72% reduction from its native value. The impact was even more pronounced on the saturation uptake capacity. Cd uptake was 72 mg/g when the breakthrough curve intercepted the C/Co = 1 line. However, that was not the final value. Due to the higher affinity of Pb, it then dispelled previously bound Cd from the sorbent. The presence of this desorbed Cd in the effluent caused the effluent concentration to exceed the influent concentration, which is usually termed "overshoot". The replacement of Cd ions by Pb ions reached its peak rate at the breakthrough of Pb (Figure 5.4a), when the Cd overshoot reached 1.76 times the feed concentration. By the time that the Pb concentration approached that in the feed, all

sites were saturated with Pb and almost all of the previously adsorbed Cd was lost. Overshoot of Cd in presence of Pb confirms the higher selectivity of Pb as observed in single metal system. Vilar et al. [13] studied the same binary system using immobilized algal biosorbent but at a higher ratio of Cd (Cd: Pb = 1.8:1) in the feed. Still 58% of the biosorbed Cd was found to be displaced by Pb, causing a 69% drop in saturation uptake. Sag et al. [12] also noticed the decrease of Cu overshoot due to replacement by Cr with increasing ratio of Cu in the feed.

From a commercial aspect, the overshoot problem can be eliminated by terminating column operation at the breakthrough of weaker metal, i.e., when the Cd uptake is 18 mg/g.

5.5.2.1.2 Effect of presence of other metals (Cd, Pb) on Zn biosorption

The biosorption of Zn was also most strongly reduced by Pb (Table 5.1, run# 3, 5, 6 and Figure 5.3b). While the breakthrough capacity was almost equally affected by the presence of either Cd (64 % reduction) or Pb (55 % reduction) the final uptake was drastically reduced by Pb. Like Cd in the Pb-Cd system, the exit concentration of Zn also showed an overshoot in the presence of Pb (Figure 5.4b) with a peak of $C/C_0 = 1.57$, confirming the same sequence of affinity (Pb>Zn) as obtained in the single metal study (5.5.1).

A seaweed derived biosorbent [14] also showed a higher overshoot of Cd than that of Zn in the presence of Cu (which was the preferred metal in that study).

Comparing with Cd in the Pb-Cd system, the overall impact on Zn in the Pb-Zn system was a little less, as 47% of initially bound Zn (Figure 5.4) was displaced by Pb. There was a 70 % reduction in the saturation uptake of Zn in Pb-Zn system compared to the monometal system. In contrast, the presence of Cd (Zn-Cd system) only caused a 45% reduction in the saturation capacity of Zn compared to the monometal system and did not produce any overshoot. This implies a very similar affinity of Zn and Cd, also indicated by similar values of their overshoot peaks (1.76 for Cd, 1.57 for Zn) in the presence of Pb.

5.5.2.1.3 Effect of presence of other metals (Cd, Zn) on Pb biosorption

Compared to both Cd and Zn, the biosorption of Pb was least influenced by the presence of competing metals (Table 5.1, Run# 1, 4, 5; Figure 5.3c). Unlike Zn and Cd, the breakthrough curve of Pb followed the usual sigmoid shape without any overshoot. That behavior is due to its higher affinity towards the biosorbent. Figure 5.3c shows that the three breakthrough curves of Pb are very closely positioned, i.e., neither Zn nor Cd affected Pb binding. Breakthrough and saturation time remained almost the same as for the monometal system. Addition of Cd decreased the breakthrough and saturation capacity of Pb by 14 and 16% respectively, whereas addition of Zn did not alter those parameters significantly.

Vilar et al. [13] found a 31% decrease in saturation capacity of Pb in a Pb-Cd system using a seaweed biosorbent. In the same study, Pb biosorption onto an algal derived biomass was found to remain unchanged. In another study using black gram husk as the biosorbent [15], Pb did not show any overshoot in presence of Ni or Zn. It was found that in a 10 mg/L binary mixture of Pb and Zn, saturation time of Pb remained almost same but breakthrough time was reduced by 38%. The article, however, did not show the breakthrough curve of co-ions of Pb.

5.5.2.2 Comparison of the binary system with its mono-component counterparts

5.5.2.2.1 Comparison with respect to individual uptake

To compare the biosorption efficiency between an M_1-M_2 binary system and the corresponding single metal systems, the function F (X_i) was defined as

$$F(X_i) = 100\frac{X_{i,b}}{X_{i,s}} \tag{14}$$

Whereby $X_{i,b}$ is any variable (e.g., uptake, or breakthrough time) for metal i in the binary system and $X_{i,s}$ is the same value for the respective single metal system. F values are given in Table 5.4. This shows that for the Cd-Zn binary system, both Cd and Zn retained

comparatively similar percentages of their mono-metal uptake both at breakthrough (33% and 36%) and at saturation (45 and 55%), which is due to their similar affinities for the sorbent. In contrast, for the Pb-Cd and Pb-Zn systems, the high affinity metal Pb was always able to retain its full capacity but at the expense of hampering its co-ion adsorption. For example, Pb retained 86 and 100% of its mono-metal uptake at breakthrough respectively in the presence of Cd and Zn but these co-ions retained only 28 and 45% of their mono-metal uptake at breakthrough. Saturation uptake of Cd and Zn in presence of Pb was critically hampered due to overshoot as explained in 5.5.2.1.

5.5.2.2.2 Comparison with respect to total uptake

On the other hand, a comparison of the combined saturated capacity of the binary system ($q_{s1}+q_{s2}$) with the saturated capacity of the stronger metal of the pair in mono-metal system expressed in molar units reveals two different scenarios (Table 5.4). The Pb-Zn system showed a minor increase in the total uptake compared to the Pb uptake in the monometal system, which is expected as the combined influent concentration was doubled in the binary system even though most of the bound Zn was replaced by Pb. On the other hand, the combined saturated capacity of the Pb-Cd and Cd-Zn systems was a little lower than the uptake capacity of Pb or Zn alone. This may be due to the scatter in the experimental data (especially for Pb) which were used to determine the uptake by numerical integration.

5.5.2.3 Effect of calcium ions

Biosorption is primarily intended to 'polish' the effluent that is for treating effluent from which the majority of the pollutant has been removed by other methods. Often these methods such as chemical precipitation use reagents containing sodium or calcium salts. As a result, alkali and alkaline earth metals may often be present in an amount high enough to influence the biosorption of the target metal. At a constant influent target metal concentration (20 mg/L, i.e., 0.1 mmol/L for Pb and 5 mg/L, i.e., 0.04 mmol/L for Cd), a total of 11 fixed bed experiments were conducted (Table 5.5, Run# 7-12 for Pb, 13-17 for

Cd) with gradually increasing concentration of Ca in the influent (0-100 mg/L, i.e., 0-2.5 mmol/L in systems with Pb and 0-20 mg/L, i.e., 0-0.4 mmol/L in the presence of Cd). By comparing Figure 5.3a and 5.3b, it can be said that the presence of calcium affects cadmium biosorption much more than lead biosorption. While 5 mg/L of calcium had no discernible effect on the Pb breakthrough curve, the same Ca concentration had a huge impact on the breakthrough curve for Cd, reducing the breakthrough time from 36 to 10 h. This is expected as the Pb has a higher affinity than Cd. With the Ca concentration increasing from zero to 100 mg/L, the capacity for Pb at saturation decreased from 73 to 51 mg/g and breakthrough capacity decreased from 45 to 5 mg/g (Table 5.5). Similarly, when the calcium concentration was increased to four times the influent concentration of cadmium (20 vs. 5 mg/L), the saturation capacity was decreased from 44 to 10 mg/g and breakthrough capacity was decreased from 18 to 1 mg/g. In both instances, the mass transfer zone was found to increase linearly with increasing Ca concentration:

for Pb: $MTZ = 0.15\ C_0 + 7.99$ ($R^2 = 0.94$);

for Cd: $MTZ = 0.41\ C_0 + 13.46$ ($R^2 = 0.96$).

Unlike the influence of other heavy metals, the inhibitory effect of Ca for Pb binding, however, is only significant when it is present at 50 mg/L or higher concentration. In contrast, Cd uptake was affected at relatively low Ca concentration of 5 mg/L. Comparing run# 6 (Table 5.1) and run# 14 (Table 5.5), it seems 0.125 mmol/L (5 mg/L) of Ca has same effect as 0.05 mmol/L of Zn on Cd biosorption.

There are no published articles focusing on the effect of alkali metals on fixed bed biosorption of Pb or Cd, but a batch study [16] with as high as 100 mg/L (0.9 mmol/L) of Cd using a seaweed showed 20% and 35% reduction in uptake capacity in presence of 65 mg/L (1.62 mmol/L) and 130 mg/L (3.24 mmol/L) Ca respectively. Another batch study using a bacterial biomass showed 80% reduction of Cd biosorption in presence of 4 mmol/L calcium. Calcium inhibition was also indicated in another study of the present author [Chapter 3]. Ca-salt solution was also used for desorption of Cd bound to seaweed [17]. Another batch study using palm kernel fiber [18] showed that the Pb uptake capacity was decreased with increase in initial Ca concentration. This extent of alkali

metal inhibition is still much lower compared to commercial ion exchange materials; for example, at a low aqueous concentration of Pb (37-49 mg/L), a cation exchanger IRA 120 Amberlite was found [19] to lose 94% of its Pb sorption capacity in presence of Ca as co-ions (0-12 g/L).

In conclusion, Pb could still be effectively be removed in column applications even if the molar concentration of Ca was much higher than that of Pb (2.5 mmol/L of Ca vs. 0.1 mmol/L Pb), while Cd uptake was severely impacted even by low Ca concentrations.

5.5.2.4 Desorption

Metals, unlike organic matter, cannot be 'degraded' or 'mineralized', but can only be concentrated and reused and hence desorption is essential for a meaningful metal sequestration technology. Figure 5.6 and Figure 5.7 show the recovery of metals using 0.1 M nitric acid as the desorption agent. Desorption was faster than biosorption, the curve reached at its peak (C_p) within 10-12 minutes (t_p) (Table 5.6). In the present study, desorption was achieved in similar timeframes both in mono-metal and binary systems. Compared to that, it was reported that the amount of acid required for desorption of Pb increases with the addition of a second metal in the Pb-Ni and Pb-Zn system using black gram husk as biosorbent [15].

It can be seen that the peak of Pb concentration was much higher than that for the other co-cations in Pb-Cd and Pb-Zn desorption (Figure 5.7) which confirms that hardly any of the weaker bound Cd or Zn remained on the sorbent after being displaced by Pb during the overshoot. For the Pb-Cd system, the amount of remaining Cd was insignificant and was not incorporated within Table 5.6 as desorption parameters were not calculated.

Maximum desorption efficiency (E_{max}) was moderately high (> 85%) except for Zn in the Pb-Zn system. In some cases, E_{max} values exceed 100% due to the measurement of concentrations near the detection limit and error associated with the numerical integration of experimental data.

It may be noticed from the ratio of $t_{0.9}/t_d$ (Table 5.5), that for Pb desorption (single and binary system), 90% of this E_{max} was achieved within less than 20% of the total

desorption time (t_d), while the remaining 80% of the time were utilized only to accomplish the remaining (10% of E_{max}) desorption. The long tail (i.e., long t_d) in Pb desorption curves can be explained by the higher covalent index of Pb (Table 5.3) implying a higher proportion of covalent bonding with Pb. For practical purposes this means that in industrial applications it would be advantageous to terminate desorption at t_{90} to achieve a mostly complete desorption using a much lower volume of eluent than required for complete desorption.

For single metal desorption, the concentration factor (CF) and recovery ratio (R) followed the order Cd<Pb<Zn. Most published studies [20, 21] define CF (i.e., CF_p in Table 5.6) on the basis of the peak desorbed metal concentration (C_p) instead of C_{av}. However, CF_p is of little practical relevance since for any industrial desorption process the entire volume of desorbent used has to be considered, i.e., an average concentration within this solution should be the basis for calculating CF as proposed in equation (5.10). As shown in Table 5.6, using C_p to calculate CF may lead to an overestimated CF depending on the extent of dilution occurring between this peak time and the time when desorption was terminated. Within binary systems, CF of Pb was decreased from 113 to 70 in the presence of Zn, but was marginally increased in presence of Cd. Similarly, CF of Zn was decreased with the addition of a second metal (Cd or Pb).

5.5.2.5 Treatment of mining wastewater

Figure 5.8 showed that 5.40 L (i.e., 85 times bed volume) of wastewater can be treated by 5 g of sorbent without any breakthrough. The breakthrough times of Zn and Cd were 10 h and 12 h respectively. None of them showed any overshoot. Since a limited quantity of effluent was collected, the experiment was terminated after 25 hours. Even though the concentrations of target metals in the wastewater were lower than previous experiments (section 5.3.3), the breakthrough time was shorter than in the single-metal solutions due to the presence of other salts such as Ca at a concentration (180 mg/L) which was higher than the experimental range (0 to 100 mg/L). Oliveira et al. [22] also noted a similar

decrease (around 50%) in capacity of peanut hulls in the treatment of electroplating effluent.

5.6 Conclusions

Protonated citrus peels can be used as a potential alternative to ion exchange resins in packed bed columns for the removal of Cd, Zn and Pb from monometal solution and in the presence of competing metals. Uptake at saturation decreased in the order Pb>Cd>≈Zn. Presence of co-ions may hinder the target metal removal; especially the saturation uptake of the weaker metal ion, such as Cd or Zn, may be substantially reduced due to its overshoot, i.e., displacement by a stronger metal such as Pb in the feed. The Cd-Zn pair did not show any overshoot due to similar binding strength of both metals. The presence of non-regulated alkali metals such as Ca may also inhibit the biosorption of a target metal, particularly of Cd. Real mining effluent is challenging to treat due to the simultaneous presence of different interfering regulated and non-regulated metals. Nevertheless, 5.40 L of mining effluent was treated by 5 g of protonated citrus peels before breakthrough. Using 0.1 N nitric acid, the saturated column can be desorbed completely for each of the single or binary systems. The concentration factor calculated based on the peak metal concentration in desorption effluent, as commonly done in the literature, was 104-352. However, this value is misleading since it is not relevant for practical applications. It is therefore recommended to calculate the concentration factor based on the average concentration of desorbed metal in spent eluent solution, which lead to CF values in the range of 34-128, whereby monometal CF decreased in the order Zn>Pb>Cd. Even this lower, more realistic value indicates that during an adsorption/desorption cycle metals were successfully concentrated in solution with the help of citrus peel biosorbents.

Based on the experimental data (influent composition, amount of peels, breakthrough time and flow rate) model parameters (Chapter 2, 3) such as k_{BA} and q_{BA} can be determined. The same parameters are typically assumed to be valid both for laboratory scale and full scale sorption systems in industrial scale-up. Therefore the

determined k_{BA} and q_{BA} may be utilized to scale up the system to a commercial level by applying breakthrough models (Chapter 3). Assuming a desired operation time (i.e., t_b) of one week, the amount of citrus peels required and bed volume can be calculated by applying the breakthrough curve model so that break through does not occur before 7 days for a known flow rate of the mining effluent and inlet concentration. For example, for typical k_{BA} and q_{BA} values of 0.3 ml/(mg.min) and 20 mg/g, as determined in Chapter 3, and considering the actual Greens Creek metal concentrations, it was calculated that 0.75 kg of citrus peels would be required per unit flow rate in m^3/day. This corresponds to a 10 ft column for the treatment of mining effluent at the flow rate of 33 m^3/day. The same aspect ratio as used for the laboratory experiment was considered for the calculation of column height.

5.7 Acknowledgement

This research was supported in part by the National Research Initiative of the USDA Cooperative State Research, Education, and Extension Service, grant number 2005-35504-16092 and by a USGS NIWR grant. Orange peels were provided by Alarma Consulting Corporation in Florida. We thank the geochemist Pete Condon for collecting mining effluent.

Table 5.1 Breakthrough curve parameters for removal of Pb, Zn and Cd from single and binary systems using protonated citrus peels.

Run #	M1	M2	C_0 (1) (mg/L)	C_0 (2) (mg/L)	t_{b1} (h)	t_{b2} (h)	t_{s1} (h)	t_{s2} (h)	q_{b1} (mg/g)	q_{b2} (mg/g)	q_{s1} (mg/g)	q_{s2} (mg/g)
1	Pb	-	10.36	-	50	-	120	-	57	-	85	-
2	Cd	-	5.62	-	37	-	120	-	22	-	44	-
3	Zn	-	3.27	-	30	-	110	-	11	-	20	-
4	Pb	Cd	10.36	5.62	50	9	114	108	49	5	71	0
5	Pb	Zn	10.36	3.27	48	12	113	95	57	5	88	6
6	Cd	Zn	5.62	3.27	10	11	77	80	6	4	20	11

Table 5.2 Comparison of mono-component saturation uptake for Pb, Cd and Zn biosorption in fixed bed columns

Sorbent	Saturation uptake mg/g (mmol/g)*			Feed concentration mg/L	Order of uptake (on mass basis)	Ref
	Pb	Cd	Zn			
Amberlite IRC 718	20 (0.10)	119 (1.06)	68 (1.04)	Pb 250 Cd, Zn 600	Cd>Zn>Pb	[11]
Chelex 100 (Bio-Rad)	23 (0.11)	112 (1.00)	83 (1.27)	Pb 375 Cd 350 or 600 Zn 400	Cd>Zn>Pb	[11]
Wetland Sediment	97 (0.47)	18 (0.16)	9 (0.14)	50 each	Pb>Cd>Zn	[23]
Grape Stalk waste	56 (0.27)	33 (0.29)	-	Cd 60 Pb 120	Pb>Cd	[24]
Tea waste	46 (0.22)			100		[24]
Orange waste			29 (0.44)	20-40		[25]
Wheat Straw		17 (0.15)		100		[26]
Green Coconut Shell	55 (0.27)	38 (0.34)	17 (0.26)	100	Pb>Cd>Zn	[27]
Waste from Boron enrichment plant		86-138 (0.76-1.23)	80-110 (1.22-1.68)	150 each	Cd>Zn	[28]
Citrus Peels	85 (0.41)	44 (0.39)	20 (0.31)	Pb 10.36 Cd 5.62 Zn 3.27	Pb>Cd>Zn	this study

* Values within parenthesis show uptake in molar units (mmol/g)

Table 5.3 Physicochemical properties characterizing the binding strength of metals [29]

Parameter	Zn	Cd	Pb
Crystal radius (r) (pm)	88	95	119
Hydrated radius (pm)	430	426	401
Hydrolysis constant (-log K)	8.96	10.08	7.7
Covalent Binding χ^2 (r +85) (pm)	536	551	718

Table 5.4 Comparison of removal of Pb, Zn and Cd from single and binary metal mixtures using protonated citrus peels.

Run #	M1	M2	F (q_{b1}) (%)	F (q_{b2}) (%)	F (q_{s1}) (%)	F (q_{s2}) (%)	$q_{s1}+q_{s2}$ (mmol/g)	Monometal q_{s1} (mmol/g)
4	Pb	Cd	86	28	84	0	0.34	0.41
5	Pb	Zn	100	45	104	30	0.52	0.41
6	Cd	Zn	33	36	45	55	0.35	0.39

The function F is defined according to equation (5.14)

Table 5.5 Biosorption performance of protonated citrus peels for removal of Pb or Cd in presence of variable amount of Ca.

Run #	Target Metal	C_0 of Metal mg/L	C_0 of Ca mg/L	t_b h	t_s h	q_b mg/g	q_s mg/g	MTZ cm
7	Pb	20	0	21	56	45	73	9
8	Pb	20	5	23	49	51	72	7
9	Pb	20	20	22	66	51	100	12
10	Pb	20	50	10	58	24	60	15
11	Pb	20	75	3	58	7	58	21
12	Pb	20	100	2	58	5	51	22
13	Cd	5	0	36	146	18	44	14
14	Cd	5	5	10	62	5	14	15
15	Cd	5	10	12	93	6	21	17
16	Cd	5	15	2	36	1	7	20
17	Cd	5	20	2	46	1	10	21

Table 5.6 Desorption curve parameters for breakthrough curves 1- 6

Run #	M1	t_d	$t_{0.9}$	t_p	$(t_{0.9}/t_d)$ *100	C_p	$C_{av,de}$	CF_P	CF	$V_{0.9}$	E_{max}	R
		min	min	min	%	mg/L	mg/L			ml	(%)	
1	Pb	241	40	12	17	2725	1167	263	113	360	108	180
2	Cd	200	100	15	50	1146	191	204	34	900	86	75
3	Zn	78	24	10	31	1007	421	308	129	216	99	275
4*	Pb	555	34	12	6	3647	1219	352	118	306	115	201
5	Pb	420	54	14	13	2580	728	249	70	486	86	126
5	Zn	65	18	12	28	340	123	104	38	162	73	317
6	Cd	65	20	10	31	1141	456	203	81	180	90	231
6	Zn	56	20	10	36	667	306	204	93	180	109	240

* negligible amount of Cd present

1. Influent Reservoir
2. Peristaltic Pump
3. Rotameter
4. Packed bed Column
5. Fraction Collector
6. Effluent Reservoir

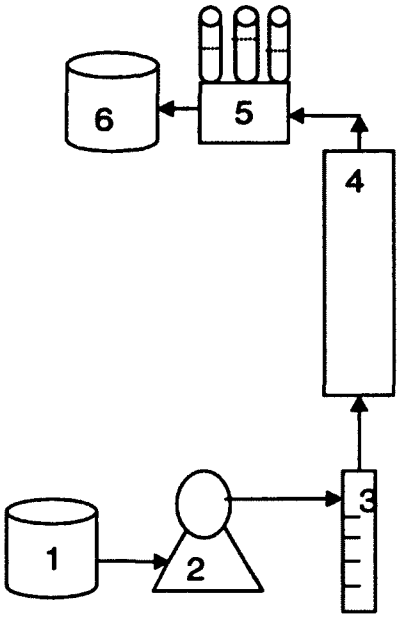

Figure 5.1 Schematic diagram of experimental set-up for packed bed column study.

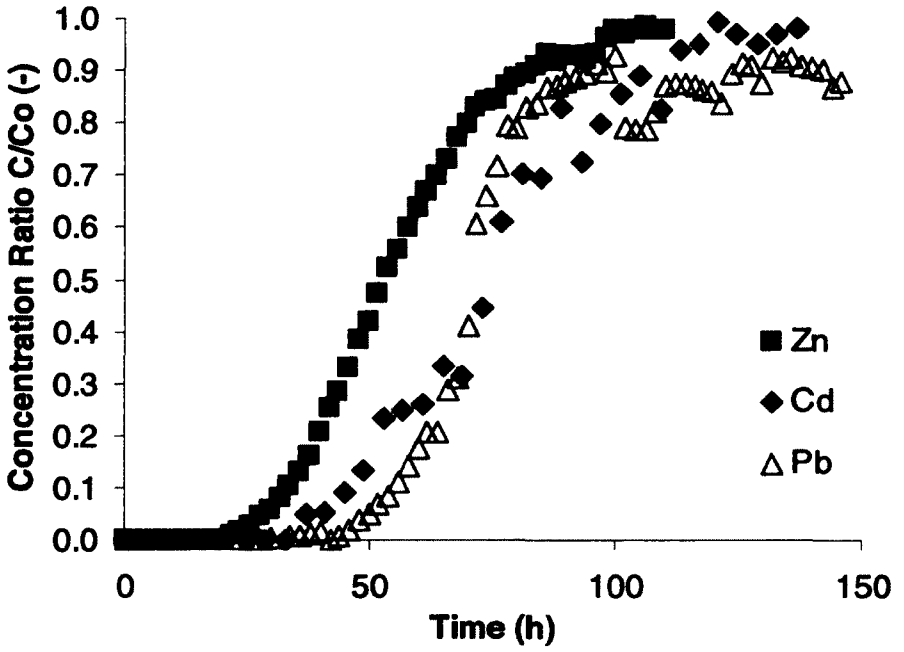

Figure 5.2 Breakthrough curves for single metal biosorption of Cd, Zn and Pb onto protonated citrus peels. (inlet concentration 0.1meq/L, bed height 24 cm, flow rate 9 ml/min and pH 5.0)

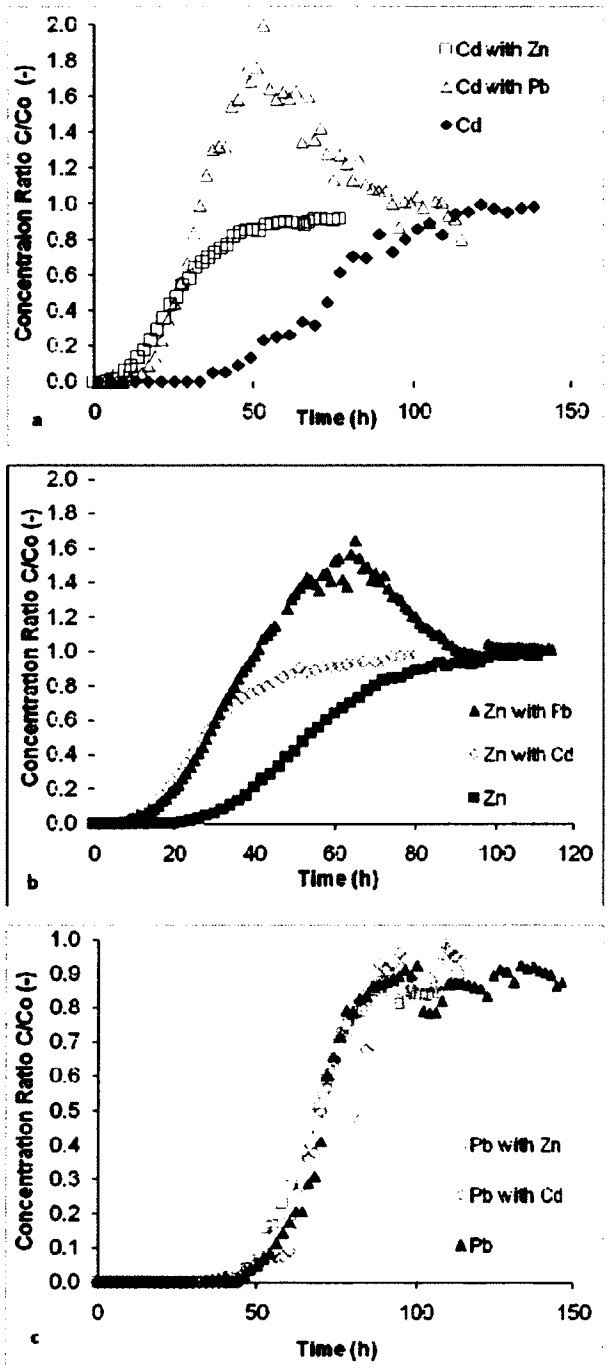

Figure 5.3 Comparison of single and binary metal breakthrough curves to account for the influence of co-ions. (inlet concentration of each ion 0.1meq/L, bed height 24 cm, flow rate 9 ml/min and pH 5.0) a) Cd in presence of Pb and Zn, b) Zn in presence of Pb and Cd, c) Pb in presence of Cd and Zn.

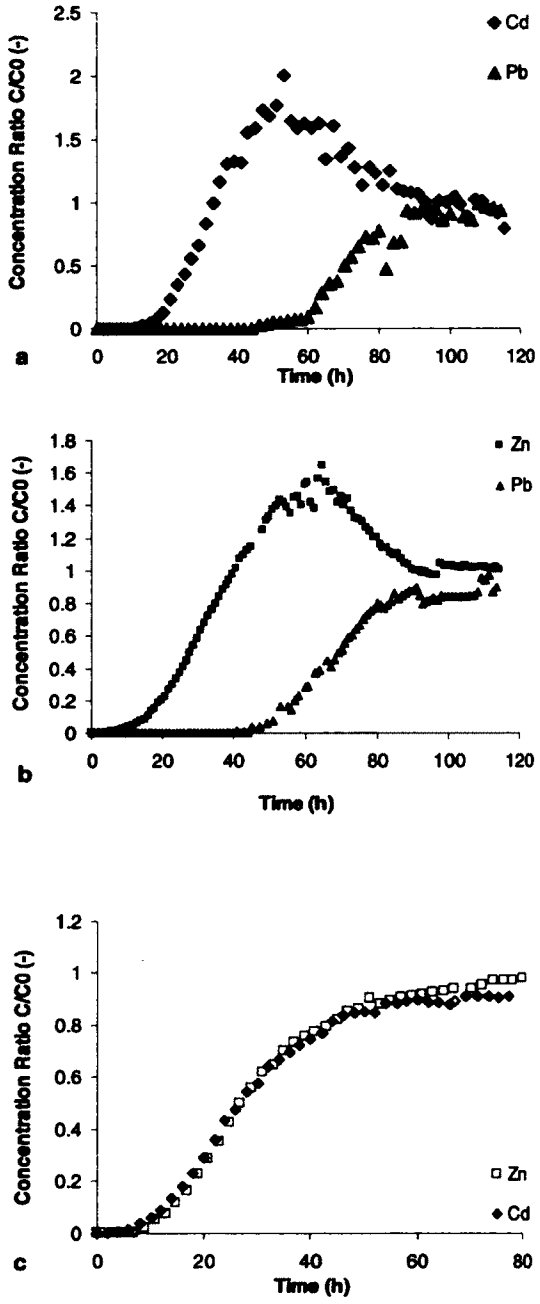

Figure 5.4 Experimental breakthrough curves for binary biosorption onto protonated citrus peels in presence of co-ions. (inlet concentration of each ion 0.1meq/L, bed height 24 cm, flow rate 9 ml/min and pH 5.0) a) Pb-Cd, b) Pb-Zn, c) Zn-Cd.

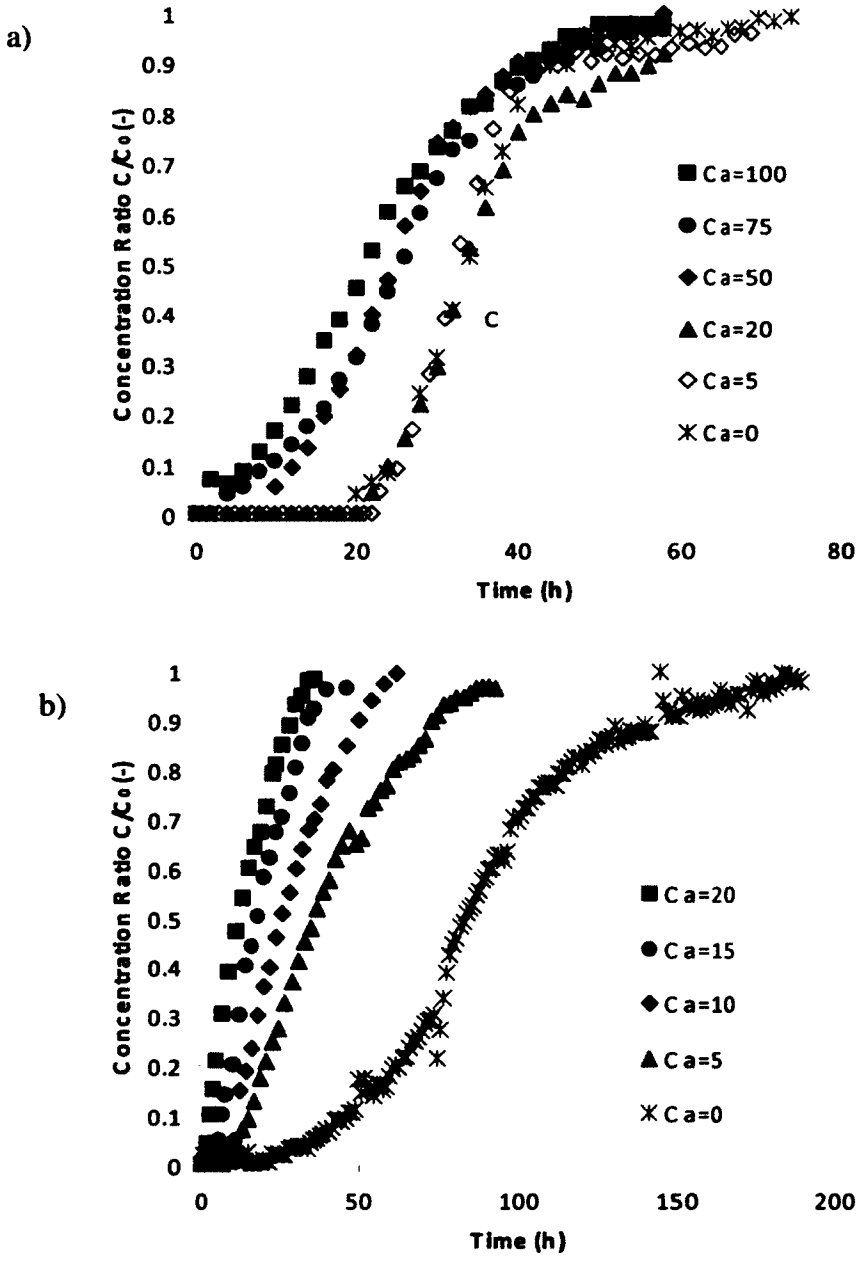

Figure 5.5 Breakthrough curves for heavy metal biosorption onto protonated citrus peels in presence of different inlet concentrations of Ca (mg/L). (bed height 24 cm, flow rate 9 ml/min and pH 5.0) a) Pb inlet concentration of 20 mg/L, b) Cd inlet concentration 5 mg/L.

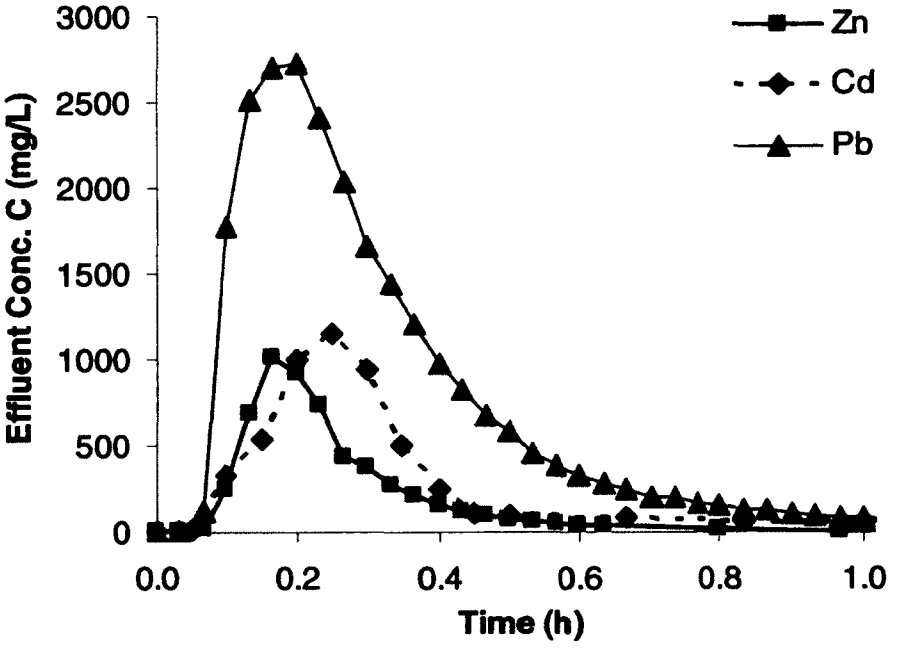

Figure 5.6 Desorption curve for Cd, Zn and Pb using 0.1(N) nitric acid after mono-metal sorption.

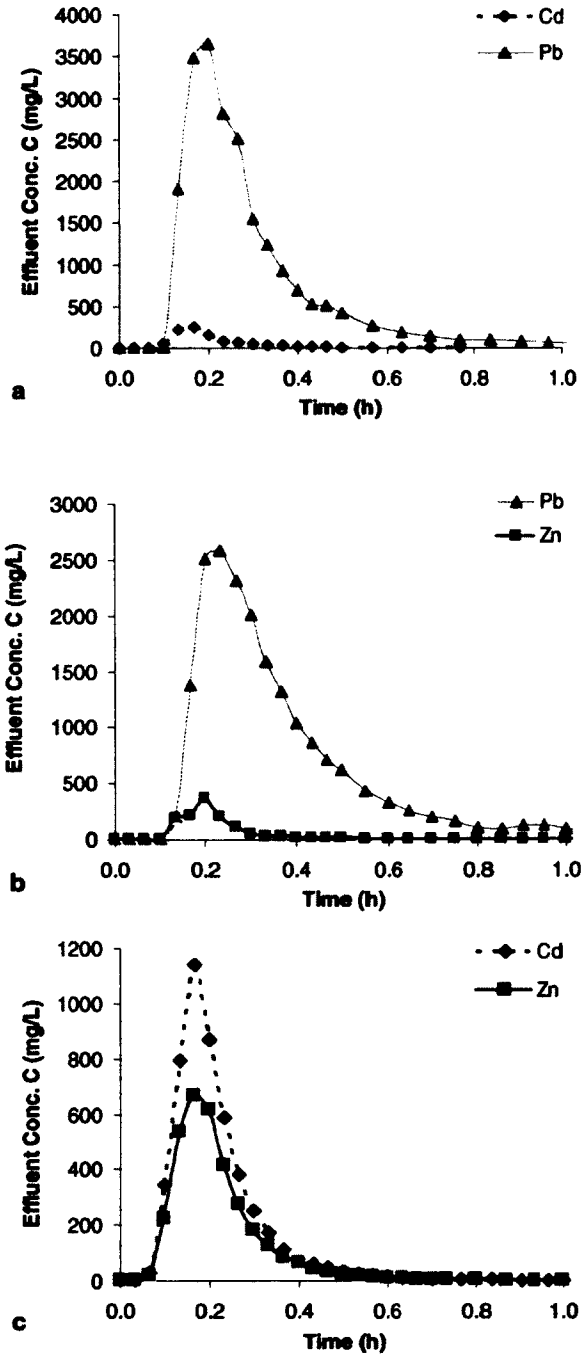

Figure 5.7 Desorption curve for binary systems using 0.1 N nitric acid. a) Pb-Cd, b) Pb-Zn, c) Zn-Cd

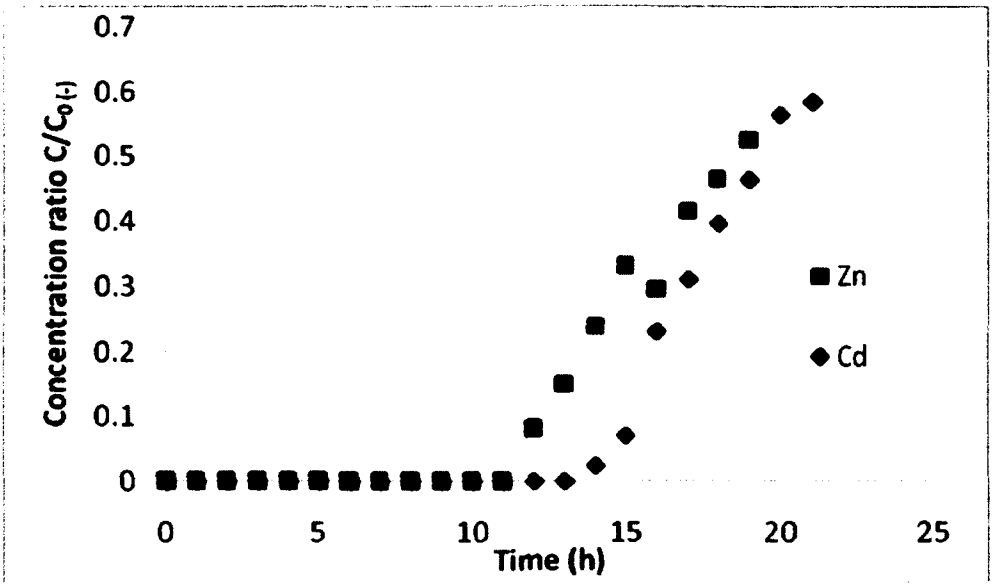

Figure 5.8 Treatment of mining effluent (bed height 24 cm, flow rate 9 ml/min)

5.8 References

1. Arief, V.O., et al., *Recent Progress on Biosorption of Heavy Metals from Liquids Using Low Cost Biosorbents: Characterization, Biosorption Parameters and Mechanism Studies.* Clean-Soil Air Water, 2008. **36**(12): p. 937-962.
2. Demirbas, A., *Heavy metal adsorption onto agro-based waste materials: A review.* Journal of Hazardous Materials, 2008. **157**(2-3): p. 220-229.
3. Vijayaraghavan, K. and Y.S. Yun, *Bacterial biosorbents and biosorption.* Biotechnology Advances, 2008. **26**(3): p. 266-291.
4. Bae, W., et al., *Enhanced mercury biosorption by bacterial cells with surface-displayed MerR.* Applied and Environmental Microbiology, 2003. **69**(6): p. 3176-3180.
5. Schiewer, S. and M. Iqbal, *The role of pectin in Cd binding by orange peel biosorbents: A comparison of peels, depectinated peels and pectic acid.* Journal of Hazardous Materials, 2010. **177**(1-3): p. 899-907.
6. Balaria, A. and S. Schiewer, *Assessment of biosorption mechanism for Pb binding by citrus pectin.* Separation and Purification Technology, 2008. **63**(3): p. 577-581.
7. Chatterjee, A. and S. Schiewer, *Biosorption of Cadmium(II) Ions by Citrus Peels in a Packed Bed Column: Effect of Process Parameters and Comparison of Different Breakthrough Curve Models.* Clean-Soil Air Water, 2011. **39**(9): p. 874-881.
8. Iqbal, M., S. Schiewer, and R. Cameron, *Mechanistic elucidation and evaluation of biosorption of metal ions by grapefruit peel using FTIR spectroscopy, kinetics and isotherms modeling, cations displacement and EDX analysis.* Journal of Chemical Technology and Biotechnology, 2009. **84**(10): p. 1516-1526.
9. Schiewer, S. and A. Balaria, *Biosorption of Pb2+ by original and protonated citrus peels: Equilibrium, kinetics, and mechanism.* Chemical Engineering Journal, 2009. **146**(2): p. 211-219.

10. Department of Natural Resources, Available from: http://dnr.alaska.gov/mlw/mining/largemine/greenscreek/.
11. Malla, M.E., M.B. Alvarez, and D.A. Batistoni, *Evaluation of sorption and desorption characteristics of cadmium, lead and zinc on Amberlite IRC-718 iminodiacetate chelating ion exchanger.* Talanta, 2002. **57**(2): p. 277-287.
12. Sag, Y., I. Atacoglu, and T. Kutsal, *Simultaneous biosorption of chromium(VI) and copper(II) on Rhizopus arrhizus in packed column reactor: Application of the competitive Freundlich model.* Separation Science and Technology, 1999. **34**(16): p. 3155-3171.
13. Vilar, V.J.P., et al., *Continuous biosorption of Pb/Cu and Pb/Cd in fixed-bed column using algae Gelidium and granulated agar extraction algal waste.* Journal of Hazardous Materials, 2008. **154**(1-3): p. 1173-1182.
14. Kratochvil, D. and B. Volesky, *Multicomponent biosorption in fixed beds.* Water Research, 2000. **34**(12): p. 3186-3196.
15. Saeed, A., M. Iqbal, and M.W. Akhtar, *Removal and recovery of lead(II) from single and multimetal (Cd, Cu, Ni, Zn) solutions by crop milling waste (black gram husk).* Journal of Hazardous Materials, 2005. **117**(1): p. 65-73.
16. Hashim, M.A. and K.H. Chu, *Biosorption of cadmium by brown, green, and red seaweeds.* Chemical Engineering Journal, 2004. **97**(2-3): p. 249-255.
17. Lee, H.S. and B. Volesky, *Interaction of light metals and protons with seaweed biosorbent.* Water Research, 1997. **31**(12): p. 3082-3088.
18. Ho, Y.S. and A.E. Ofmaja, *Effects of calcium competition on lead sorption by palm kernel fibre.* Journal of Hazardous Materials, 2005. **120**(1-3): p. 157-162.
19. Wilke, A., R. Buchholz, and G. Bunke, *Selective biosorption of heavy metals by algae.* Environmental Biotechnology 2, 2006. **2**: p. 47-56.
20. Martin-Lara, M.A., et al., *Multiple biosorption-desorption cycles in a fixed-bed column for Pb(II) removal by acid-treated olive stone.* Journal of Industrial and Engineering Chemistry. **18**(3): p. 1006-1012.

21. Barron-Zambrano, J., et al., *Biosorption of Reactive Black 5 from aqueous solutions by chitosan: Column studies.* Journal of Environmental Management, 2010. **91**(12): p. 2669-2675.

22. Oliveira, F.D., et al., *Copper, Nickel and Zinc Removal by Peanut Hulls: Batch and Column Studies in Mono, Tri-Component Systems and with Real Effluent.* Global Nest Journal, 2010. **12**(2): p. 206-214.

23. Seo, D.C., K. Yu, and R.D. DeLaune, *Comparison of monometal and multimetal adsorption in Mississippi River alluvial wetland sediment: Batch and column experiments.* Chemosphere, 2008. **73**(11): p. 1757-1764.

24. Miralles, N., et al., *Cadmium and Lead Removal from Aqueous Solution by Grape Stalk Wastes: Modeling of a Fixed-Bed Column.* Journal of Chemical and Engineering Data, 2010. **55**(9): p. 3548-3554.

25. Marin, A.B.P., et al., *Biosorption of Zn(II) by orange waste in batch and packed-bed systems.* Journal of Chemical Technology and Biotechnology, 2010. **85**(10): p. 1310-1318.

26. Muhamad, H., H. Doan, and A. Lohi, *Batch and continuous fixed-bed column biosorption of Cd2+ and Cu2+.* Chemical Engineering Journal, 2010. **158**(3): p. 369-377.

27. Sousa, F.W., et al., *Green coconut shells applied as adsorbent for removal of toxic metal ions using fixed-bed column technology.* Journal of Environmental Management, 2010. **91**(8): p. 1634-1640.

28. Atar, N., A. Olgun, and S. Wang, *Adsorption of cadmium (II) and zinc (II) on boron enrichment process waste in aqueous solutions: Batch and fixed-bed system studies.* Chemical Engineering Journal, 2012. **192**: p. 1-7.

29. Wulfsberg, G., *Principles of Descriptive Inorganic Chemistry.* 1992: Univ Science Books.

6 Overall conclusions and recommendations

6.1 Conclusions

Citrus peels were found to be generally suitable for biosorption of Cd, Pb and Zn in fixed bed columns, confirming the first hypothesis which said that citrus peels can be used in a packed bed reactor without any processing. Citrus peels were also immobilized within an alginate matrix. This supports the fourth hypothesis which said that immobilization using commonly used polymeric materials can be customized to immobilize citrus peels such that they can be successfully applied in a column. Being an industrial waste, the 'quality' of peels varies from batch to batch with a potential for disintegration, swelling or clogging the column. It was found [Chapter 3] that these problems can be avoided by using this immobilized peels.

Metal uptake of immobilized peels was even higher than that of native peels. Metal uptake at breakthrough or saturation depended on different factors such as influent concentration, bed height and flow rate, as presumed by the second hypothesis. It was found that if the residence time of the metals in the column is not sufficient for mass transfer to occur (e.g., at high flow rates), uptake at breakthrough was reduced. An empty bed contact time of 10 minutes was found to be sufficient for effective sorbent utilization. Uptake at breakthrough was increased with increasing bed height, as found by most published articles, because less of the sorption capacity is "wasted" since the mass transfer zone, where the sorbent is not completely saturated, occupies a smaller fraction of the total column volume. Nevertheless, a normalized plot considering concentration vs. number of bed volumes treated revealed the fact that for a column long enough to have non-zero breakthrough time and negligible dispersion, increasing bed height proportionately increased the breakthrough and saturation time.

This study also focused on unifying the different modeling approaches available. Typically, biosorption articles follow a set of equations to model equilibrium and kinetics in batch and fixed bed reactor without verifying the suitability of using those models

under the prevailing conditions. This study identified the following major flaws in numerous biosorption articles:

1) Several model equations are used in the same article without recognition that they are mathematically analogous. Application of one equation makes the use of others redundant.

2) There are model equations which are not exactly analogous, but different approximations of a same parent model. The reason for making these approximations is often historical; usually to simplify the data fitting process to the extent that no software or other similar tools would be required, which was important in the pre-computer era. Incidentally, theses approximated versions are still used today, even violating the assumptions used in the derivation of the parent model.

3) There are articles where original rate equations were used and numerically solved using software packages, estimating model parameters by fitting those models to experimental data. Often times only one dominant resistance or rate limiting step was considered, which led to an average overall parameter (incorporating the effect of other parameters which were not considered in the model) as opposed to an 'intrinsic' one. Such apparent parameters are useless for a-priori prediction of breakthrough curves.

This study used rate equations for which analytical solutions were available. Breakthrough curves were predicted from the model by determining model parameters from other sources. This supports the third hypothesis. The diffusion coefficients of Cd in protonated citrus peels and in alginate immobilized peels were estimated to be 1.9E-05 and 1.0E-04 cm^2/min respectively based on batch kinetic experiments, whereas the film diffusion coefficient was estimated from published correlations.

For single metal biosorption, uptake on a mass basis in both batch and fixed bed reactors (at breakthrough and saturation) was found to follow the order Pb>Cd>≈Zn. However on

a molar basis, Zn had a higher uptake than Cd in batch mode. A comparison among different equilibrium models showed that a two parameter model was sufficient; the F test confirmed that no significant improvement was found by the introduction of third parameter.

It was found that the presence of other co-ions (regulated heavy metals such as Pb, Cd, Zn or the non-regulated commonly occurring divalent light metal Ca) affects the biosorption of target metals both in batch and fixed-bed reactors. The influence of regulated metals on equilibrium uptake was modeled as competitive, uncompetitive and partially competitive type interaction. This supports the fifth hypothesis.

The saturated column was regenerated using 0.1 (N) nitric acid. Desorption was almost complete for each of the single and binary systems. The concentration factor (CF), which is the ratio of concentration of desorbed metal to that in the influent stream, was calculated to be in the range of 34-128. The common practice is to calculate the CF based on the peak concentration of eluate but here the CF was determined based on the average concentration of desorbed metal in spent eluent solution so that it can measure the effectiveness of metal pre-concentration from the dilute influent stream. For single metal systems, CF decreased in the order Zn>Pb>Cd. Finally, 5.40 L of mining effluent containing a number of regulated and non-regulated metals was purified using 5 g of citrus peels. Overall, citrus peels were found to be efficient for the removal of heavy metals from aqueous phase.

6.2 Recommendations for future research

The current work presents in-depth studies on biosorption of heavy metals by citrus peels using a fixed bed reactor. Further work is recommended for practical application of this process:

Laboratory Work:

1) Modification of reactor
    a. Use of a recycled stream for better utilization of unused portion of the packed-bed column.

b. Use of Continuous Stirred Tank Reactor (CSTR).

2) Modification of influent
    a. Fixed bed experiment using a mixture of three or more metals.
3) Modification of biosorbent
    a. Cross-linking using suitable chemicals such as glutaraldehyde to provide mechanical rigidity without granulation.

Modeling:

1) Mathematical modeling of breakthrough curves showing overshoot of the weaker metal in multi-metal biosorption.
2) Deriving the external and intra-particle mass transfer coefficients of each metal in multi-metal biosorption.
3) Mathematical modeling of desorption curves.

Economic analysis:

For industrial applications, design of biosorption processes must be based on process economics considering multiple adsorption-desorption cycles. For immobilized peels on the one hand the initial sorbent cost is higher, which however could be counterbalanced by more frequent reuse of this more stable sorbent compared to untreated peels. Savings made by reusing native citrus peels, however, may not be profitable due to the eluent requirement, as well as investment cost for equipment. Eluent volume, on the other hand, controls the concentration ratio within a limit (Chapter 5). Again, performance of a cycle can be judged from the concentration ratio and/or recovery ratio all of which are connected by a single equation (Chapter 5). The recovery ratio can be controlled by choice of the eluent volume. Accordingly, a model may be constructed to determine the optimum usage of citrus peels and other biosorbents (Chapter 4).